2015-06-09

Rotary Inertial Navigation System with a Low-cost MEMS IMU and Its Integration with GNSS

Du, Shuang

UNIVERSITY OF CALGARY

Rotary Inertial Navigation System with a Low-cost MEMS IMU and Its Integration with GNSS

by

Shuang Du

A THESIS

SUBMITTED TO THE FACULTY OF GRADUATE STUDIES

IN PARTIAL FULFILMENT OF THE REQUIREMENTS FOR THE

DEGREE OF DOCTOR OF PHILOSOPHY

GRADUATE PROGRAM IN GEOMATICS ENGINEERING

CALGARY, ALBERTA

MAY, 2015

Abstract

Micro-electro-mechanical-systems (MEMS) inertial measurement unit (IMU) outputs are corrupted by significant sensor errors, such as noises, biases, scale factors, and installation errors. Consequently, the navigation errors of a low-cost inertial system with the MEMS IMU will accumulate quickly over time in stand-alone mode. Methods that can effectively mitigate the navigation errors without a need for external aiding, will be of great value for many applications. This research proposed a rotary inertial navigation system (INS) to mitigate navigation errors caused by MEMS inertial sensor errors when external aiding information is not available. A rotary INS is an inertial navigator in which the IMU is installed on a rotation platform. Application of proper rotation schemes can effectively cancel and reduce sensor errors. For example, the rotation of an IMU with a constant angular rate can modulate the constant inertial bias into periodic signals, and an integration of the modulated inertial data over a complete rotation cycle can eliminate the effect of the bias on the navigation solutions.

Improvement of current inertial system's observability in the absence of system maneuvers is also highly desired in applications. It is well known that the position and velocity from external aiding are extensively used to estimate the INS errors, and the weak maneuvers result in poor system observability and eventually degrade the navigation performance due to inaccurate estimation of INS errors. As the rotation changes the position of the IMU, the system observability is significantly improved in a rotary inertial system.

Although the rotary INS has been applied to inertial system with high-end IMUs, it has not been investigated for low-cost MEMS IMUs. Given the fact that the MEMS IMU features significant

sensor errors, as well as large and fast error variations, there are many issues and challenges that need to be addressed for effective navigation error mitigation and applications by rotary INS with MEMS IMUs. The conducted turntable tests and kinematic field tests indicate that with proper data processing, the horizontal position errors can be reduced by about 2~5 times in an inertial system with a rotating low-cost MEMS IMU, compared to those errors in a non-rotating system. Moreover, the observability of the roll and pitch errors, the accelerometer biases in the horizontal axes, and the gyro bias in the vertical direction can be significantly improved by IMU rotations.

Acknowledgements

First of all, I would like to express my sincere gratitude to my supervisor, Dr. Yang Gao. He continuously encouraged me to go through all the research and provided the financial support during my graduate studies. Without the supervision and the support from him, this study cannot be done.

Dr. Yang Gao, Dr. Naser El-Sheimy, Dr. Kyle O'Keefe, Dr. Abu Sesay, and Dr. Chiang Kai-Wei, members of my examination committee, are greatly acknowledged for your time to read this thesis and your valuable opinions. Dr. Wei Sun is also acknowledged for the valuable suggestions on this research and providing the equipments for test data collections.

Finally, and most importantly, I would like to thank my parents, Liping Du and Furong Lan, who unconditionally loved me, guided me, believed me, encouraged me and of course helped me financially for all these years. They are the source of all my achievements, and this work would not have been possible without their support.

Table of Contents

List of Tables

List of Figures and Illustrations

List of Symbols, Abbreviations and Nomenclature

Symbol	Definition
A	Azimuth angle
C_b^n	Transformation matrix from the body frame to the navigation frame
C_b^s	Transformation matrix from the body frame to the sensor frame
C_s^n	Transformation matrix from the sensor frame to the navigation frame
D^{-1}	relationship matrix between the position rate and velocity in the navigation frame
F_{rr}	Relationship matrix between the 1st derivative of position error vector and position error vector
F_{rv}	Relationship matrix between the 1st derivative of position error vector and velocity error vector
F_{vr}	Relationship matrix between the 1st derivative of velocity error vector and position error vector
F_{vv}	Relationship matrix between the 1st derivative of velocity error vector and velocity error vector
$F_{v\varepsilon}$	Relationship matrix between the 1st derivative of velocity error vector and attitude error vector
$F_{\varepsilon r}$	Relationship matrix between the 1st derivative of attitude error vector and position error vector
$F_{\varepsilon v}$	Relationship matrix between the 1st derivative of attitude error vector and velocity error vector
$F_{\varepsilon\varepsilon}$	Relationship matrix between the 1st derivative of attitude error vector and attitude error vector
H_j	The design matrix corresponding to the j^{th} measurement

K_{aij}	Accelerometer installation error between the i and j axes
K_{ax}	Accelerometer scale factor in the X axis
K_{ay}	Accelerometer scale factor in the Y axis
K_{az}	Accelerometer scale factor in the Z axis
K_{gij}	Gyro installation error between the i and j axes
K_{gx}	Gyro scale factor in the X axis
K_{gy}	Gyro scale factor in the Y axis
K_{gz}	Gyro scale factor in the Z axis
M	Meridian radius of the earth curvature
N	Prime vertical radius of the earth curvature
N_a	Accelerometers installation errors
N_g	Gyroscopes installation errors
R_1	Rotation matrix about the X axis
R_2	Rotation matrix about the Y axis
R_3	Rotation matrix about the Z axis
S_a	Accelerometers scale factor
S_g	Gyroscopes scale factor
X	Unknown vector for the rotary INS calibration
Z_j	The j^{th} measurement for rotary INS calibration
b^n	Accelerometer bias vector in the navigation frame
b^s	Accelerometer bias vector in the sensor frame
d^n	Gyroscope bias vector in the navigation frame
d^s	Gyroscope bias vector in the sensor frame
f	True accelerations
$\tilde{f}$	Sensed accelerations by accelerometers

f_{ib}^{b}	Specific force in the body frame with respect to the inertial frame
f_{is}^{s}	Specific force in the sensor frame with respect to the inertial frame
f_{sb}^{b}	specific force in the body frame with respect to the sensor frame
g^{n}	Local gravity vector in the navigation frame
n_{f}	Accelerometers noises
n_{w}	Gyroscopes noises
p	Pitch angle
r	Roll angle
r^{n}	Position vector in the navigation frame
v^{n}	Velocity vector in the navigation frame
Ω_{ie}^{n}	skew-symmetric matrix of the earth rotation rate in the navigation frame
Ω_{en}^{n}	skew-symmetric matrix of the transport rate caused by the change of orientation of the navigation frame
Ω_{ib}^{b}	Skew-symmetric matrix of the angular rate in the body frame with respect to the inertial frame
δf^{n}	Accelerometer error vector in the navigation frame
δr^{n}	Position error vector in the navigation frame
δv^{n}	Velocity error vector in the navigation frame
$\delta\omega_{sb}^{b}$	IMU rotation rate error
$\delta\omega^{n}$	Gyroscope error vector in the navigation frame
$\tilde{\omega}$	Sensed angular rates by gyroscopes
ω	True angular rate
ω_{ib}^{b}	Angular rate in the body frame with respect to the inertial frame

ω_{is}^{s}	Angular rate in the sensor frame with respect to the inertial frame
ω_{sb}^{b}	Angular rate in the body frame with respect to the sensor frame
$\phi^{\times}$	Matrix representing the rotation angle error of the rotation platform
φ	Latitude
λ	Longitude
ε^{n}	Attitude error vector in the navigation frame
σ_{b}	Uncertainty of estimates for gyro biases
σ_{s}	Uncertainty of estimates for gyro scale factor and installation error.

Abbreviations	Definition
ARW	Angle Random Walk
AUV	Autonomous Underwater Vehicle
ECEF	Earth Centered Earth Fixed
EKF	Extended Kalman Filter
FOG	Fiber Optic Gyroscope
GNSS	Global Navigation Satellite System
IMU	Inertial Measurement Unit
INS	Inertial Navigation System
MEMS	Microelectromechanical System
NATO	North Atlantic Treaty Organization
PPM	Parts Per Million
PVA	Position, Velocity and Attitude
RLG	Ring Laser Gyroscope
RMS	Root Mean Square
STD	Standard Deviation
ZUPT	Zero Velocity Updates

Chapter One: Introduction

Inertial navigation is the process whereby the measurements provided by an inertial measurement unit (IMU) are used to determine the position of the vehicle in which they are installed (Schwarz and Wei, 2000; Titterton and Weston, 2004). The IMU normally contains a triad of accelerometers and gyroscopes (gyros), and the combination of the two sets of measurements is able to define the translational motion of the vehicle with respect to the inertial reference frame, which allows its position to be calculated based on the initial states (position and attitude). As a self-contained navigation system, the inertial navigation system (INS) has been used for a wide range of applications. For geomatics applications, the INS is an essential geo-referencing device in mobile mapping systems for infrastructure and street surveys, in underwater navigation systems for offshore geophysical exploration, and in unmanned aerial vehicles for disaster monitoring, to mention just a few. INS navigation errors include errors in its position, velocity and attitude solutions. Due to its self-contained characteristic, the INS navigation errors accumulate over time, which deteriorate its long term navigation accuracy.

A rotary INS is an INS in which the IMU is installed on a rotation platform as shown in Figure 1.1. This technique was initially proposed for the gimbaled inertial system by Geller (1968). Afterwards, Levinson and Giovanni (1980) applied it to strapdown inertial system. The proper rotation of the IMU can average out the inertial sensor biases (Weston and Titterton, 2000) and eventually improve the navigation performance. For example, the rotation of the IMU with a constant angular rate can modulate the constant inertial bias into periodic signals, and an integration of the modulated inertial data over a complete rotation cycle can eliminate the effect

of the bias on the navigation solutions (Giovanni and Levinson, 1981; Sun et al., 2013; Du et al., 2014). In the sequel, an INS with a non-rotating IMU is referred to as a conventional INS to distinguish it from a rotary INS.

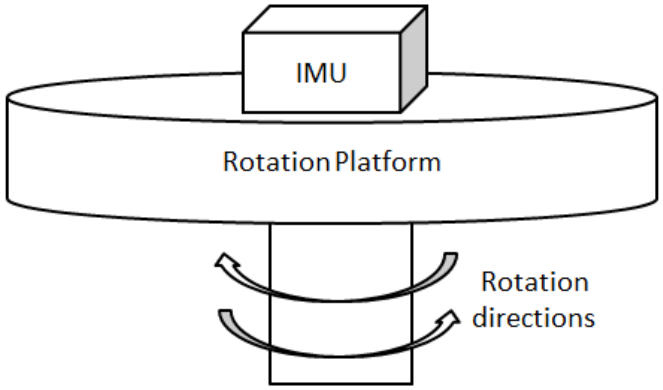

Figure 1.1 Structure of rotary INS

As the rotary INS can mitigate the INS navigation errors without the requirement of external information, it has been extensively employed for the warship or submarine. The rotary systems can be divided into single-axis and dual-axis rotary systems. In 1980, Sperry Marine, Inc. proposed and developed the single-axis rotary INS based on ring laser gyro (RLG) for the long-term marine navigation, which can meet U.S. Navy Type I at-sea performance requirements (Levinson and Giovanni 1980; Giovanni and Levinson 1981). Afterwards, they developed other two single-axis rotary inertial systems, MK39Mod3C and WSN-7B, which were extensively equipped in warships and submarines in many countries and areas (Tucker and Levinson, 2000; Yuan, 2007; Sun, 2011). Both systems can achieve the marine navigation performance of better than 1 nmile/24h, and they also meet U.S. Navy navigation requirements, as well as velocity and

attitude specifications (Terry and Emanuel, 2000). Figure 1.2 shows the structure of WSN-7B, and the MK39Mod3C has a similar structure.

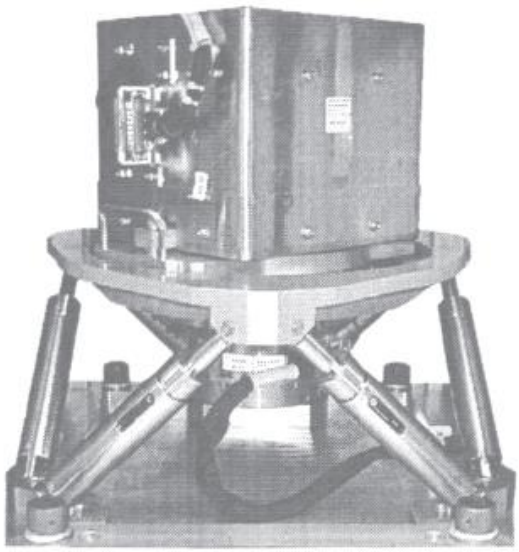

Figure 1.2 Structure of WSB-7B single-axis rotary RLG inertial system (Yuan 2007)

Sperry Marine, Inc. and Honeywell, Inc. jointly developed the dual-axis, high performance rotary marine RLG navigator, MK-49, which has advantages in comparison to the single-axis system. In 1989, MK-49 was chosen as the standard navigation system for the warships of North Atlantic Treaty Organization (NATO). In 1994, 56 systems were producing for the navies of the Netherlands, Spain, and the United Kingdom and 20 systems were manufacturing for the navies of Australia and New Zealand (Lahham and Brazell, 1992; Levinson et al., 1994; Hibbard et al., 1996). The Canadian Navy also spent $970 million on MK-49 to equip their submarines in 2005, while Australia expended $680 million to upgrade their marine navigator in 2006. The navigation accuracy of MK-49 can achieve 0.39 nmile/30h. Based on MK-49, Sperry Marine, Inc. developed another dual-axis rotary inertial system, WSN-7A, in the 1990s, which was only equipped in U.S. Navy; however, its navigation accuracy is yet unclear (Yuan 2007; Sun 2011).

Table 1.1 lists the comparisons between the conventional and rotary marine navigators in terms of navigation accuracy and costs (Yuan 2007). Because of the additional rotation devices, the rotary systems are much more expensive than the conventional systems; however the rotation of the IMU significantly improves the navigation accuracy, especially for the dual-axis rotary systems.

Table 1.1 Comparisons between non-rotary and rotary systems (Yuan 2007)

	Non-rotary INS	Single-axis rotary INS	Dual-axis rotary INS
Products	MK39Mod3A	MK39Mod3C, WSN-7B	MK-49, WSN-7A
Navigation Accuracy	<1 nmile/8h	<1 nmile/24h	<0.39 nmile/30h
Costs	$30 million	$90 million	$250 million

As production and maintenance are very expensive for the rotary system based on RLG, Pennsylvania State University ARL (Applied Research Laboratory), NRL (Naval Research Laboratory), as well as Boeing and Honeywell, started in 1995 to develop the rotary system based on fiber optic gyro (FOG) (Morrow and Heckman, 1998; Heckman and Baretela, 2000). It was reported that such a system can achieve the navigation performance better than 10 nmile/100h (Sun 2011). So far, both single-axis and dual-axis rotary systems are still only produced based on high-end inertial sensor, such as RLG and FOG, and are extensively equipped in warships and submarines for navies. The development of tri-axis rotary system is also underway (Sun 2011).

1.1 Background and Problem Statement

As a self-contained navigation system, the accumulated INS navigation errors are highly dependent upon the sensor errors. Although very small sensor errors are contained in high-end inertial sensors, such as RLG and FOG (Du, 2010), their large size (usually also very heavy) and high cost have limited their use to various applications. With the development of microelectromechanical system (MEMS) technology, MEMS inertial sensors became available to the commercial market in the 1990s. MEMS inertial sensors quickly found applications for motion detection, indoor pedestrian and robotic navigation because of their low-cost, small size, light weight, and low-power consumption (Liu, 2006; Wang, 2006; Hide et al., 2010; Karumuri et al., 2011). The MEMS IMU outputs however, are corrupted with significant sensor errors, such as high frequency noises, biases, scale factors, and installation errors. As a result, the navigation errors will accumulate quickly and deteriorate the navigation solution over a short period of time (Nassar et al., 2003; Shin et al., 2005; Du, 2010). For example, the position errors of an inertial system with a low-cost MEMS IMU will grow to kilometers within several minutes (Du et al., 2014).

With external aiding, the accumulated INS navigation errors can be effectively mitigated. For example, the position and velocity information obtained from the Global Navigation Satellite System (GNSS) can be used to estimate the INS errors using an extended Kalman filter (EKF) and eventually limit the navigation error accumulation (Shin, 2001; Shin, 2005; Niu et al., 2006; Antonio, 2010; Fang and Gong, 2010; Du and Gao, 2012a). Various investigations have been conducted to employ external navigation information to aid the INS. Carvalho et al. (1997) and Ren and Ke (2010) applied the particle filter to dampen the navigation error accumulation of the

INS. Wang and Gao (2005) and Noureldin et al. (2007) applied the fuzzy logic to adaptively adjust the parameters of the estimation algorithm. More precise stochastic model, such as auto-regressive model, is used to interpret the randomness of MEMS-based inertial sensor errors (Nasser, 2003; Nasser and El-Sheimy, 2005; Du and Gao, 2012b). Other sensors, such as wheel speed sensors (Li, 2009) and vision sensors (Huang et al., 2011; Du et al., 2012; Du et al., 2013), are also employed in an aided-INS to limit the navigation error accumulations.

Although the navigation error accumulations can be effectively reduced in an aided-INS, the errors still accumulate quickly when aiding sensors are not available. For example, GNSS will not be available for land vehicles travelling through tunnels or underwater vehicles, and the vision sensors are unusable in severe weather conditions as clear images cannot be obtained. Previous research indicate that the positioning solutions with decimetre accuracy can be obtained by a conventional MEMS-based inertial system with continuous GNSS updates at data rate of 1 Hz, nevertheless, position errors would quickly drift to 30~50 metres within 30 seconds in the presence of GNSS outages (Godha, 2006; Du, 2010). Thus, methods that can effectively mitigate the navigation errors, without a need for external aiding, will be of great value for many applications. Such benefits include not only a reduction of dependence on external aiding information, but also good autonomous navigation performance over a longer period when no external aiding is available (Yuksel, 2011; Du et al., 2015). .

Improvement of current inertial system's observability in the absence of system maneuvers is also highly desired in applications. The position and velocity information from the GNSS and Doppler velocity sensors has been widely used as external measurements to estimate INS errors (Meskin and Bar-Itzhack, 1992; Godha and Cannon 2007; Niu et al., 2007). However, position

information is only weakly related to the attitude and inertial sensor errors, which causes the velocity information to become the main measurements to estimate all other error parameters (Rhee et al., 2004; Hong et al., 2005). Although the INS position and velocity errors can be directly observed in the filter, with the measurements of position and velocity, the observability of other INS error terms (except the accelerometer bias in vertical direction) is highly related to the system maneuvers (Goshen-Meskin and Bar-Itzhack, 1992; Hong et al., 2005). Weak maneuvers results in poor observability of these errors and eventually degrades the navigation performance due to inaccurate estimation of INS sensor errors. For instance, in precision agriculture, the GNSS/INS integrated system is employed to determine the position, velocity and attitude of the tractors for guidance and steering control. Since parallel straight lines are typical for ploughing and cultivating with tractors (Li et al., 2012), the vehicle maneuvers become very weak when the tractors are travelling at a constant velocity along straight lines. As a result, the observability of the filter parameters of attitude errors, accelerometer biases in the horizontal plane, and gyro biases are very poor. In particular, the azimuth solution will be drifted away from its true value due to poor observability for the azimuth error and the gyro biases in the vertical direction.

Given the ability of a rotary INS to mitigate the error accumulation in high-end inertial systems, this technique is investigated and applied to MEMS-based inertial systems in this research to mitigate the navigation error accumulation in stand-alone mode. Moreover, this technique is also employed to improve the observability of INS errors, as the rotation changes the position of the IMU.

1.2 Literature Review

As early as 1968, Geller (1968) described a gimbaled inertial system with continuous rotation of platform relative to the local level frame, and he concluded that the system position error was greatly reduced by rotation frequencies larger than twice that of Schuler frequency. Levinson and Giovanni (1980) and Giovanni and Levinson (1981) applied such technique to a strapdown system and presented a marine RLG navigator, in which the assembly was sequenced between four orthogonal dwell positions relative to the longitudinal axis. The rotation rate between dwell positions was 10 degree per second and the dwell time in each position was 11 minutes. Although promising results were reported in the above research, the error equations and analyses were seldom provided. At the beginning of 20^{th} century, with the maturation of FOG technology, most of the research focused on the rotary system based on FOG. The error modulation principle with IMU continuous rotation about vertical axis was analyzed in Yang and Miao (2004), Zhang et al. (2009) and Ben et al. (2010). Yang and Miao (2004) concluded that the constant sensor errors in horizontal axes are modulated into periodic signals and can be well mitigated after a complete rotation cycle; however, the errors in vertical axis cannot be modulated. Simulations are used to verify the reduction on navigation errors. Zhang et al. (2009) and Ben et al. (2010) derived the differential equations for navigation errors and employed Laplace transform to obtain solutions, which indicated analytically that the navigation errors can be reduced through IMU rotation, and a higher rotation rate can more effectively mitigate navigation errors. Although IMU rotation can effectively mitigate navigation errors, it also motivates additional sensor errors. Sun et al. (2009) found that the IMU rotation induced a gyro bias in vertical axis, due to scale factor, and gyro biases in both horizontal axes, due to installation errors, which severely degrade the navigation performance. A reciprocating rotation scheme was proposed, in which the IMU

rotates about vertical axis 360 degrees in clockwise direction, and then rotates in counter-clockwise direction 360 degrees, to eliminate the effect on navigation errors by rotation induced gyro biases. Their results indicated that only the effect of the rotation-induced gyro bias by scale factor can be mitigated in such a rotation scheme. Similar methods were also proposed in Ishibashi (2006a; 2006b), which applied the rotary technique for the navigation of an autonomous underwater vehicle (AUV).

As the continuous rotation of the IMU may cause mechanical problems in the rotational platform, the rotation-dwell scheme was also designed for the rotary INS with FOG (Yuan and Rao, 2006; Yuan 2007; Sun 2011). A Two-position and a four-position rotation-dwell schemes were proposed by Yuan (2007), which pointed out that the integration of the modulated sensor errors must be zeroes after a complete rotation cycle to reduce the navigation errors. Similar to Giovanni and Levinson (1981), the dwell positions are symmetric in the reference frame, and the dwell time for each position is the same. Sun (2011) also proposed the four-position rotation-dwell scheme and concluded that the continuous rotation outperforms the rotation-dwell scheme in terms of error mitigations. As the sensor errors in rotation axis cannot be modulated, Zha et al. (2012) proposed a method, in which two inertial sensors with similar error characteristics are mounted on the opposite direction of the rotation axis to reduce the navigation error caused by the sensor bias in rotation axis. Simulation results indicated that the proposed system with additional sensor in rotation axis can further reduce the navigation errors in comparison to other single-axis systems.

Proper IMU rotations not only reduce the navigation errors, but also improve the accuracy of alignment, as constant sensor biases can be auto-compensated after a complete rotation cycle.

Yang and Miao (2004), Yuan (2007) and Sun (2011) studied the alignment for a single-axis rotary system, and the turntable tests and simulations demonstrated that the alignment accuracy can be improved by at least 1 order of magnitude. Currently, only rotation about the vertical axis is employed for the single-axis system, as it can effectively remove the navigation errors in the east-north plane.

As the sensor errors in the rotation axis cannot be modulated in the single-axis system, dual-axis rotation technique was developed to further improve the navigation performance of rotary INS, though such technique is much more complex than single-axis indexing and requires more expensive rotation devices. In Levinson and Majure (1987), the dual-axis indexing was applied to the RLG inertial system and the results shows that such a system can further reduce the navigation errors by about 50%, in comparison to the single-axis system. Different dual-axis rotation schemes were also applied to FOG inertial systems. Yuan and Rao (2006) and Yuan (2007) presented an eight-position and a sixteen-position rotation-dwell schemes. The turntable tests indicated that the navigation errors are reduced by at least 4~5 times in a dual-axis system, compared to the single-axis system. Moreover, the dual-axis system offers better repeatability of navigation errors. Sun (2011) also proposed a sixteen-position rotation-dwell scheme and pointed out that the error mitigation performance is highly associated with the rotation between dwell positions and the dwell time at each position. With dual-axis rotation devices, the multi-position calibration algorithms were also proposed to calibrate the gyro scale factors and installation errors for a rotary system (Lu and Wang, 2010; Yuan 2007; and Sun 2011).

1.3 Research Objectives and Contributions

The main objective of this research is to investigate the rotary INS technique to reduce the navigation errors in inertial systems with low-cost MEMS IMUs in stand-alone mode, and to improve the navigation system's observability by rotation of the IMU. Although the rotary INS has been applied to inertial systems with high-end IMUs, it has not been investigated for low-cost MEMS IMUs. Given the fact that the MEMS IMU features significant sensor errors, as well as large and fast error variations, there are many issues and challenges that need to be addressed for effective navigation error mitigation and applications by rotary INS with MEMS IMUs. Two MEMS IMUs, namely NAV440 and MTi-G, are employed in this research, and both tri-axial and single-axis rotation tables are used to rotate the IMUs. The rotation tables are usually very expensive and cumbersome, but the error compensations for the MEMS IMUs can be better understood by using them, as the rotation tables isolate factors that affect error mitigations, such as vibrations and unstable rotation. Three different rotation schemes, each continuously rotating about X, Y and Z axes, respectively, are proposed and investigated for INS navigation error mitigation without external aiding. An integrated GNSS/rotary INS with MEMS IMU is also proposed and investigated for bridging GNSS outages. An outline of the specific objectives of this research is given below:

i. Development of the mathematical equations for error mitigation in rotary INS and performance analysis by simulation computations. This work will also include the identification of potential IMU rotation induced sensor errors and the development of methods to estimate and remove such sensor errors.

ii. Static and kinematic field tests on rotary INS with MEMS IMUs. The static tests will be conducted in a laboratory to assess the developed calibration method for accurate sensor error determination, to analyze the error mitigation performance of rotary INS with MEMS IMUs, and to investigate the relationship between the IMU rotation rate and the error mitigation efficiency of the rotary INS. The kinematic field tests will focus on the evaluation of the error mitigation performance of rotary INS in a dynamic environment due to frequent variations in acceleration, velocity and azimuth.

iii. Analysis of the system observability of conventional INS and rotary INS in the absence of system maneuvers and the improvements of the system observability by IMU rotations.

iv. Development of an integrated system of GNSS and rotary INS with MEMS IMU for bridging GNSS outages and field tests to verify the improvements of navigation performance by IMU rotations.

The major contributions of this thesis include the following:

i. The investigation of rotary INS with MEMS IMU from mathematical equations of error mitigations, IMU rotation schemes and the rotation-induced sensor errors, as well as their calibrations, simulation analysis, turntable tests in laboratory and kinematic field tests, and results analysis;

ii. The investigation of the observability of both conventional and rotary inertial navigation systems and its improvement by IMU rotation, as well as turntable tests in laboratory and results analysis;

iii. The development of integrated GNSS and rotary INS based on MEMS IMUs to bridge GNSS outages, including system observability analysis, as well as kinematic field tests and results analysis

The rotary INS with MEMS IMU and its integrated system with GNSS are able to provide enhanced navigation performance with potential to various applications; some such applications are provided below. Despite the fact that rotary inertial systems with MEMS IMU require a rotation platform, which increases hardware complexity and cost compared to the conventional systems, such obstacles will be overcome by technology advances in the future driven by applications demanding continuous navigation in challenging environments.

1) Underwater Navigation

Autonomous underwater vehicles (AUVs) are widely used in recent years for underwater search and mapping, climate change assessment, marine habitat monitoring, and shallow water mine countermeasures. Inertial systems are used as the primary navigator for AUVs due to the unavailability of GNSS (Hartman et al., 2008). The observability issue is a concern in an underwater environment, where strong maneuvers are difficult due to water resistance. Although Doppler velocity sensor and depth sensor can be used to aid the inertial navigation, the observability for attitude errors and most sensor errors is still poor, which not only results in inaccurate estimation of those error terms, but also causes navigation errors to quickly accumulate over time. With improved observability from IMU rotation, the inertial sensor errors and attitude errors can be more accurately determined with measurements from Doppler velocity sensor or depth sensor. Moreover, the rotation can also mitigate error accumulation when

external sensors are unavailable. Therefore, the rotary inertial systems with MEMS IMU have the potential to improve the autonomous navigation performance of AUVs for different applications.

2) Land Vehicle Navigation

The integrated GNSS/INS system is extensively accepted as the current navigation system for land vehicles (manned or unmanned). In such a system, the navigation solutions can be derived from the inertial data with high data rate, and the GNSS measurements are used to estimate the inertial sensor errors and corrections for position, velocity and attitude errors. As GNSS outages are frequently experienced, such as in situations where the vehicle is travelling in a tunnel or urban canopy, the navigation errors quickly accumulate due to significant sensor errors. Such an issue can be well-overcome by IMU rotation in an integrated system with rotary INS, with the potential to improve overall system navigation performance.

3) Precision Agriculture

Precision agriculture has revolutionized traditional farming. By integrating precision agriculture, farmers can operate more efficiently and productively during every stage of their farming applications. The GNSS/INS integrated system is employed to determine the position, velocity and attitude of the tractors for guidance and steering control. As mentioned previously, the observability of attitude errors, accelerometer biases in horizontal axes, and gyro bias in vertical axis become poor due to the lack of strong maneuvers when vehicle travels along straight lines with relatively stable velocity. As a result, less accurate attitude solutions are obtained in such conditions, and in particular, the azimuth solution will be drifted away from its true value. Such

issues can be well handled by an integrated system with rotary INS, which can substantially improve the system observability in the absence of maneuvers. The roll and pitch errors are reduced by improving their own observability and the observability of accelerometer biases in the horizontal axes, while the azimuth errors can be limited by accurate estimation of the gyro bias in the vertical axis.

1.4 Thesis Outline

Chapter Two presents the fundamentals of rotary INS. The definitions of different coordinate frames, including inertial frame, local level frame, body frame and a newly introduced sensor frame are provided, as well as the transformations between these frames. The mechanization of rotary INS is described in the local level frame, followed by the inertial sensor error model, as well as the rotary INS error model in the local level frame.

Chapter Three analyzes the error mitigations of rotary INS. Mathematical equations are derived for conventional INS and rotary INS with IMU rotations about X, Y and Z axes, respectively. Error mitigations and motivated sensor errors by IMU rotations are identified and verified through simulation analysis. Then a calibration process is introduced to remove the motivated sensor errors.

Chapter Four presents the static and kinematic field tests for rotary INS with two different MEMS IMUs. The static tests are conducted in laboratory based on a tri-axial rotation table to assess the calibration method for accurate determination of sensor errors, to evaluate the error mitigations for MEMS IMU using rotary technique, and to investigate the relationship between rotation rate and error mitigations. The kinematic field tests are conducted based on a single-axis

rotation table, to study the error mitigation performance of rotary INS in dynamic conditions due to frequent variations on acceleration, velocity and azimuth.

Chapter Five presents the observability analysis for conventional INS and rotary INS with IMU rotations about X, Y and Z axes, respectively, in the absence of system maneuvers. Then turntable tests are conducted based on the tri-axial rotation table in laboratory to verify the improvement on observability by IMU rotations.

Chapter Six presents the development of the integrated GNSS/rotary INS with MEMS IMU to bridge GNSS outages. Kinematic field tests are conducted based on a single-axis rotation table to verify the navigation error mitigations by IMU rotations during GNSS outages.

Chapter Seven summarizes the work presented in this thesis, and draws conclusions from the test results and analysis. Finally, recommendations for the future work are provided.

Chapter Two: Fundamentals of Rotary Inertial Navigation System

The fundamentals of rotary INS are introduced in this chapter, including the coordinate frames and the transformations among them, as well as the mechanization algorithm, the error mitigation principle, the inertial sensor error model, and the model for the navigation errors.

2.1 Coordinate Frames and Transformations

The inertial frame, earth centered earth fixed frame, local-level frame, and body frame are employed in rotary INS, and their definitions are given as follows:

Inertial frame (i-frame): it is a non-rotating and non-accelerating frame with respect to fixed stars. Its origin is the Earth's center of mass, X axis is pointing towards the mean vernal equinox, Z axis is parallel to the spin axis of the Earth, and Y axis is orthogonal to X and Z axes completing a right-handed system.

Earth Centered Earth Fixed frame (ECEF or e-frame): as shown in Figure 2.1, the origin of the frame is the Earth's mass center, and its Z axis is parallel to the mean spin axis of the Earth, its X axis is pointing towards the mean meridian of Greenwich, while the Y axis is orthogonal to both X and Z axes completing a right-handed system.

Local level frame (l-frame or n-frame): it is a local geodetic frame with the origin coinciding with the sensor, the X and Y axes pointing towards geodetic east and north, respectively, and the Z axis pointing up, as shown in Figure 2.1. This frame is also referred as the navigation frame.

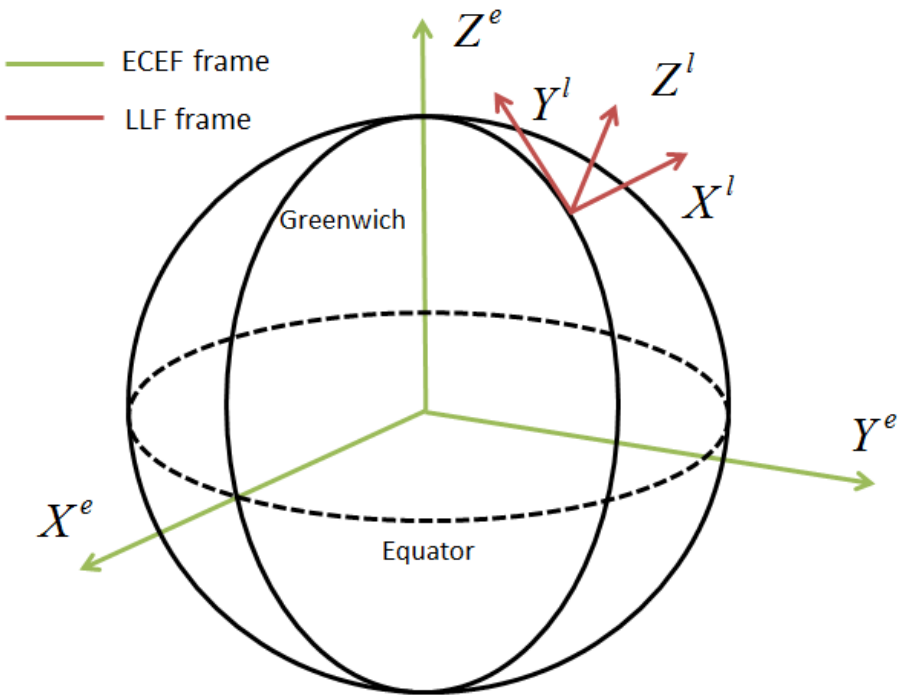

Figure 2.1 Earth centered earth fixed and local level frames

Body frame (b-frame): the origin of the frame is the center of the IMU, the X and Y axes are pointing forward and right directions of the vehicle (or carrier), in which the IMU is installed, respectively, and the Z axis is orthogonal to the XY plane completing a right-handed system.

As the IMU rotates in the rotary INS, a new frame in which the inertial readings are collected is introduced in addition to the above coordinate frames. This new coordinate frame is referred as the inertial sensor frame with the definition provided below.

Inertial sensor frame (s-frame): the inertial sensor frame is also referred as the IMU frame. Its axes are aligned with the sensitive axes of the inertial sensors with the origin defined as the origin of the IMU.

The transformations between different coordinate frames are frequently used in inertial navigations. Some of the transformations used in this research are given as follows:

The transformation from the b-frame to the n-frame can be performed by three consecutive rotations around the X, Y and Z axes, as described by Eq. (2.1).

$$
\begin{aligned}
C_b^n &= R_3(A)R_2(r)R_1(p) \\
&= \begin{bmatrix} \cos A\cos r & \cos A\sin r\sin p + \sin A\cos p & -\cos A\sin r\cos p + \sin A\sin p \\ -\sin A\cos r & -\sin A\sin r\sin p + \cos A\cos p & \sin A\sin r\cos p + \cos A\sin p \\ \sin r & -\cos r\sin p & \cos r\cos p \end{bmatrix}
\end{aligned} \tag{2.1}
$$

where, $R_3(A) = \begin{bmatrix} \cos A & \sin A & 0 \\ -\sin A & \cos A & 0 \\ 0 & 0 & 1 \end{bmatrix}, R_2(r) = \begin{bmatrix} \cos r & 0 & -\sin r \\ 0 & 1 & 0 \\ \sin r & 0 & \cos r \end{bmatrix}, R_1(p) = \begin{bmatrix} 1 & 0 & 0 \\ 0 & \cos p & \sin p \\ 0 & -\sin p & \cos p \end{bmatrix}$

are the rotation matrix about Z, Y and X axes, respectively, A represents the azimuth, r represents the roll, and p represents the pitch.

The transformation matrix between the s-frame and the b-frame is associated with the IMU rotations. For the IMU rotation about the Z-axis in the positive direction, the transformation matrix from the b-frame to the s-frame is given in Eq. (2.2).

$$
C_b^s = \begin{bmatrix} \cos\beta & \sin\beta & 0 \\ -\sin\beta & \cos\beta & 0 \\ 0 & 0 & 1 \end{bmatrix} = (C_s^b)^T \tag{2.2}
$$

where β is the rotation angle about Z axis.

With the transformation matrix from the sensor frame to the body frame, the transformation matrix from the sensor frame to the navigation frame can be obtained using Eq. (2.3).

$$C_s^n = C_b^n C_s^b \tag{2.3}$$

2.2 Rotary INS Mechanization

Generally speaking, the mechanization algorithm of rotary INS is similar to the one of conventional INS. As the inertial readings are collected in the sensor frame, a transformation process is required as shown in Eq. (2.4).

$$\begin{aligned} f_{ib}^b &= C_s^b f_{is}^s + f_{sb}^b \\ \omega_{ib}^b &= C_s^b \omega_{is}^s + \omega_{sb}^b \end{aligned} \tag{2.4}$$

where f_{ib}^b and ω_{ib}^b are the specific force and angular rate in the body frame with respect to the inertial frame, respectively, f_{is}^s and ω_{is}^s are the specific force and angular rate in the sensor frame with respect to the inertial frame, respectively, f_{sb}^b and ω_{sb}^b are the specific force and angular rate of the body frame with respect to the sensor frame, respectively. As the IMU rotation does not introduce any linear movement, f_{sb}^b is a zero vector, while ω_{sb}^b is associated with the IMU rotations.

Obviously, the rotation angle between the body frame and the sensor frame is required in the transformation process, and this information is usually measured by a device installed in the rotation platform. With the transformed specific force and angular rate in the body frame, the

mechanization of the conventional INS can be used to derive position, velocity and attitude solutions as shown in Eq. (2.5).

$$\begin{bmatrix} \dot{r}^n \\ \dot{v}^n \\ \dot{C}_b^n \end{bmatrix} = \begin{bmatrix} D^{-1}v^n \\ C_b^n f^b - (2\Omega_{ie}^n + \Omega_{en}^n)v^n + g^n \\ C_b^n(\Omega_{ib}^b - \Omega_{in}^b) \end{bmatrix} \tag{2.5}$$

where dot represents the time derivatives, and the superscript 'n' and 'b' represent the n-frame and the b-frame, respectively, $D^{-1} = \begin{bmatrix} 0 & \frac{1}{M+h} & 0 \\ \frac{1}{(N+h)\cos\varphi} & 0 & 0 \\ 0 & 0 & 1 \end{bmatrix}$ is the relationship matrix between the position rate and velocity in the n-frame, M represents the meridian radius of the earth curvature, N represents the prime vertical radius of the earth curvature, $r^n = [\varphi \quad \lambda \quad h]$ presents the position vector in the n-frame, $v^n = [V_E \quad V_N \quad V_U]^T$ represents the velocity vector in the n-frame, $g^n = [0 \quad 0 \quad -g]$ represents the earth's local gravity vector, g can be obtained from a normal gravity model, Ω_{ab}^c represents the skew-symmetric matrix of the rotation rate ω_{ab}^c, which represents the rotation rate from the frame 'b' relative to the frame 'a', expressed in the frame 'c', ω_{ie}^n and ω_{en}^n represent the earth rotation rate projected in the n-frame and the transport rate caused by the change of orientation of the n-frame, respectively, ω_{in}^n represents the sum of the ω_{ie}^n and ω_{en}^n.

The above rotary INS mechanization equations can also be illustrated as a flowchart given in Figure 2.2

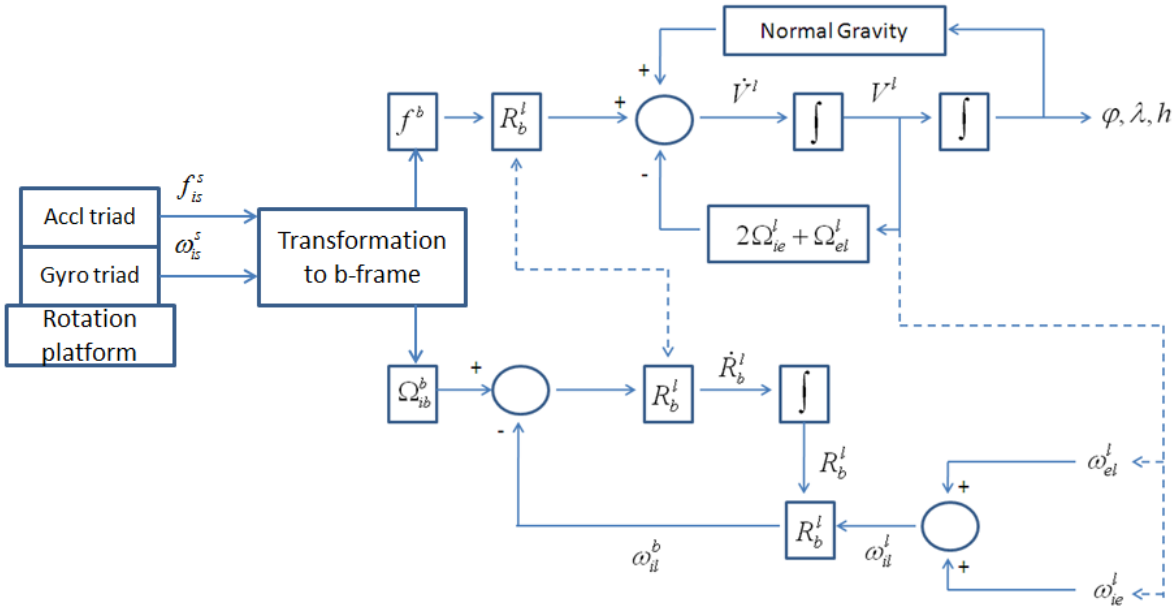

Figure 2.2 Flowchart of rotary INS mechanization

2.3 Error Modulation by IMU Rotation

A simple scenario, in which the IMU rotates in counter-clockwise direction about the Z axis with a constant rotation rate ω, as shown in Figure 2.3, is employed to explain the principle of rotation error modulation.

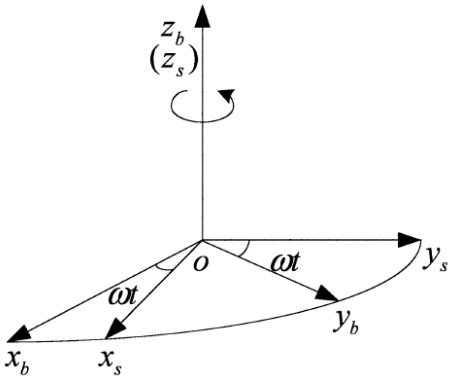

Figure 2.3 Scenario of IMU rotation about Z axis

Based on the transformation matrix between the body frame and the sensor frame given in Eq. (2.2), the gyro and accelerometer biases in the navigation frame at time t can be described by Eq. (2.6) and (2.7), respectively, if the body frame is aligned with the navigation frame (Sun et al., 2013; Du et al., 2014).

$$d^n = \begin{bmatrix} d_E \\ d_N \\ d_U \end{bmatrix} = C_s^n d^s = C_b^n C_s^b d^s = \begin{bmatrix} d_x^s \cos\omega t - d_y^s \sin\omega t \\ d_x^s \sin\omega t + d_y^s \cos\omega t \\ d_z^s \end{bmatrix} \tag{2.6}$$

$$b^n = \begin{bmatrix} b_E \\ b_N \\ b_U \end{bmatrix} = C_s^n b^s = C_b^n C_s^b b^s = \begin{bmatrix} b_x^s \cos\omega t - b_y^s \sin\omega t \\ b_x^s \sin\omega t + b_y^s \cos\omega t \\ b_z^s \end{bmatrix} \tag{2.7}$$

where $d^s = \begin{bmatrix} d_x^s & d_y^s & d_z^s \end{bmatrix}^T$ and $b^s = \begin{bmatrix} b_x^s & b_y^s & b_z^s \end{bmatrix}^T$ represent the gyro drift and accelerometer bias in the sensor frame, respectively, $d^n = \begin{bmatrix} d_E & d_N & d_U \end{bmatrix}^T$ and $b^n = \begin{bmatrix} b_E & b_N & b_U \end{bmatrix}^T$ represent the gyro drift and accelerometer bias in the navigation frame, respectively.

As shown in above equations, the gyro and accelerometer biases in the east and north directions are converted into periodic signals through continuous IMU rotation about the Z axis, if the biases are constants. As the integrations of these periodic errors are zeroes after a complete rotation cycle, the navigation errors caused by the sensor constant biases in the X and Y axes are self-eliminated. However, the inertial sensor bias in the Z-axis (rotation axis) cannot be modulated, and the navigation errors caused by such errors propagate in the same way as in the conventional INS.

The above analysis is based on that the body frame is aligned with the navigation frame and it remains static while IMU rotating. If we consider a specific scenario, in which the IMU rotates in counter-clockwise direction about the Z axis with a constant rotation rate ω and the body frame also rotates in clockwise direction about the Z axis with ω, then the gyro and accelerometer biases in the navigation frame can be described by Eq. (2.8) and (2.9), respectively. Apparently, the rotation of the body frame removes the modulation on sensor biases. This demonstrates that the dynamics of vehicle (or carrier), in which the IMU is installed, will affect the error modulation by IMU rotations.

$$d^n = \begin{bmatrix} d_E \\ d_N \\ d_U \end{bmatrix} = C_s^n d^s = C_b^n C_s^b d^s = \begin{bmatrix} d_x^s \\ d_y^s \\ d_z^s \end{bmatrix} \tag{2.8}$$

$$b^n = \begin{bmatrix} b_E \\ b_N \\ b_U \end{bmatrix} = C_s^n b^s = C_b^n C_s^b b^s = \begin{bmatrix} b_x^s \\ b_y^s \\ b_z^s \end{bmatrix} \tag{2.9}$$

2.4 Inertial Sensor Error Model

The specific force and angular rate collected by the accelerometer and gyro contain different errors, such as the noise, the turn on biases, the scale factor errors, and the installation errors. The sensor errors are the major error source of the navigation errors of inertial navigation systems. Usually the sensor error models for the gyro and accelerometer can be described by Eq. (2.10) and (2.11), respectively.

$$\tilde{\omega} = \omega + d + S_g\omega + N_g\omega + n_w \tag{2.10}$$

$$\tilde{f} = f + b + S_a f + N_a f + n_f \tag{2.11}$$

where $\tilde{\omega}$ represents the actual gyro outputs, ω represents the true angular rate, d represents the gyro bias, S_g represents the gyro scale factor, N_g represents the gyro installation errors, and n_ω represent the gyro noise, $\tilde{f}$ represents the actual accelerometer outputs, f represents the true specific force, b represents the accelerometer bias, S_a represents the accelerometer scale factor, N_a represents the accelerometer installation errors, and n_f represent the accelerometer noise.

Both accelerometer and gyro biases normally contain two parts, namely, the deterministic part and the random part. The deterministic part is constant, but differs each time the sensor is turned on, and is also known as the turn on bias in some literatures. The random part of bias varies with time and it is quantified by the bias instability. The high-end IMU features very small gyro bias instability, e.g. 0.01°/h or even lower, but for MEMS IMU it is very significant, e.g. 10 °/h ~ 100 °/h or even higher.

The scale factors of the gyro and accelerometer cause sensor errors from the true value. Usually the scale factors for gyro and accelerometer are represented by matrices in Eq. (2.12) and (2.13), respectively, and they are quantified in the unit of parts per million (ppm). Normally the scale factor for MEMS IMU varies as a function of temperature (Guo and Zhong 2013; Niu et al., 2013).

$$S_g = \begin{bmatrix} K_{gx} & 0 & 0 \\ 0 & K_{gy} & 0 \\ 0 & 0 & K_{gz} \end{bmatrix} \tag{2.12}$$

$$S_a = \begin{bmatrix} K_{ax} & 0 & 0 \\ 0 & K_{ay} & 0 \\ 0 & 0 & K_{az} \end{bmatrix} \tag{2.13}$$

where K_{gx}, K_{gy}, K_{gz} represent the scale factors for gyros along X, Y and Z axes, respectively, K_{ax}, K_{ay}, K_{az} represent the scale factors for accelerometers along X, Y and Z axes, respectively.

Due to the imperfection of inertial sensor assembling and installation, the 3 sensitive axes of the sensor triad are not perfectly orthogonal with each other, which causes the sensed inertial value of one axis to project into the other two axes. The installation error for gyros and accelerometers can be described by Eq. (2.14) and (2.15), respectively, and they are quantified using the unit of angle or PPM. Similarly, the installation errors are also temperature-dependent (Niu et al. 2013).

$$N_g = \begin{bmatrix} 0 & K_{gxy} & K_{gxz} \\ K_{gyx} & 0 & K_{gyz} \\ K_{gzx} & K_{gzy} & 0 \end{bmatrix} \tag{2.14}$$

$$N_a = \begin{bmatrix} 0 & K_{axy} & K_{axz} \\ K_{ayx} & 0 & K_{ayz} \\ K_{azx} & K_{azy} & 0 \end{bmatrix} \tag{2.15}$$

where K_{gij} represents the installation error parameter between i axis and j axis (i, j = X, Y, Z), K_{aij} represents the installation error parameter between i axis and j axis (i, j = X, Y, Z).

2.5 Rotary INS Error Model

As IMU rotation does not introduce any linear movement, the error model for the conventional INS errors in the local level frame, which can be described by a series of differential equations, can be used to describe the position, velocity and attitude errors for a rotary INS in the same frame. The first time derivative of the position errors is related to the position errors and velocity errors, which can be described as Eq. (2.16) (Jekeli, 2001; Du, 2010).

$$\dot{\delta r}^n = F_{rr}\delta r^n + F_{rv}\delta v^n \tag{2.16}$$

where, $F_{rr} = \begin{bmatrix} 0 & 0 & -\frac{\dot{\varphi}}{M+h} \\ \dot{\lambda}\tan\varphi & 0 & -\frac{\dot{\lambda}}{N+h} \\ 0 & 0 & 0 \end{bmatrix}$ and $F_{rv} = \begin{bmatrix} 0 & \frac{1}{M+h} & 0 \\ \frac{1}{(N+h)\cos\varphi} & 0 & 0 \\ 0 & 0 & -1 \end{bmatrix}$, $\dot{\varphi}$ and $\dot{\lambda}$ represent the latitude and longitude rate, respectively.

The first time derivative of the velocity errors is related to the position errors, the velocity errors, and the attitude errors, as well as the accelerometer sensor errors, as shown Eq. (2.17) (Jekeli, 2001; Du, 2010).

$$\dot{\delta v}^n = F_{vr}\delta r^n + F_{vv}\delta v^n + F_{v\varepsilon}\varepsilon^n + \delta f^n \tag{2.17}$$

where $F_{vr} = \begin{bmatrix} 2\omega_e(V_U \sin\varphi + V_N \cos\varphi) + V_N \dot{\lambda}/\cos\varphi & 0 & 0 \\ -2\omega_{ie} V_E \cos\varphi - V_E \dot{\lambda}/\cos\varphi & 0 & 0 \\ -2\omega_{ie} V_E \sin\varphi & 0 & \frac{2\gamma}{R} \end{bmatrix}$,

$F_{vv} = \begin{bmatrix} \frac{-V_U + V_N \tan\varphi}{N+h} & (2\omega_{ie} + \dot{\lambda})\sin\varphi & -(2\omega_{ie} + \dot{\lambda})\cos\varphi \\ -(2\omega_{ie} + \dot{\lambda})\sin\varphi & \frac{-V_U}{M+h} & -\dot{\varphi} \\ (2\omega_{ie} + \dot{\lambda})\cos\varphi & 2\dot{\varphi} & 0 \end{bmatrix}$,

$F_{v\varepsilon} = \begin{bmatrix} 0 & f_U & -f_N \\ -f_U & 0 & f_E \\ f_N & -f_E & 0 \end{bmatrix}$, and f_E, f_N, f_U represent the specific force in the navigation frame, γ represents the normal gravity that varies with the altitude, δf^n represents the accelerometer sensor error in the navigation frame, and $R = \sqrt{MN}$.

The first derivative of the attitude errors is related to the position errors, the velocity errors, and the attitude errors, as well as the gyro sensor errors, as shown in Eq. (2.18) (Jekeli, 2001; Du, 2010).

$$\dot{\varepsilon}^n = F_{\varepsilon r}\delta r^n + F_{\varepsilon v}\delta v^n + F_{\varepsilon\varepsilon}\varepsilon^n + \delta\omega^n \tag{2.18}$$

where $F_{\varepsilon r} = \begin{bmatrix} 0 & 0 & \frac{\dot{\varphi}}{M+h} \\ -\omega_{ie}\sin\varphi & 0 & -\frac{\dot{\lambda}\cos\varphi}{N+h} \\ \omega_{ie}\cos\varphi + \dot{\lambda}/\cos\varphi & 0 & -\frac{\dot{\lambda}\sin\varphi}{N+h} \end{bmatrix}$,

$$F_{\varepsilon v} = \begin{bmatrix} 0 & -\frac{1}{M+h} & 0 \\ \frac{1}{N+h} & 0 & 0 \\ \frac{\tan\varphi}{N+h} & 0 & 0 \end{bmatrix}, \text{ and } F_{\varepsilon\varepsilon} = \begin{bmatrix} 0 & (\omega_{ie}+\dot{\lambda})\sin\varphi & -(\omega_{ie}+\dot{\lambda})\cos\varphi \\ -(\omega_{ie}+\dot{\lambda})\sin\varphi & 0 & -\dot{\varphi} \\ (\omega_{ie}+\dot{\lambda})\cos\varphi & \dot{\varphi} & 0 \end{bmatrix},$$

ω_{ie} represents the earth rotation rate and $\delta\omega^n$ represents the gyro sensor error in navigation frame.

According to Eq. (2.4), the transformation process of inertial data from the b-frame to the s-frame requires the IMU rotation rate and the rotation angle measurement, which usually contain errors associated with the rotation platform. The effects of these errors on navigation errors are analyzed as follows. By considering the rotation angle error, the transformation matrix from the s-frame to the b-frame can be described by Eq. (2.19).

$$\tilde{C}_s^b = \begin{bmatrix} \cos(\beta+\delta\theta) & -\sin(\beta+\delta\theta) & 0 \\ \sin(\beta+\delta\theta) & \cos(\beta+\delta\theta) & 0 \\ 0 & 0 & 1 \end{bmatrix} = (I-\phi^{\times})C_s^b \tag{2.19}$$

where $\tilde{C}_s^b$ represents the calculated transformation matrix from the s-frame to the b-frame, $\delta\theta$ represents the measured rotation angle error, and $\phi^{\times} = \begin{bmatrix} 0 & \delta\theta & 0 \\ -\delta\theta & 0 & 0 \\ 0 & 0 & 0 \end{bmatrix}$ is the matrix representing the rotation angle error of the rotation platform.

Based on the calculated transformed specific force and angular rate in the b-frame described by Eq. (2.20) and (2.21), respectively, the velocity errors in the n-frame caused by the rotation angle

error can be described by the term, $C_b^n \phi^{\times} C_s^b f_{is}^s$, while the attitude errors in the n-frame can be described by the term, $C_b^n \phi^{\times} C_s^b \omega_{is}^s$. Obviously, the effects of the rotation angle error on the velocity and attitude errors are associated with the vehicle dynamics. Although the IMU rotation rate error does not affect the velocity errors, the resulted attitude errors in the n-frame can be described by the term, $C_b^n \delta\omega_{sb}^b$.

$$\tilde{f}_{ib}^b = \tilde{C}_s^b \tilde{f}_{is}^s = (I - \phi^{\times}) C_s^b (f_{is}^s + \delta f_{is}^s) \approx C_s^b f_{is}^s + C_s^b \delta f_{is}^s - \phi^{\times} C_s^b f_{is}^s \tag{2.20}$$

$$\tilde{\omega}_{ib}^b = \tilde{C}_s^b \tilde{\omega}_{is}^s + \tilde{\omega}_{sb}^b \approx C_s^b \omega_{is}^s + C_s^b \delta\omega_{is}^s + \omega_{sb}^b + \delta\omega_{sb}^b - \phi^{\times} C_s^b \omega_{is}^s \tag{2.21}$$

where $\tilde{f}_{ib}^b$ and $\tilde{\omega}_{ib}^b$ represent the calculated specific force and angular rate in the b-frame, respectively, δf_{is}^s and $\delta\omega_{is}^s$ represent the errors in specific force and angular rate, respectively, and $\delta\omega_{sb}^b$ represents the IMU rotation rate error.

Chapter Three: Rotary INS Error Mitigation, Calibration and Analysis

A rotary INS relies on proper IMU rotations to modulate the inertial sensor errors, mitigate the navigation error accumulation, and eventually improve the system autonomous navigation performance. But IMU rotations may also induce certain additional sensor errors, which have to be calibrated (Sun et al., 2009; Du et al., 2014). This chapter first analyzes the error mitigation for the rotary INS with three IMU rotation schemes, each rotating about the X, Y and Z axes, respectively, in comparison to the conventional INS. Constant biases, scale factors and installation errors for both gyros and accelerometers are considered for the error mitigation analysis. Simulations are given to verify the effectiveness of a rotary INS for navigation error mitigation and to identify the IMU rotation induced sensor errors. All analyses are conducted in a static mode, with the body frame assumed to be aligned with the local level frame to simplify the analysis. A calibration process has been proposed to estimate the gyro scale factor and installation errors, and to eliminate their effect on the error mitigation performance of a rotary INS.

3.1 Error Accumulation for Conventional INS

Although the sensor biases, scale factors and installation errors vary in nature (Guo and Zhong 2013; Niu et al., 2013), they are considered to be constants in a short time period (e.g. during a complete rotation cycle) under stable temperature conditions, in order to simplify the analysis. For the conventional INS, the accumulated velocity and attitude errors caused by the constant accelerometer and gyro biases during the time period T can be obtained using Eq. (3.1) and (3.2), respectively.

$$\int_0^T d^n dt = \begin{bmatrix} Td_x^s \\ Td_y^s \\ Td_z^s \end{bmatrix} \tag{3.1}$$

$$\int_0^T b^n dt = \begin{bmatrix} Tb_x^s \\ Tb_y^s \\ Tb_z^s \end{bmatrix} \tag{3.2}$$

Given the fact that the inertial sensors only sense the earth rotation rate and the local gravity when IMU remains static, the gyro and accelerometer errors caused by their scale factors can be described by Eq. (3.3) and (3.4), respectively.

$$\delta\omega_{SF}^n = S_g \omega_{is}^n = \begin{bmatrix} K_{gx} & 0 & 0 \\ 0 & K_{gy} & 0 \\ 0 & 0 & K_{gz} \end{bmatrix} \begin{bmatrix} 0 \\ \omega_{ie}\cos\varphi \\ \omega_{ie}\sin\varphi \end{bmatrix} = \begin{bmatrix} 0 \\ K_{gy}\omega_{ie}\cos\varphi \\ K_{gz}\omega_{ie}\sin\varphi \end{bmatrix} \tag{3.3}$$

$$\delta f_{SF}^n = S_a f^n = \begin{bmatrix} K_{ax} & 0 & 0 \\ 0 & K_{ay} & 0 \\ 0 & 0 & K_{az} \end{bmatrix} \begin{bmatrix} 0 \\ 0 \\ g \end{bmatrix} = \begin{bmatrix} 0 \\ 0 \\ K_{az}g \end{bmatrix} \tag{3.4}$$

where $\delta\omega_{SF}^n$ and δf_{SF}^n are gyro and accelerometer errors caused by their scale factor in the local level frame, respectively. The accumulated attitude and velocity errors during the time period T then can be described by Eq. (3.5) and (3.6), respectively.

$$\int_0^T \delta\omega_{SF}^n dt == \begin{bmatrix} 0 \\ TK_{gy}\omega_{ie}\cos\varphi \\ TK_{gz}\omega_{ie}\sin\varphi \end{bmatrix} \tag{3.5}$$

$$\int_0^T \delta f_{SF}^n dt = \begin{bmatrix} 0 \\ 0 \\ TK_{az}g \end{bmatrix} \tag{3.6}$$

With the assumption that the body frame is aligned to the local level frame, the accumulated attitude errors are only observed in the north and vertical directions whereas the velocity errors are only observable in the vertical direction.

The gyro and accelerometer errors caused by installation errors can be described by Eq. (3.7) and (3.8), respectively.

$$\delta\omega_N^n = N_g \omega_{is}^n = \begin{bmatrix} 0 & K_{gxy} & K_{gxz} \\ K_{gyx} & 0 & K_{gyz} \\ K_{gzx} & K_{gzy} & 0 \end{bmatrix} \begin{bmatrix} 0 \\ \omega_{ie}\cos\varphi \\ \omega_{ie}\sin\varphi \end{bmatrix} = \begin{bmatrix} K_{gxy}\omega_{ie}\cos\varphi + K_{gxz}\omega_{ie}\sin\varphi \\ K_{gyz}\omega_{ie}\sin\varphi \\ K_{gzy}\omega_{ie}\cos\varphi \end{bmatrix} \tag{3.7}$$

$$\delta f_N^n = N_a \delta f_N^n = \begin{bmatrix} 0 & K_{axy} & K_{axz} \\ K_{ayx} & 0 & K_{ayz} \\ K_{azx} & K_{azy} & 0 \end{bmatrix} \begin{bmatrix} 0 \\ 0 \\ g \end{bmatrix} = \begin{bmatrix} K_{axz}g \\ K_{ayz}g \\ 0 \end{bmatrix} \tag{3.8}$$

where $\delta\omega_N^n$ and δf_N^n are the gyro and accelerometer errors caused by their installation errors in the local level frame, respectively. The sensed earth rotation rate and local gravity are projected to the other two axes, and the resulted attitude and velocity errors over T can be described by Eq. (3.9) and (3.10), respectively.

$$\int_0^T \delta\omega_N^n dt == \begin{bmatrix} T(K_{gxy}\omega_{ie}\cos\varphi + K_{gxz}\omega_{ie}\sin\varphi) \\ TK_{gyz}\omega_{ie}\sin\varphi \\ TK_{gzy}\omega_{ie}\cos\varphi \end{bmatrix} \tag{3.9}$$

$$\int_0^T \delta f_N^n dt = \begin{bmatrix} TK_{axz}g \\ TK_{ayz}g \\ 0 \end{bmatrix} \tag{3.10}$$

3.2 Rotary INS Error Mitigation

The sensor biases, scale factors and installation errors are still assumed to be constants in a short time period (e.g. a complete rotation cycle) under stable temperature. The error mitigation for IMU rotation about the X axis is first analyzed, and then followed with the analysis of error mitigation for IMU rotation about the Y and Z axes, respectively.

3.2.1 Error Mitigation by Rotating IMU about X Axis

With the IMU rotation about the X axis at the rate of ω, the transformation matrix between the body frame and the sensor frame can be described by Eq. (3.11).

$$C_b^s = \begin{bmatrix} 1 & 0 & 0 \\ 0 & \cos\omega t & \sin\omega t \\ 0 & -\sin\omega t & \cos\omega t \end{bmatrix} = (C_s^b)^T \tag{3.11}$$

By applying the above transformation matrix, the gyro and accelerometer biases in the local level frame can be described by Eq. (3.12) and (3.13), respectively. These errors are modulated into periodic signals in the north and vertical directions, and the attitude and velocity errors caused by such errors are self-eliminated after a complete rotation cycle, as shown in Eq. (3.14) and (3.15). As the sensor biases in the rotation axis cannot be modulated, the attitude and velocity error in the east direction propagates in the same way as in the conventional INS.

$$d^n = C_b^n C_s^b d^s = \begin{bmatrix} d_x^s \\ d_y^s \cos\omega t + d_z^s \sin\omega t \\ -d_y^s \sin\omega t + d_z^s \cos\omega t \end{bmatrix} \tag{3.12}$$

$$b^n = C_b^n C_s^b b^s = \begin{bmatrix} b_x^s \\ b_y^s \cos\omega t + b_z^s \sin\omega t \\ -b_y^s \sin\omega t + b_z^s \cos\omega t \end{bmatrix} \tag{3.13}$$

$$\int_0^T d^n dt = \begin{bmatrix} Td_x^s \\ 0 \\ 0 \end{bmatrix} \tag{3.14}$$

$$\int_0^T b^n dt = \begin{bmatrix} Tb_x^s \\ 0 \\ 0 \end{bmatrix} \tag{3.15}$$

Due to the IMU rotation about the X axis, the gyro triad senses both the earth rotation rate and the IMU rotation rate, as shown in Eq. (3.16). Subsequently, the gyro errors caused by the scale factors in the local level frame can be obtained by Eq. (3.17), and the resulting attitude errors after a complete rotation cycle can be described by Eq. (3.18).

$$\omega_{is}^s = C_b^s \omega_{ib}^b + \omega_{bs}^s = \begin{bmatrix} \omega \\ \omega_{ie}\cos\varphi\cos\omega t + \omega_{ie}\sin\varphi\sin\omega t \\ -\omega_{ie}\cos\varphi\sin\omega t + \omega_{ie}\sin\varphi\cos\omega t \end{bmatrix} \tag{3.16}$$

$$\delta\omega_{SF}^{n} = C_s^n S_g \omega_{is}^s = \begin{bmatrix} K_{gx}\omega \\ K_{gy}(\omega_{ie}\cos\varphi\frac{1+\cos 2\omega t}{2} + \omega_{ie}\sin\varphi\frac{\sin 2\omega t}{2}) \\ -K_{gz}(-\omega_{ie}\cos\varphi\frac{1-\cos 2\omega t}{2} + \omega_{ie}\sin\varphi\frac{\sin 2\omega t}{2}) \\ K_{gy}(\omega_{ie}\cos\varphi\frac{\sin 2\omega t}{2} + \omega_{ie}\sin\varphi\frac{1-\cos 2\omega t}{2}) \\ +K_{gz}(-\omega_{ie}\cos\varphi\frac{\sin 2\omega t}{2} + \omega_{ie}\sin\varphi\frac{1+\cos 2\omega t}{2}) \end{bmatrix} \tag{3.17}$$

$$\int_0^T \delta\omega_{SF}^{n} dt = \begin{bmatrix} TK_{gx}\omega \\ \frac{1}{2}T(K_{gy}+K_{gz})\omega_{ie}\cos\varphi \\ \frac{1}{2}T(K_{gy}+K_{gz})\omega_{ie}\sin\varphi \end{bmatrix} \tag{3.18}$$

Although the resulting attitude errors in the north and vertical directions are similar to those in the conventional INS, the IMU rotation induces an attitude error in the east direction (pitch) because of the gyro scale factor in the X axis. As the rotation rate is usually much more significant than the earth rotation rate, the induced attitude error will severely degrade the navigation performance of the inertial system.

As the local gravity is projected into the north direction with the IMU rotation about the X axis, the accelerometer errors in the local level frame caused by the scale factor can be described by Eq. (3.19).

$$\delta f_{SF}^{n} = C_s^n S_a C_b^s f^b = \begin{bmatrix} 0 \\ K_{ay} g \dfrac{\sin 2\omega t}{2} - K_{az} g \dfrac{\sin 2\omega t}{2} \\ K_{ay} g \dfrac{1-\cos 2\omega t}{2} + K_{az} g \dfrac{1+\cos 2\omega t}{2} \end{bmatrix} \tag{3.19}$$

Similar to the conventional INS, the velocity errors caused by the scale factor after a complete rotation cycle are only observed in the vertical direction, as shown in Eq. (3.20).

$$\int_0^T \delta f_{SF}^{n} dt = \begin{bmatrix} 0 \\ 0 \\ \dfrac{1}{2} T (K_{ay} + K_{az}) g \end{bmatrix} \tag{3.20}$$

It is clear that the IMU rotation rate is projected to the Y and Z axes due to the installation errors when the IMU rotates about the X axis, resulting in gyro errors in the Y and Z axes, as shown in Eq. (3.21).

$$\delta\omega_N^s = N_g \omega_{is}^s = \begin{bmatrix} K_{gxy}(\omega_{ie}\cos\varphi\cos\omega t + \omega_{ie}\sin\varphi\sin\omega t) \\ \quad + K_{gxz}(-\omega_{ie}\cos\varphi\sin\omega t + \omega_{ie}\sin\varphi\cos\omega t) \\ K_{gyx}\omega + K_{gyz}(-\omega_{ie}\cos\varphi\sin\omega t + \omega_{ie}\sin\varphi\cos\omega t) \\ K_{gzx}\omega + K_{gzy}(\omega_{ie}\cos\varphi\cos\omega t + \omega_{ie}\sin\varphi\sin\omega t) \end{bmatrix} \tag{3.21}$$

Thus, the rotation induced gyro errors by installation errors in the local level frame can be described by Eq. (3.22), while the resulting attitude errors after a complete cycle are given in Eq. (3.23).

$$\delta\omega_N^n = C_s^n \delta\omega_N^s = \begin{bmatrix} K_{gxy}(\omega_{ie}\cos\varphi\cos\omega t + \omega_{ie}\sin\varphi\sin\omega t) + K_{gxz}(-\omega_{ie}\cos\varphi\sin\omega t \\ + \omega_{ie}\sin\varphi\cos\omega t) \\ K_{gyx}\omega\cos\omega t - K_{gzx}\omega\sin\omega t + K_{gyz}\omega_{ie}(\sin\varphi\dfrac{1+\cos 2\omega t}{2} - \cos\varphi\dfrac{\sin 2\omega t}{2}) \\ - K_{gzy}\omega_{ie}(\cos\varphi\dfrac{\sin 2\omega t}{2} + \sin\varphi\dfrac{1-\cos 2\omega t}{2}) \\ K_{gyx}\omega\sin\omega t + K_{gzx}\omega\cos\omega t + K_{gyz}\omega_{ie}(\sin\varphi\dfrac{\sin 2\omega t}{2} - \cos\varphi\dfrac{1-\cos 2\omega t}{2}) \\ + K_{gzy}\omega_{ie}(\cos\varphi\dfrac{1+\cos 2\omega t}{2} + \sin\varphi\dfrac{\sin 2\omega t}{2}) \end{bmatrix} \quad (3.22)$$

$$\int_0^T \delta\omega_N^n = \begin{bmatrix} 0 \\ \dfrac{1}{2}(K_{gyz} - K_{gzy})\omega_{ie}\sin\varphi \\ \dfrac{1}{2}(-K_{gyz} + K_{gzy})\omega_{ie}\cos\varphi \end{bmatrix} \quad (3.23)$$

Apparently, the rotation induced gyro biases are modulated by IMU rotation, and the resulting attitude errors are only observed in the north and vertical directions with similar magnitude to those present in the conventional INS. The rotation induced gyro errors, however, will lead to velocity and position errors due to significant IMU rotation rate.

The accelerometer errors caused by the installation errors in the local level frame are given in Eq. (3.24).

$$\delta f_N^n = C_s^n N_a C_b^s f^b = \begin{bmatrix} K_{axy} g\sin\omega t + K_{axz} g\cos\omega t \\ K_{ayz} g\dfrac{1+\cos 2\omega t}{2} - K_{azy} g\dfrac{1-\cos 2\omega t}{2} \\ K_{ayz} g\dfrac{\sin 2\omega t}{2} + K_{azy} g\dfrac{\sin 2\omega t}{2} \end{bmatrix} \quad (3.24)$$

After a complete rotation cycle, the resulting velocity errors have a similar magnitude, as in the conventional INS, which are observable only in the north direction, as shown in Eq. (3.25).

$$\int_0^T \delta f_N^n dt = \begin{bmatrix} 0 \\ \frac{T}{2}(K_{ayz} - K_{azy})g \\ 0 \end{bmatrix} \tag{3.25}$$

3.2.2 Error Mitigation by Rotating IMU about Y Axis

When IMU rotates about the Y axis, both gyro and accelerometer biases in the X and Z axes are modulated, so the attitude and velocity errors in the east and vertical directions caused by those errors are automatically removed after a complete rotation cycle. However, the attitude and velocity errors in the north direction are not removed, which propagate in the same way as in the conventional INS (Du et al., 2014).

The rotation induced gyro errors by the scale factor in the local level frame can be described by Eq. (3.26), and the resulting attitude errors after a complete rotation cycle can be obtained by Eq. (3.27). Obviously, IMU rotation induces a significant attitude error in the north direction.

$$\delta\omega_{SF}^n = C_s^n S_g \omega_{is}^s = \begin{bmatrix} -K_{gx}\omega_{ie}\sin\varphi\frac{\sin 2\omega t}{2} + K_{gz}\omega_{ie}\sin\varphi\frac{\sin 2\omega t}{2} \\ K_{gy}(\omega_{ie}\cos\varphi + \omega) \\ K_{gx}\omega_{ie}\sin\varphi\frac{1-\cos 2\omega t}{2} + K_{gz}\omega_{ie}\sin\varphi\frac{1+\cos 2\omega t}{2} \end{bmatrix} \tag{3.26}$$

$$\int_0^T \delta\omega_{SF}^n dt = \begin{bmatrix} 0 \\ TK_{gy}(\omega_{ie}\cos\varphi + \omega) \\ \frac{T}{2}(K_{gx} + K_{gz})\omega_{ie}\sin\varphi \end{bmatrix} \tag{3.27}$$

The IMU rotation induced accelerometer errors by scale factor and the resulting velocity errors can be described by Eq. (3.28) and (3.29), respectively.

$$\delta f_{SF}^{\ n} = C_s^n S_a C_b^s f^b = \begin{bmatrix} -K_{ax} g \frac{\sin 2\omega t}{2} + K_{az} g \frac{\sin 2\omega t}{2} \\ 0 \\ K_{ax} g \frac{1-\cos 2\omega t}{2} + K_{az} g \frac{1+\cos 2\omega t}{2} \end{bmatrix} \tag{3.28}$$

$$\int_0^T \delta f_{SF}^{\ n} dt = \begin{bmatrix} 0 \\ 0 \\ \frac{1}{2}T(K_{ax} + K_{az})g \end{bmatrix} \tag{3.29}$$

Gyro installation errors project the IMU rotation rate into the X and Z axis, resulting in gyro errors as shown in Eq. (3.30).

$$\delta\omega_N^s = N_g \omega_{is}^s = \begin{bmatrix} K_{gxy}(\omega_{ie}\cos\varphi + \omega) + K_{gxz}\omega_{ie}\sin\varphi\cos\omega t \\ -K_{gyx}\omega_{ie}\sin\varphi\sin\omega t + K_{gyz}\omega_{ie}\sin\varphi\cos\omega t \\ -K_{gzx}\omega_{ie}\sin\varphi\sin\omega t + K_{gzy}(\omega_{ie}\cos\varphi + \omega) \end{bmatrix} \tag{3.30}$$

Although the resulting attitude errors after a complete rotation cycle are similar to those in the conventional INS, as shown in Eq. (3.31), the rotation induced gyro errors lead to velocity and position errors due to the significant rotation rate.

$$\int_0^T \delta\omega_N^n = \int_0^T C_s^n \delta\omega_N^s = \begin{bmatrix} \frac{T}{2}(K_{gxz} - K_{gzx})\omega_{ie}\sin\varphi \\ 0 \\ 0 \end{bmatrix} \tag{3.31}$$

Different from the rotation induced velocity errors caused by the installation errors, which are observable in the north direction when IMU rotates about the X axis, the velocity errors are observable in the east direction for the IMU rotating about the Y axis as shown in Eq. (3.32).

$$\int_0^T \delta f_N^n dt = \int_0^T C_s^n \delta f_N^s dt = \begin{bmatrix} \frac{T}{2}(K_{axz} - K_{azx})g \\ 0 \\ 0 \end{bmatrix} \tag{3.32}$$

3.2.3 Error Mitigation by Rotating IMU about Z Axis

The gyro and accelerometer biases in the X and Y axes are modulated when the IMU rotates about the Z axis. The attitude and velocity errors caused by such biases are therefore self-eliminated in the east-north plane after a complete rotation cycle; though the errors in the vertical direction still propagate in the same way as in the conventional INS. Because of the scale factor in the Z axis, the IMU rotation will induce a gyro error, which leads to an accumulated azimuth error, as shown in Eq. (3.33) and (3.34).

$$\delta\omega_{SF}^n = C_b^n C_s^b \delta\omega_{SF}^s = \begin{bmatrix} (K_{gx} - K_{gy})\omega_{ie}\cos\varphi\sin\omega t\cos\omega t \\ (K_{gx}\sin^2\omega t + K_{gy}\cos^2\omega t)\omega_{ie}\cos\varphi \\ K_{gz}(\omega_{ie}\sin\varphi + \omega) \end{bmatrix} \tag{3.33}$$

$$\int_0^T \delta\omega_{SF}^n dt = \begin{bmatrix} 0 \\ \dfrac{T\omega_{ie}\cos\varphi(K_{gx}+K_{gy})}{2} \\ K_{gz}(\omega_{ie}\sin\varphi+\omega)T \end{bmatrix} \tag{3.34}$$

As with the conventional INS, the accelerometer scale factor induces a velocity error in the vertical direction because of the local gravity, as shown in Eq. (3.35).

$$\int_0^T \delta f_{SF}^n dt = \int_0^T C_s^n \delta f_{SF}^s dt = \begin{bmatrix} 0 \\ 0 \\ TK_{az}g \end{bmatrix} \tag{3.35}$$

When the IMU rotates about the Z axis, the projection of the IMU rotation rate results in gyro errors in the X and Y axes, as shown in Eq. (3.36). Although the rotation induced errors are modulated and the resulted attitude errors are self-eliminated after a complete rotation cycle, as shown in Eq. (3.37), the induced gyro errors lead to velocity and position errors.

$$\delta\omega_N^s = N_g\omega_{is}^s = \begin{bmatrix} K_{gxy}\omega_{ie}\cos\varphi\cos\omega t + K_{gxz}(\omega_{ie}\sin\varphi+\omega) \\ K_{gyx}\omega_{ie}\cos\varphi\sin\omega t + K_{gyz}(\omega_{ie}\sin\varphi+\omega) \\ K_{gzx}\omega_{ie}\cos\varphi\sin\omega t + K_{gzy}\omega_{ie}\cos\varphi\cos\omega t \end{bmatrix} \tag{3.36}$$

$$\int_0^T \delta\omega_N^n dt = \begin{bmatrix} \dfrac{T\omega_{ie}\cos\varphi(K_{gxy}-K_{gyx})}{2} \\ 0 \\ 0 \end{bmatrix} \tag{3.37}$$

The local gravity is projected to the X and Y axes resulting accelerometer errors, which are modulated through IMU rotation. Consequently, resulting velocity errors are self-eliminated after a complete rotation cycle, as shown in Eq. (3.38).

$$\int_0^T \delta f_N^n dt = \begin{bmatrix} 0 \\ 0 \\ 0 \end{bmatrix} \tag{3.38}$$

3.3 Simulations and Analysis

Simulations of both the conventional and rotary INS in a static mode are conducted in the following paragraphs to verify the error mitigation analysis given in Section 3.1 and 3.2. For the rotary INS, the simulated inertial data includes the earth rotation rate, the IMU rotation rate and the local gravity sensed by the IMU; while for the conventional INS it includes only the earth rotation rate and the local gravity. As to the inertial sensor biases, scale factors and installation errors, they are simulated separately and added to the inertial data to study their respective contributions to the navigation errors. The IMU rotation rate is set as 10 °/s. To simplify the analysis, the body frame is assumed to be aligned with the local level frame.

3.3.1 Sensor Biases and Analysis

The inertial sensor biases are simulated as constants while white noises are added to both the conventional and rotary INS data, as shown in Table 3.1. The position, velocity and attitude (PVA) solutions are derived for the conventional and rotary INS using their own mechanization algorithm.

Table 3.1 Simulation of inertial sensor biases

	X axis	Y axis	Z axis
Gyro bias (°/h)	30	30	30
Gyro white noise (°/$\sqrt{h}$)	0.2	0.2	0.2
Accelerometer bias (m^2/s)	0.2	0.2	0.2
Accelerometer white noise (m/s/$\sqrt{h}$)	0.1	0.1	0.1

For IMU rotation about the X axis, the velocity and attitude errors for the conventional and rotary INS are given in Figures 3.1 and 3.2, respectively. The green color represents the errors in the rotary INS, while the blue color represents the errors in the conventional INS. The velocity and attitude errors in the conventional INS accumulate quickly over time due to the simulated inertial sensor biases, while the IMU rotation modulate the gyro biases in the Y and Z axes into periodic signals, which significantly reduces the roll and azimuth errors in the rotary INS. As the gyro bias in the X axis cannot be modulated, the pitch error remains almost the same as the conventional INS. The modulation of the accelerometer biases in the Y and Z axes also reduce the velocity errors, as shown in the Figure 3.1.

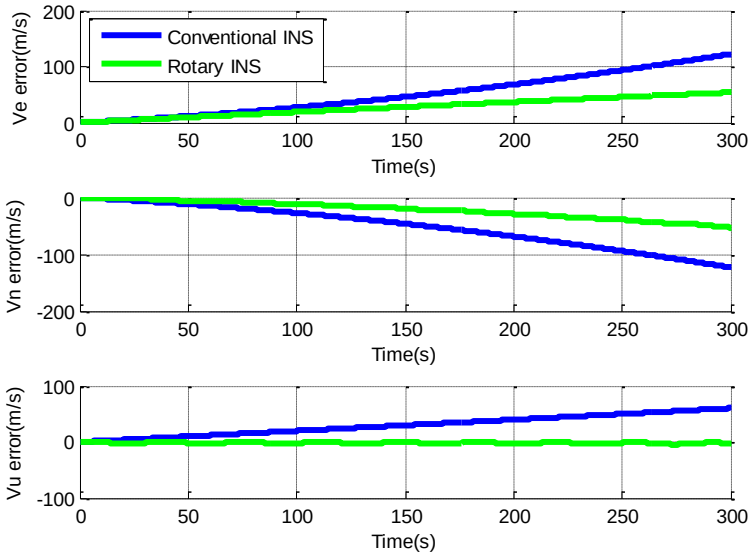

Figure 3.1 Velocity errors with rotation about X axis

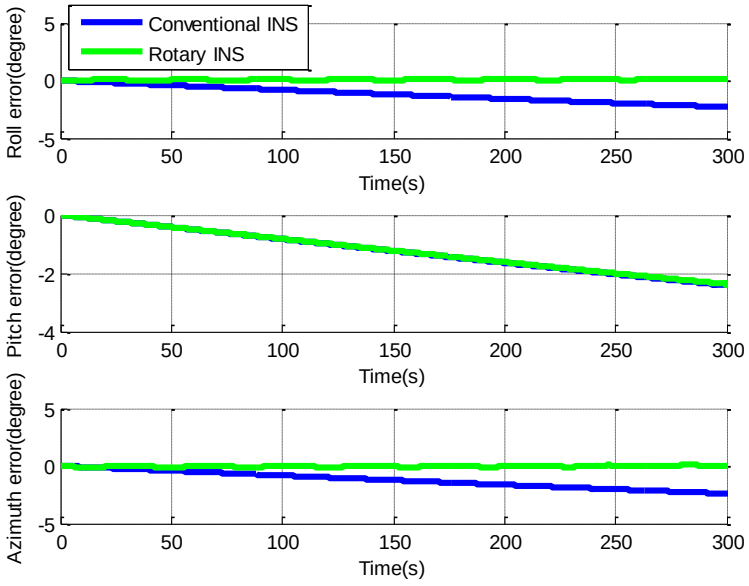

Figure 3.2 Attitude errors with rotation about X axis

With the IMU rotation about the Y axis, the pitch and azimuth errors are greatly reduced due to the modulation of the gyro biases in the X and Z axes, as shown in Figure 3.4, although the roll errors remain the same as the ones in the conventional INS. Similar velocity errors are obtained compared to the ones for IMU rotation about the X axis.

When the IMU rotates about the Z axis, the modulation of accelerometer and gyro biases in the horizontal axes (both X and Y axes) significantly reduce the velocity errors in the east-north plane as well as the roll and pitch errors, as shown in Figures 3.5 and 3.6. The vertical velocity error and the azimuth error, however, are almost the same as the ones in the conventional INS, as the sensor errors in rotation axis cannot be modulated.

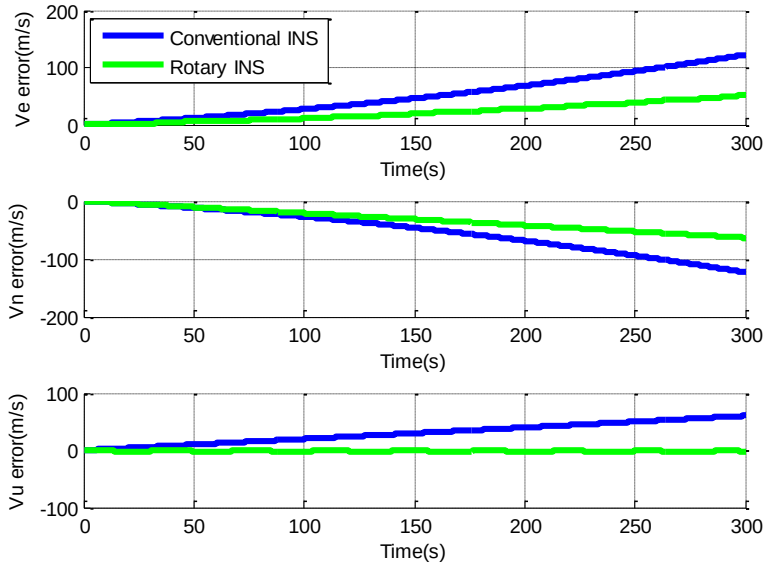

Figure 3.3 Velocity errors with rotation about Y axis

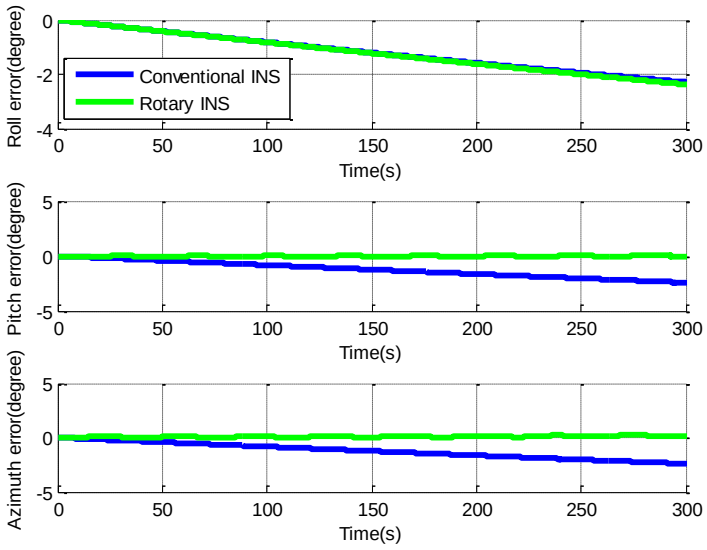

Figure 3.4 Attitude errors with rotation about Y axis

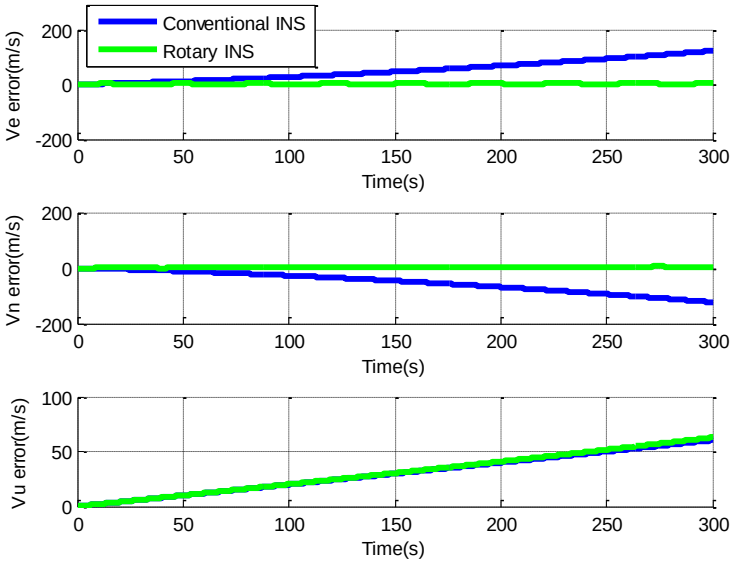

Figure 3.5 Velocity error with rotation about Z axis

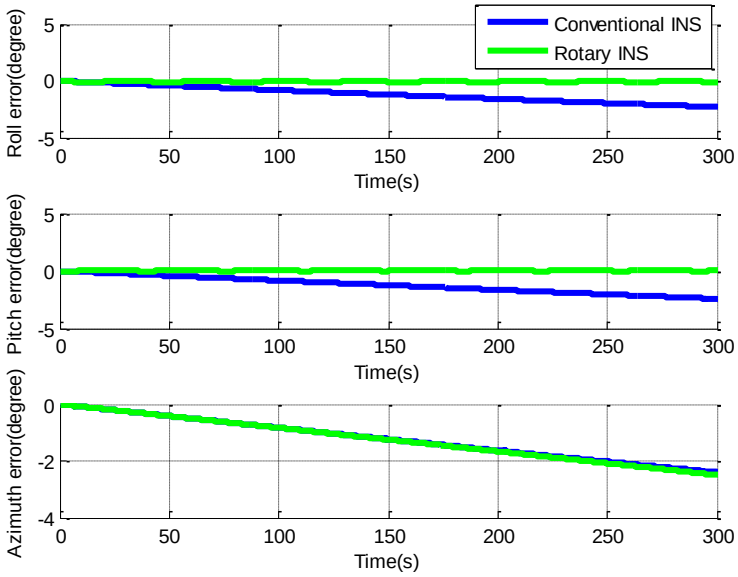

Figure 3.6 Attitude errors with rotation about Z axis

It has been demonstrated that the rotary INS can reduce the velocity and attitude errors using three different rotation schemes. For the IMU rotation about the X or Y axes, the velocity and attitude errors in the vertical direction can be significantly reduced, while the errors in the east-north plane can only be partially removed, as the sensor biases in the X or Y axes cannot be modulated. In contrast, the velocity and attitude errors can be more effectively mitigated in the horizontal plane when the IMU rotates about the Z axis; however, the errors in the vertical direction are almost identical to the ones in the conventional INS.

3.3.2 Sensor Scale Factors and Analysis

According to the analysis in Section 3.2, the accelerometer scale factors have limited effect on the navigation errors in a rotary INS. Therefore, only the gyro scale factors are simulated as

shown in Table 3.2, while the white noise is also added to both the conventional and rotary INS data.

Table 3.2 Simulation of gyro scale factors

	X axis	**Y axis**	**Z axis**
Gyro scale factor (PPM)	3000	3000	3000
Gyro white noise (°/$\sqrt{h}$)	0.2	0.2	0.2
Accelerometer white noise (m/s/$\sqrt{h}$)	0.1	0.1	0.1

Consistent with the previous analysis, the IMU rotation about the X or Y axes induces gyro errors due to the scale factors, which result in the accumulated pitch or roll error in the rotary INS, as shown in Figure 3.7 or 3.8, respectively. The blue and green lines represent the navigation errors of the conventional and rotary INS with only gyro scale factor, respectively, and the blue dash line represents the navigation errors of conventional INS, with simulated gyro and accelerometer biases given in Section 3.3.1. Significant velocity errors in the north or east direction are also motivated by the rotation induced gyro errors as shown in the figures.

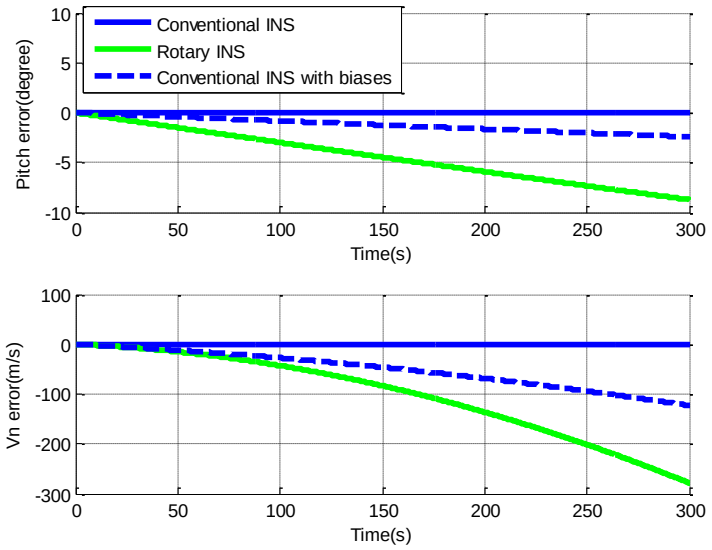

Figure 3.7 Pitch and velocity errors in north direction induced by gyro scale factors with rotation about X axis

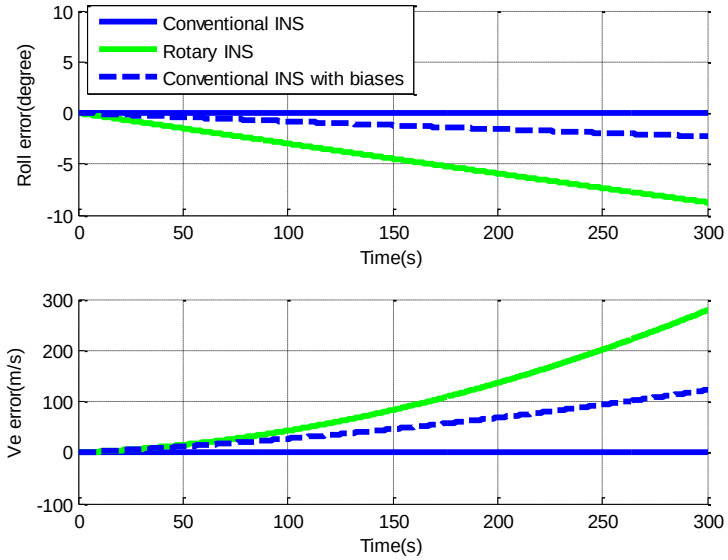

Figure 3.8 Roll and velocity errors in east direction induced by gyro scale factors with rotation about Y axis

When the IMU rotates about the Z axis, the induced gyro error in the Z axis results in an accumulated azimuth error, as shown in Figure 3.9. Although roll and pitch errors, as well as the velocity errors in the east-north plane, are eventually accumulated, their magnitudes are much smaller than the errors for the other two rotation schemes, as shown in Figure 3.9 and 3.10.

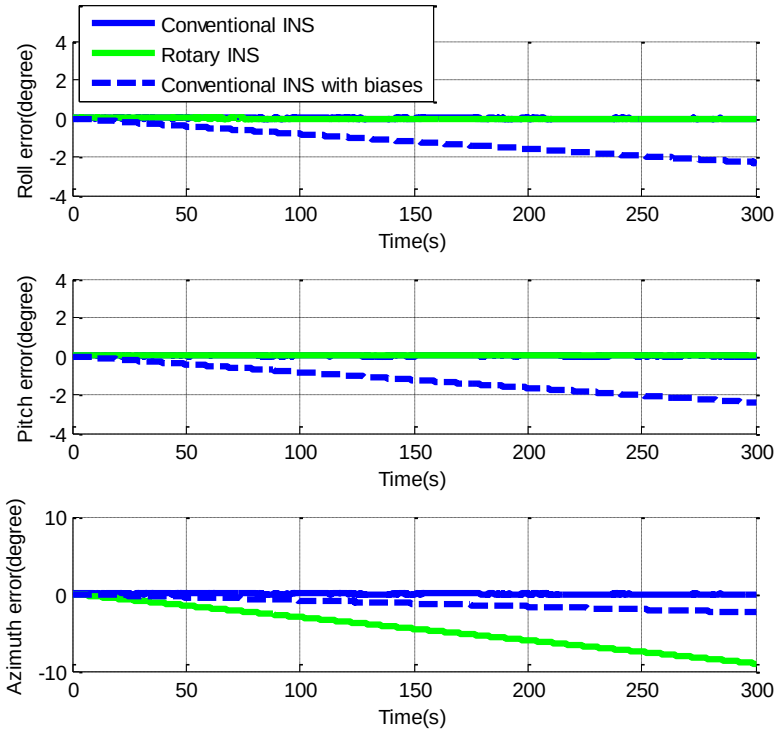

Figure 3.9 Attitude errors induced by gyro scale factors with rotation about Z axis

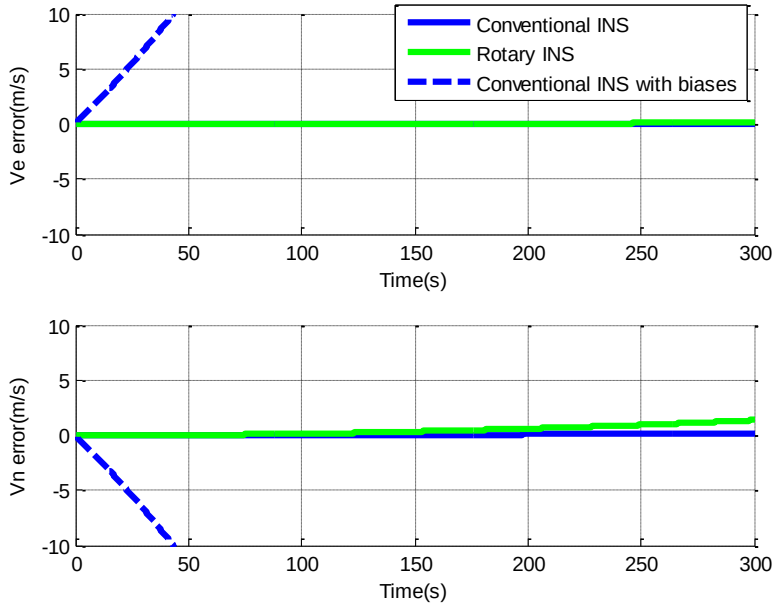

Figure 3.10 Velocity errors induced by gyro scale factors with rotation about Z axis

3.3.3 Sensor Installation Errors and Analysis

Only gyro installation errors are simulated, as shown in Table 3.3, as accelerometer installation errors have limited effect on navigation errors. The white noise is also added to both the conventional and rotary INS data.

Table 3.3 Simulation of gyro installation errors

	X axis	**Y axis**	**Z axis**
Gyro installation error (°)	0.1	0.1	0.1
Gyro white noise (°/$\sqrt{h}$)	0.2	0.2	0.2
Accelerometer white noise (m/s/$\sqrt{h}$)	0.1	0.1	0.1

When IMU rotates about the X axis, the gyro errors are induced by the installation errors, and their modulation leads to oscillating errors in roll and azimuth, as shown in Figure 3.11. Similarly, the IMU rotation about the Y axis induces gyro errors in the X and Z axes, resulting oscillated pitch and azimuth errors, as shown in Figure 3.12, while the rotation about the Z axis results oscillating roll and pitch errors as shown in Figure 3.13. The oscillating attitude errors lead to velocity and position errors.

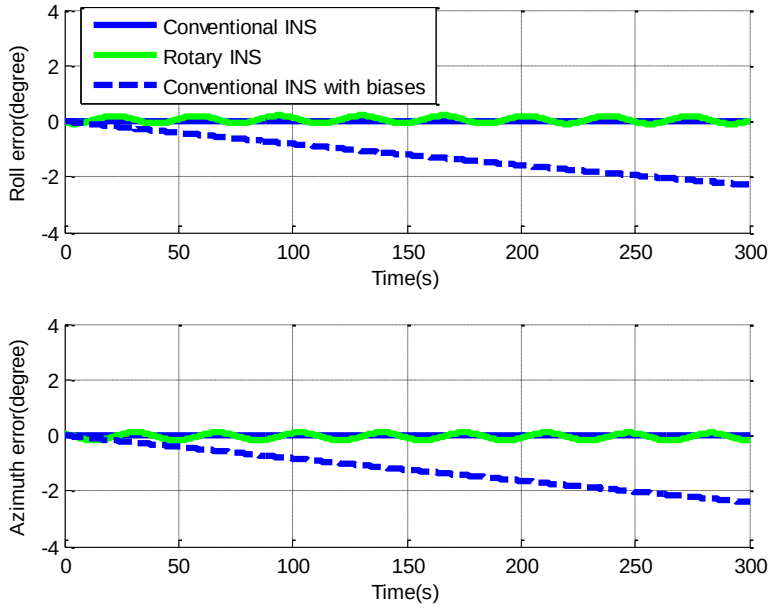

Figure 3.11 Attitude errors induced by gyro installation errors with rotation about X axis

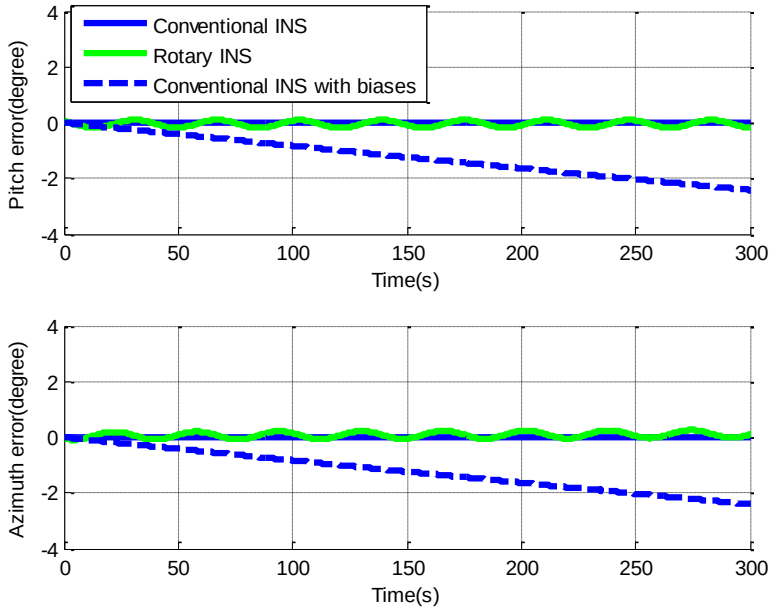

Figure 3.12 Attitude errors induced by gyro installation errors with rotation about Y Axis

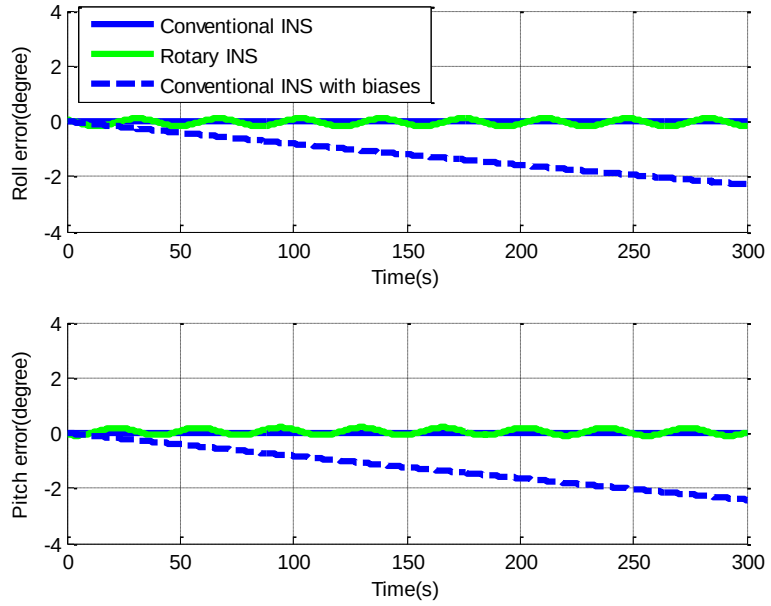

Figure 3.13 Attitude errors induced by gyro installation errors with rotation about Z axis

Based on the above error mitigation analysis and simulation results, we can conclude that:

- The IMU rotation modulates the constant biases of inertial sensors that are perpendicular to the rotation axis, and the attitude and velocity errors caused by such biases are self-mitigated after a complete rotation cycle.
- The constant biases of inertial sensors in the rotation axis cannot be modulated, and the attitude and velocity errors caused by such errors propagate in the same way as in the conventional INS.
- The accelerometer scale factors and installation errors have very limited effect on the error mitigation of a rotary INS.
- Gyro scale factor and installation errors play important roles in the rotary INS. The IMU rotation induces an extra error in the gyro of the rotation axis due to gyro scale factor, and this error results in accumulated attitude errors in the direction of the corresponding rotation axis. The IMU rotation also induces extra errors in the gyros that are perpendicular to the rotation axis due to gyro installation errors, resulting in oscillating attitude and velocity errors. Gyro scale factor and installation errors must be calibrated for a rotary INS to maintain its error mitigation performance.
- The IMU rotation about the Z axis can effectively mitigate the navigation errors in the horizontal plane, while the rotation about the X or Y axes can mainly reduce the navigation errors in the vertical direction; therefore, the IMU rotation about the Z axis is more suitable than the other two rotation schemes for the navigation applications.

3.4 IMU Rotation Induced Error Calibration

Since IMU rotation will induce additional gyro biases due to gyro scale factor and installation errors, a calibration process is proposed in the following paragraphs for a rotary INS with IMU rotation about the Z axis. Although the full gyro scale factor and installation errors are represented by 9 parameters, according to Eq. (2.12) and (2.14), the proposed method is only to calibrate the gyro scale factor of the Z axis, K_{gz}, and the installation errors, K_{gxz}, K_{gyz}, which will cause significant gyro errors when IMU rotates about the Z axis.

3.4.1 Gyro Error Model for Calibration

As the rotation does not introduce any linear motion of the IMU, the theoretical gyro outputs in the body frame can be described by Eq. (3.39), when the body frame is static relative to the local level frame.

$$\omega_{ib}^{b} = C_{n}^{b}\omega_{ib}^{n} = C_{n}^{b}\omega_{ie}^{n} = C_{n}^{b}\begin{bmatrix} 0 \\ \omega_{ie}\cos\varphi \\ \omega_{ie}\sin\varphi \end{bmatrix} = \begin{bmatrix} a\omega_{ie} \\ b\omega_{ie} \\ c\omega_{ie} \end{bmatrix} \tag{3.39}$$

where,

$$\begin{bmatrix} a \\ b \\ c \end{bmatrix} = \begin{bmatrix} (\cos A\sin r\sin p + \sin A\cos p)\cos\varphi + (-\cos A\sin r\cos p + \sin A\sin p)\sin\varphi \\ (-\sin A\sin r\sin p + \cos A\cos p)\cos\varphi + (\sin A\sin r\sin p + \cos A\sin p)\sin\varphi \\ -\cos r\sin p\cos\varphi + \cos r\cos p\sin\varphi \end{bmatrix}, \text{ and they}$$

satisfy the equality equation $a^2 + b^2 + c^2 = 1$.

The theoretical and actual gyro outputs in the sensor frame can be described by Eq. (3.40) and (3.41), respectively, then the gyro errors can be derived in Eq. (3.42).

$$\omega_{is}^{s} = C_{b}^{s}\omega_{ib}^{b} + \omega_{bs}^{s} = \begin{bmatrix} \omega_{ie}(a\cos\omega t + b\sin\omega t) \\ \omega_{ie}(-a\sin\omega t + b\cos\omega t) \\ c\omega_{ie} + \omega \end{bmatrix} \tag{3.40}$$

$$\tilde{\omega}_{is}^{s} = \omega_{is}^{s} + N\omega_{is}^{s} + d^{s} \tag{3.41}$$

$$\delta\omega_{is}^{s} = \begin{bmatrix} K_{gx}\omega_{ie}(a\cos\omega t + b\sin\omega t) + K_{gxy}\omega_{ie}(-a\sin\omega t + b\cos\omega t) + K_{gxz}(c\omega_{ie} + \omega) + d_{x}^{s} \\ K_{gyx}\omega_{ie}(a\cos\omega t + b\sin\omega t) + K_{gy}\omega_{ie}(-a\sin\omega t + b\cos\omega t) + K_{gyz}(c\omega_{ie} + \omega) + d_{y}^{s} \\ K_{gzx}\omega_{ie}(a\cos\omega t + b\sin\omega t) + K_{gzy}\omega_{ie}(-a\sin\omega t + b\cos\omega t) + K_{gz}(c\omega_{ie} + \omega) + d_{z}^{s} \end{bmatrix} \tag{3.42}$$

where, $N = \begin{bmatrix} K_{gx} & K_{gxy} & K_{gxz} \\ K_{gyx} & K_{gy} & K_{gyz} \\ K_{gzx} & K_{gzy} & K_{gz} \end{bmatrix}$, represents a 3×3 matrix representing the combination of gyro scale factors and installation errors and $d^{s} = \begin{bmatrix} d_{x}^{s} & d_{y}^{s} & d_{z}^{s} \end{bmatrix}^{T}$, represents the gyro biases in the sensor frame.

The Earth rotation rate can be ignored in the above error model because, 1) the Earth rotation rate cannot be sensed in most MEMS IMUs due to their significant gyro bias instability and noise, and 2) the IMU rotation rate is much more significant than the Earth rotation rate. Thus, the gyro error model can be simplified as shown in Eq. (3.45).

$$\delta\omega_{is}^{s} = \begin{bmatrix} K_{gxz}\omega + d_{x}^{s} \\ K_{gyz}\omega + d_{y}^{s} \\ K_{gz}\omega + d_{z}^{s} \end{bmatrix} \tag{3.45}$$

With different IMU rotation rates, the gyro scale factor, K_{gz}, the gyro installation errors, K_{gxz}, K_{gyz}, as well as the gyro biases, $\begin{bmatrix} d_x^s & d_y^s & d_z^s \end{bmatrix}^T$, can be solved based on the error model given in Eq. (3.45). The measurements are the gyro readings, which can be described by Eq. (3.46), and the measurement model for a single measurement is given by Eq. (3.47).

$$Z_j = \tilde{\omega}_{is}^s - \omega_{is}^s \approx \begin{bmatrix} \tilde{\omega}_{is,x}^s \\ \tilde{\omega}_{is,y}^s \\ \tilde{\omega}_{is,z}^s - \omega_j \end{bmatrix} \tag{3.46}$$

$$Z_j = H_j X = \begin{bmatrix} \omega_j & 0 & 0 & 1 & 0 & 0 \\ 0 & \omega_j & 0 & 0 & 1 & 0 \\ 0 & 0 & \omega_j & 0 & 0 & 1 \end{bmatrix} \begin{bmatrix} K_{gxz} \\ K_{gyz} \\ K_{gz} \\ d_x^s \\ d_y^s \\ d_z^s \end{bmatrix} \tag{3.47}$$

where Z_j represents the j^{th} measurement, and ω_j represents the IMU rotation rate with respect to the Z_j.

3.4.2 Calibration Implementation

The calibration process can be implemented in two steps: 1) the IMU remains still on the rotation platform for 60 seconds; and, 2) the IMU rotates along with the rotation platform at a designated rotation rate about the Z axis for 60 seconds. The total calibration time is 2 minutes. According to the error model in Eq. (3.45), the gyro biases can be estimated from the inertial data collected over the static period, while the gyro scale factor, K_{gz}, and the installation errors, K_{gxz}, K_{gyz}, can

be estimated from the collected data during the rotation period. It is worthwhile to mention that the MEMS IMU usually features significant non-linearity errors (Artese et al., 2008; He 2009), so the designated rotation rate for calibration process should be the same as the rotation rate employed by the rotation scheme. For example, for the MEMS-based rotary INS with IMU rotation about the Z axis at the rate of 10 °/s, the calibration process should employ the same rotation rate to estimate the gyro scale factor and installation errors.

The error sources for the calibration include the gyro sensor noise, the gyro bias instability (gyro biases are not constants, but time-correlated variables), and the ignored Earth rotation rate. The calibration errors of gyro biases caused by noise can be calculated using Eq. (3.48), while the calibration errors for scale factor and installation errors caused by noise are given by Eq. (3.49) (Niu et al. 2013).

$$\sigma_b = ARW / \sqrt{T_{static}} \tag{3.48}$$

$$\sigma_s = ARW \cdot \sqrt{T_{rotation}} / \alpha_{rotation} \tag{3.49}$$

where ARW represents the angle random walk of gyros, T_{static} represents the time period that the IMU remains still, $T_{rotation}$ represents the time period for IMU rotation, and $\alpha_{rotation}$ represents the rotated angle of the IMU. Apparently, the longer calibration time and higher IMU rotation rate can reduce the calibration errors caused by gyro noise; however, the longer time may also increase the effect of gyro bias instability on calibration results. The reason for choosing 60 seconds for the calibration time in each step will be provided in Chapter 4, along with the noise level and gyro bias instability of the tested MEMS IMU.

Chapter Four: Static and Kinematic Tests of MEMS-based Rotary INS

As the MEMS IMU usually features significant sensor errors, such as bias instability, scale factors and installation errors, tests with real data from the rotated MEMS IMU sensors should be conducted to investigate the navigation error mitigation performance. Based on a tri-axial rotation table, two MEMS IMUs, namely NAV440 and MTi-G, are tested in laboratory under static environments to verify the calibration process and analyze the error mitigation performance with different IMU rotation rates. The road kinematic field tests are also conducted with both IMUs based on a single-axis rotation table. A trajectory with different dynamic conditions is employed to study the error mitigation performance of a MEMS-based rotary system under kinematic conditions. Only the IMU rotation about the Z axis is considered in both static and kinematic tests, as it can effectively reduce the navigation errors in the east-north plane, compared to the other two rotation schemes.

4.1 Static Tests and Analysis

The rotation platform consists of a tri-axial rotation table and a console (computer), as shown in Figure 4.1. The tri-axial rotation table has three rotational frames, namely, the outer frame, middle frame and inner frame. The console controls the position and rotation of these frames.

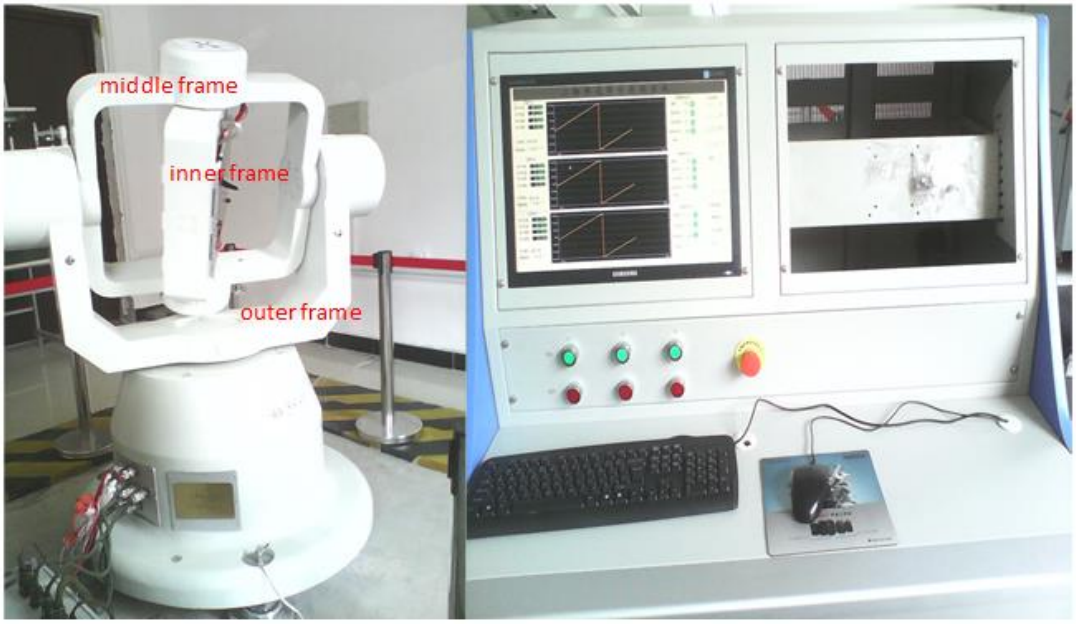

Figure 4.1 Tri-axial rotation platform

The MEMS IMUs are firmly installed on a piece of metal underneath the inner frame with screws, as shown in Figure 4.2. Different rotations, such as rotations about the X, Y and Z axes can be implemented by rotating the frames. For example, with the IMU axes defined as shown in Figure 4.3 (X axis pointing left, Z axis pointing up, and Y axis completing a right-hand system), rotation of the outer frame rotates the IMU about its Z axis, when both the middle and inner frames remain at the level position (or angle position of 0°). An initialization process, after which both the middle and inner frames are adjusted to the level position and the rotation axis of the inner frame points to the north direction, is required for the rotation table. Apparently, with the IMU installations shown in Figure 4.3, the IMU body frame is aligned to the local level frame after the initialization process.

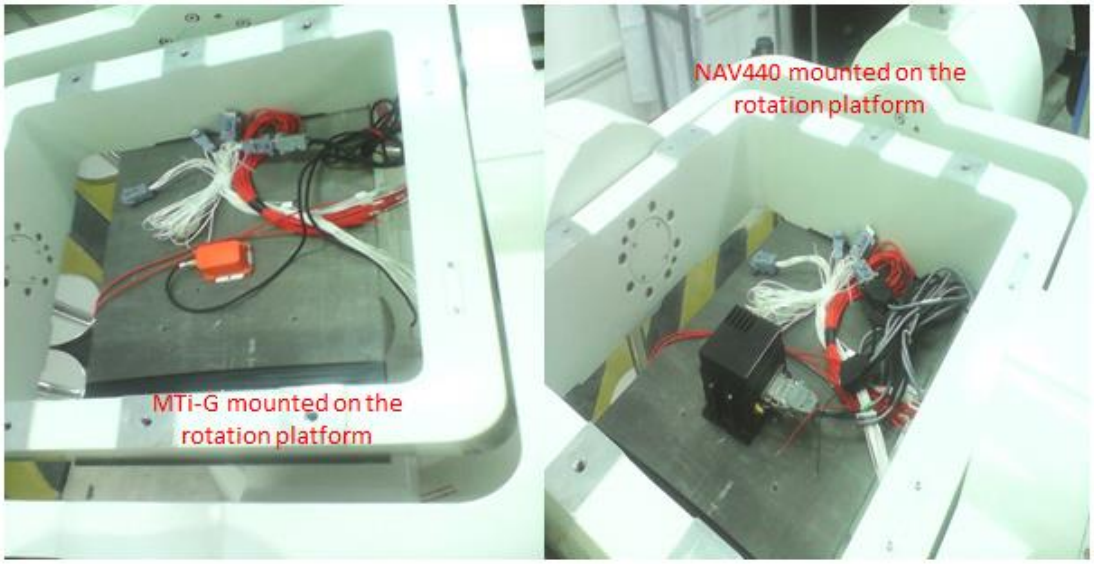

Figure 4.2 Installation of MEMS IMU on tri-axial rotation table

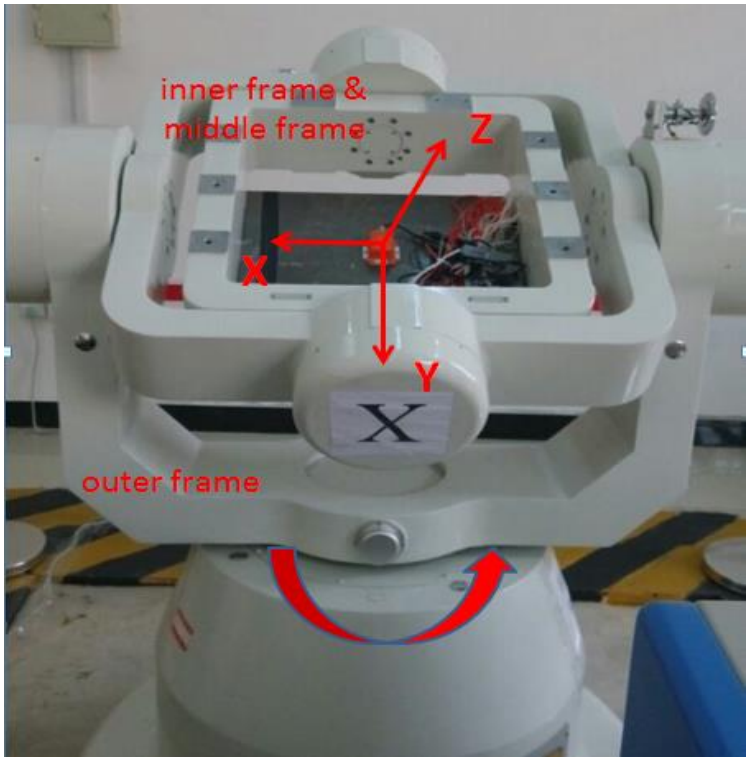

Figure 4.3 Rotation table set-up for IMU rotation about Z axis

Tables 4.1 and 4.2 present the technical parameters of the rotation platform and the characteristics of the tested MEMS IMUs, respectively. All of the data is provided by the manufacturers. Although the gyro white noise of NAV440 is not provided, the Allan variance method was conducted to obtain this value, which is about 0.4 °/$\sqrt{h}$ (Du and Gao, 2012a). With the superior rotation rate accuracy of the rotation table, the effect of the IMU rotation rate error on the attitude errors can be ignored for an inertial system based on a low-cost MEMS IMU.

Table 4.1 Technical parameters of tri-axial rotation platform

Position Accuracy (º)	**Rotation Rate Accuracy (º/s)**	**Maximum Rotation Rate (º/s)**
1e-5	1e-5	±100

Table 4.2 Characteristics of tested IMUs

Characteristics	**MTi-G**	**NAV440**
Range (°/s)	-300~300	-400~400
Gyro bias instability (°/h)	3600	20
Gyro white noise (°/$\sqrt{h}$)	3.0	-

The frame rotation angle data (the rotation angle between the body frame and the sensor frame) and the MEMS IMU data are recorded by the console, with the data rates of 50 Hz and 100 Hz,

respectively. The frame rotation angle is used to form the transformation matrix between the body frame and the sensor frame, which are required in the mechanization process.

Two types of tests are conducted in laboratory, being the conventional INS static tests and the rotary INS static tests. For the conventional INS test, the inertial data is collected with the MEMS IMU remaining still on the rotation table for 6 minutes. For the rotary tests, ten individual tests are conducted. In each individual test, the IMU rotates about the Z axis at a designated rate for 5 minutes, with a calibration process conducted at the onset. The designated rotation rates for the ten individual tests are 10 °/s, 20 °/s, 30 °/s, 40 °/s, 50 °/s, 60 °/s, 70 °/s, 80 °/s, 90 °/s and 100 °/s, respectively. As mentioned in Chapter 3, the IMU rotation rate employed in the calibration process is the same as the rate in the corresponding individual test.

4.1.1 Conventional INS Static Tests

The conventional INS static tests are conducted to investigate how fast the inertial errors accumulate over time without IMU rotation and to provide a comparison to the rotary INS. The means of the gyro data collected during the 1st minute provide the estimates of the gyro biases (Skaloud 1999). The navigation solutions are derived with the initial position, velocity and attitude from external information (the body frame is aligned to the local level frame after the initialization process of the rotation table). As expected, the position, velocity and attitude errors accumulate quickly over time, and their RMS values for MTi-G and NAV440 are summarized in Tables 4.3 and 4.4, respectively. After 5 minutes, the horizontal position errors accumulate to several kilometers for both MEMS IMUs.

Table 4.3 RMS of navigation errors for conventional INS with MTi-G in static mode

Latitude (m)	**Longitude (m)**	**Height (m)**
2412.3	1526.8	173.8
Vn (m/s)	**Ve (m/s)**	**Vu (m/s)**
33.2	20.5	1.2
Pitch (°)	**Roll (°)**	**Azimuth (°)**
1.83	1.32	2.31

Table 4.4 RMS of navigation errors for conventional INS with NAV440 in static mode

Latitude (m)	**Longitude (m)**	**Height (m)**
829.1	2820.1	1033.0
Vn (m/s)	**Ve (m/s)**	**Vu (m/s)**
4.8	26.7	9.0
Pitch (°)	**Roll (°)**	**Azimuth (°)**
0.48	0.60	0.73

4.1.2 Rotary INS Static Tests

In each individual test, the gyro scale factor of the Z axis, K_{gz}, the installation errors, K_{gxz}, K_{gyz}, and the gyro biases are estimated in the calibration process. Based on the gyro noise level of the IMUs given in Table 4.2, the calibration errors caused by gyro noise are calculated and presented

in Table 4.5 for both IMUs. For the time length of 60 seconds, the calibration errors of gyro bias are about 23 °/h and 3°/h for MTi-G and NAV440, respectively, and similar calibration errors are also obtained for the scale factor and installation errors. For both IMUs, the calibration errors caused by noise are much smaller than the gyro bias instability given in Table 4.2, which means such calibration accuracy is sufficient for MEMS-based INS. Although the longer calibration time leads to even smaller calibration errors, it may increase the effect of gyro bias instability on calibration results.

Table 4.5 Calibration errors caused by gyro noise for MEMS IMUs

Rotation Rate	**MTi-G**		**NAV440**	
(°/s)	**σ_b(°/h)**	**σ_s (ppm)**	**σ_b(°/h)**	**σ_s (ppm)**
10	23.2	645.5	3.1	86.1
20		322.7		43.0
30		215.2		28.7
40		161.4		21.5
50		129.1		17.2
60		107.6		14.2
70		92.2		12.3
80		80.7		10.8
90		71.7		9.6
100		64.5		8.6

Two data processing strategies are employed to derive the navigation solutions for the rotary INS, in order to study the effect of gyro scale factor and installation errors on navigation error mitigations. For the Data Processing Strategy I, the navigation solutions are derived with only the estimates of gyro biases from the calibration process, while the solutions are derived with the estimates of the gyro installation errors, scale factor and biases for the Data Processing Strategy II.

4.1.2.1 NAV440 with Data Processing Strategy I

Using the Data Processing Strategy I, the navigation solutions are derived for each individual rotary test using NAV440. The velocity and attitude errors in the east-north plane for the individual test with rotation rate of 30 °/s are given in Figures 4.4 and 4.5, respectively. As only the estimates of gyro biases are applied in the data processing, the oscillating roll and pitch errors indicate the modulation of motivated gyro biases by the IMU rotation. Due to the modulation of accelerometer biases and oscillated roll and pitch errors, the accumulated velocity errors also become oscillating errors. The oscillating period is the same as the IMU rotation period. The RMS of the navigation errors over the 5 minutes are calculated for each individual test. Figures 4.6 and 4.7 present the RMS values of the horizontal position and velocity errors, as well as the attitude errors for different IMU rotation rates. Although only the gyro biases are removed, the position, velocity, roll and pitch errors are reduced compared to those errors in the conventional INS. Due to the motivated gyro bias in the Z axis by IMU rotation, the azimuth error almost linearly increases over the rotation rate. The means of the RMS of the horizontal position and velocity errors for all individual tests are 544.8 m and 4.9 m/s, respectively. The remaining major error sources of the navigation errors are the rotation induced biases and the gyro bias residuals.

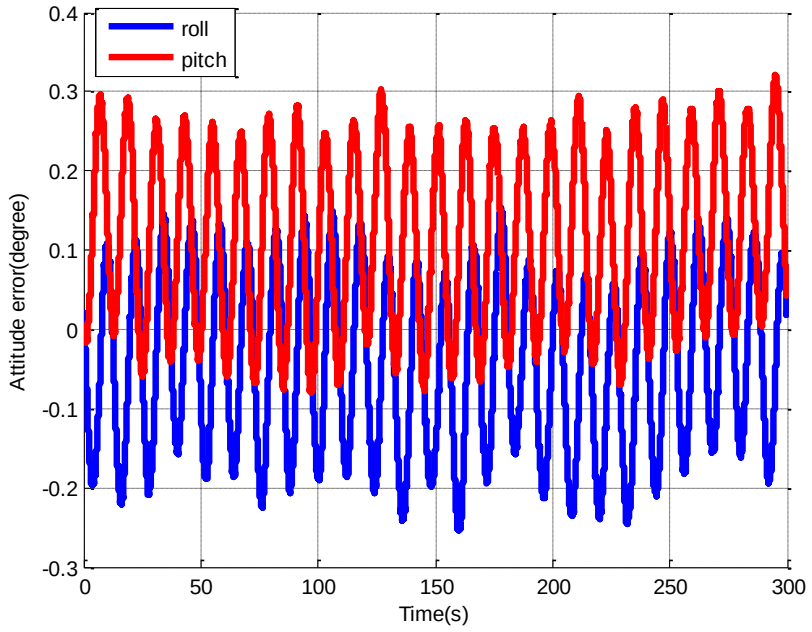

Figure 4.4 Attitude errors for rotary INS with NAV440 with Data Processing Strategy I

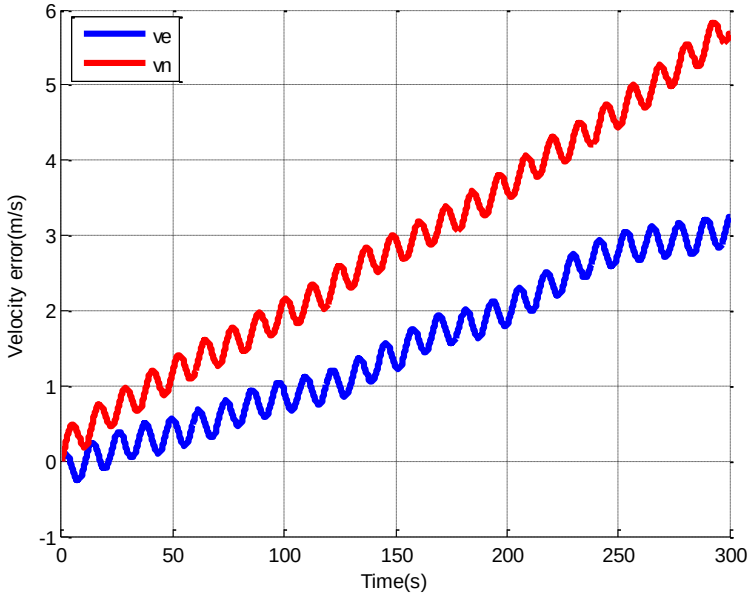

Figure 4.5 Velocity errors for rotary INS with NAV440 with Data Processing Strategy I

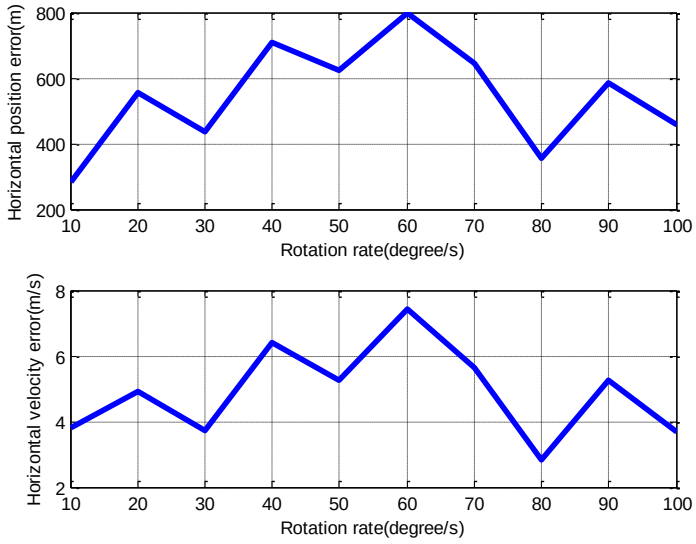

Figure 4.6 RMS of horizontal position and velocity errors for rotary INS with NAV440 with Data Processing Strategy I

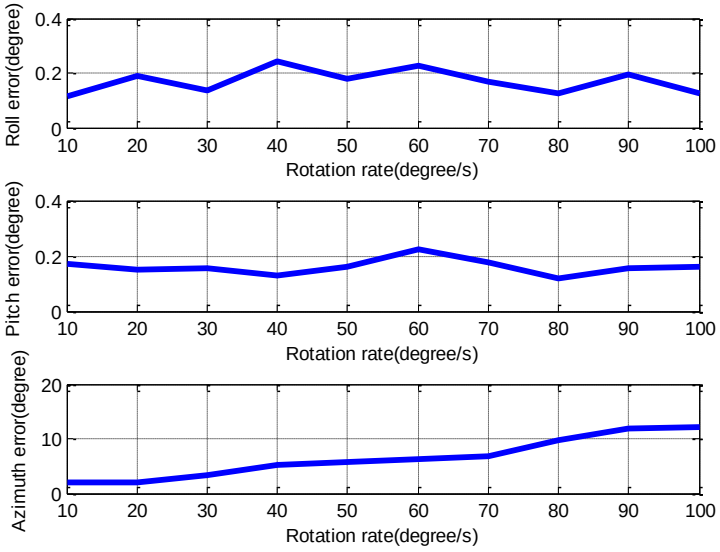

Figure 4.7 RMS of attitude errors for rotary INS with NAV440 with Data Processing Strategy I

4.1.2.2 NAV440 with Data Processing Strategy II

With the removal of the gyro scale factor and installation errors, the navigation solutions are calculated for each rotary test using NAV440. The attitude and velocity errors of the individual test with the IMU rotation rate of 30 °/s are given in Figures 4.8 and 4.9, respectively. When compared to the results obtained using Data Processing Strategy I, the oscillating amplitudes of the roll and pitch errors are greatly reduced, which indicates that the calibration process effectively removes the motivated gyro biases by IMU rotation, and the oscillating velocity errors are mainly caused by the modulation of accelerometer biases. The unstable oscillating amplitudes in the roll and pitch errors are caused by the variation of gyro bias residuals, and the oscillating period for attitude and velocity errors is the IMU rotation period.

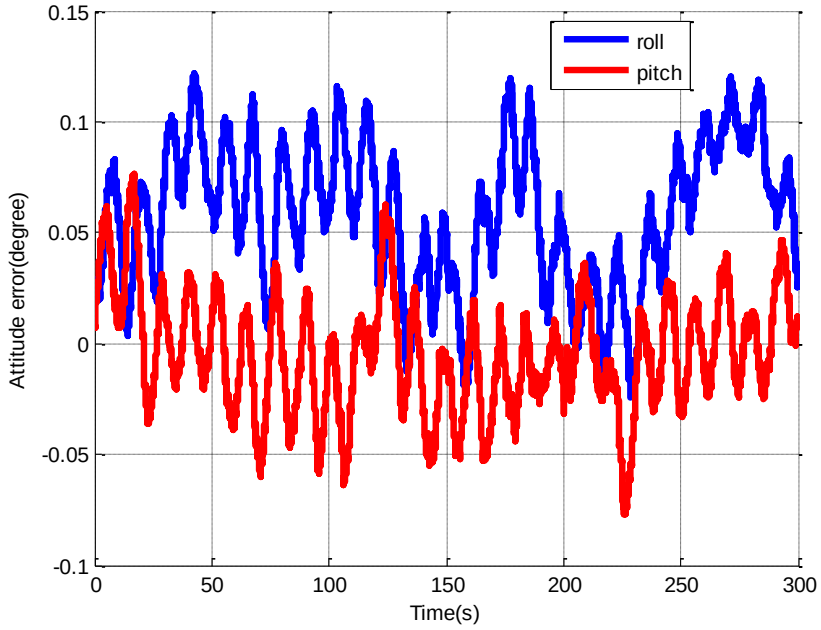

Figure 4.8 Attitude errors for rotary INS with NAV440 with Data Processing Strategy II

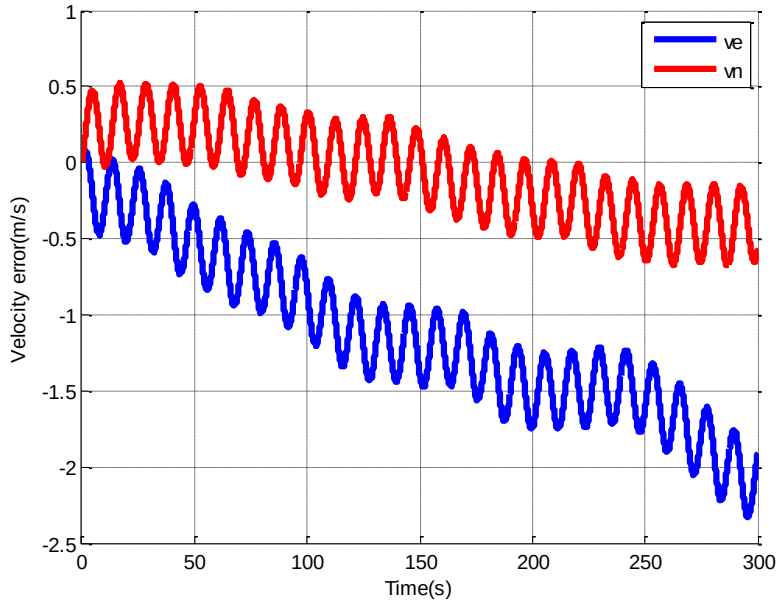

Figure 4.9 Velocity errors for rotary INS with NAV440 with Data Processing Strategy II

Figures 4.10 and 4.11 present the RMS of horizontal position and velocity errors, as well as the attitude errors for different IMU rotation rates. With the removal of the rotation induced gyro biases in the X and Y axes, the roll and pitch errors are further reduced, as well as the position and velocity errors. Also, the azimuth errors are significantly reduced due to the removal of the motivated gyro bias in the Z axis. The means of the RMS horizontal position and velocity errors are reduced to 213.8 m and 2.2 m/s, respectively, which demonstrates a significant improvement on navigation performance by IMU rotation, in comparison to the errors in the conventional INS. As shown in Figures 4.10 and 4.11, higher rotation rate basically can more effectively modulate the sensor errors, and results in smaller position and velocity errors, though fluctuations are observed.

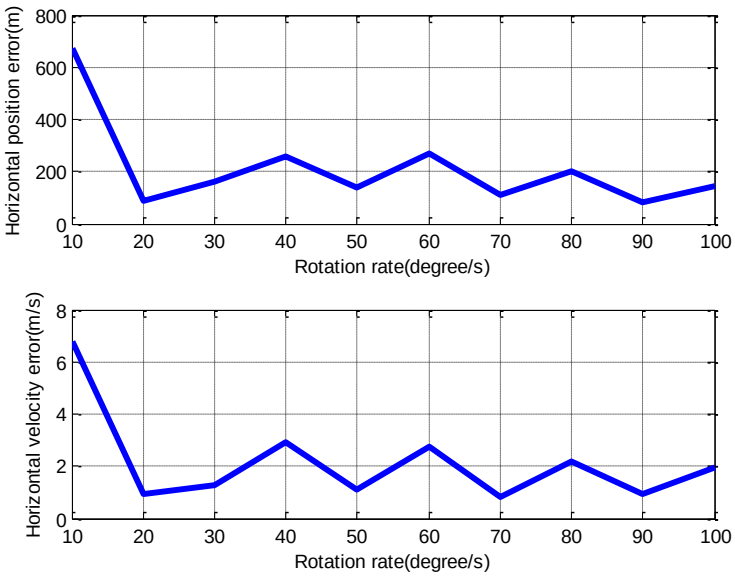

Figure 4.10 RMS of horizontal position and velocity errors for rotary INS with NAV440 with Data Processing Strategy II

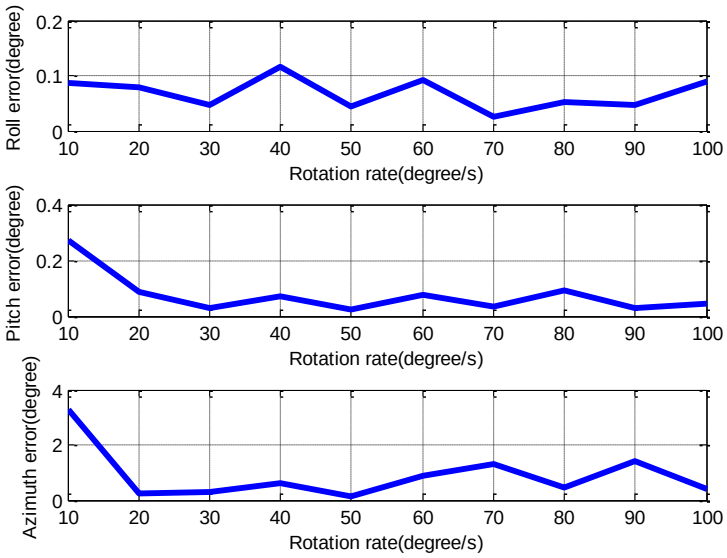

Figure 4.11 RMS of attitude errors for rotary INS with NAV440 with Data Processing Strategy II

4.1.2.3 MTi-G with Data Processing Strategy I

With Data Processing Strategy I, the navigation solutions are also derived for each rotary test using MTi-G. The attitude and horizontal velocity errors for the individual test with a rotation rate of 10 °/s are provided in Figures 4.12 and 4.13, respectively. As expected, the roll and pitch errors, as well as the velocity errors, are modulated into oscillating signals due to the modulation of motivated gyro biases and accelerometer biases.

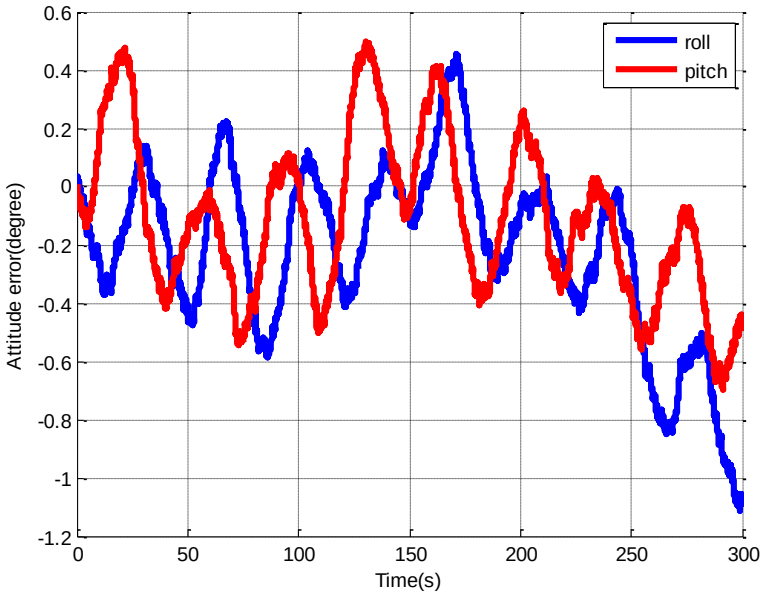

Figure 4.12 Attitude errors for rotary INS with MTi-G with Data Processing Strategy I

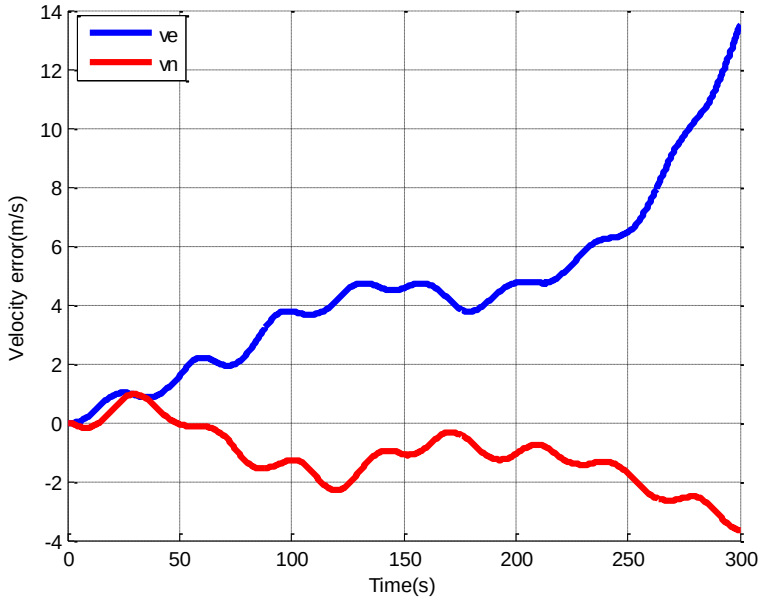

Figure 4.13 Velocity errors for rotary INS with MTi-G with Data Processing Strategy I

The RMS errors of the horizontal position and velocity solutions, as well as the attitude solutions for different IMU rotation rates, are plotted in Figures 4.14 and 4.15. Similar to the NAV440's results, the horizontal position and velocity errors, as well as the pitch and roll errors, are reduced, in comparison to those errors in the conventional INS. The azimuth error still grows almost linearly over the IMU rotation rate. The mean values of the RMS errors of the horizontal position and velocity for all tests are 1525.8 m and 14.6 m/s, respectively.

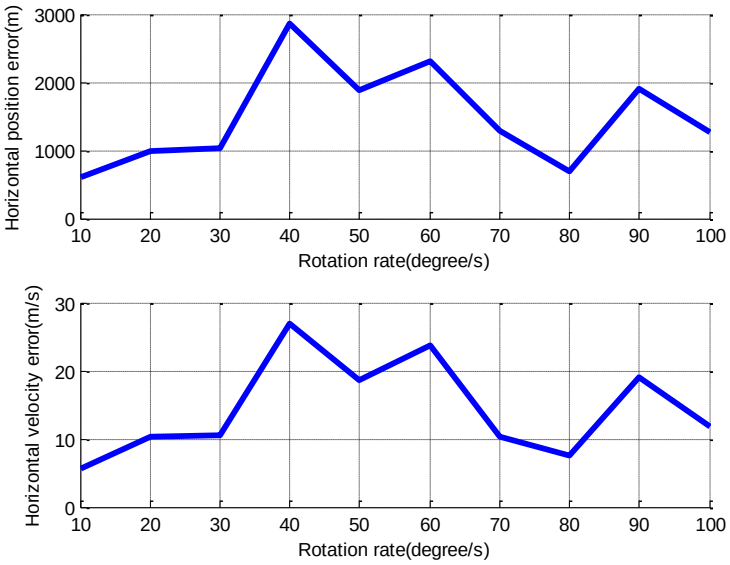

Figure 4.14 RMS of horizontal position and velocity errors for rotary INS with MTi-G with Data Processing Strategy I

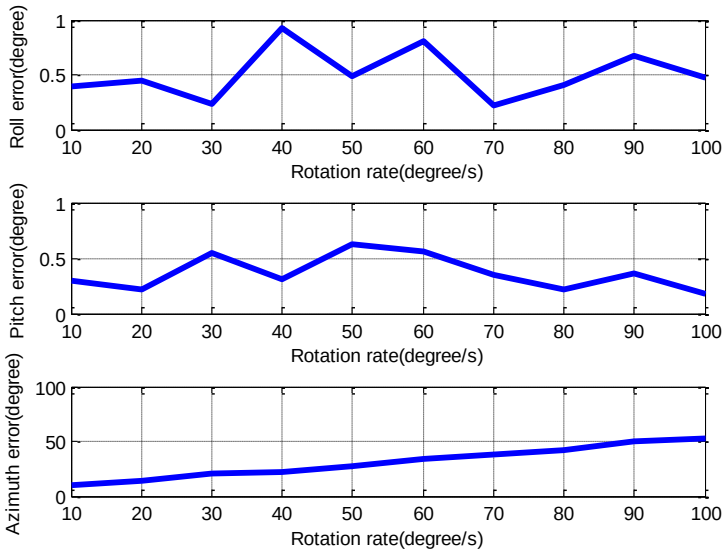

Figure 4.15 RMS of attitude errors for rotary INS with MTi-G with Data Processing Strategy I

4.1.2.4 MTi-G with Data Processing Strategy II

The navigation solutions are derived for each rotary test using Data Processing Strategy II. Figures 4.16 and 4.17 present the attitude and velocity errors in the east-north plane for the individual test with the rotation rate of 10 °/s, respectively. By applying the estimates of gyro installation errors, the oscillating amplitude of the roll and pitch errors, as well as the velocity errors are greatly reduced. The residuals of oscillating velocity errors are caused by the modulation of accelerometer biases

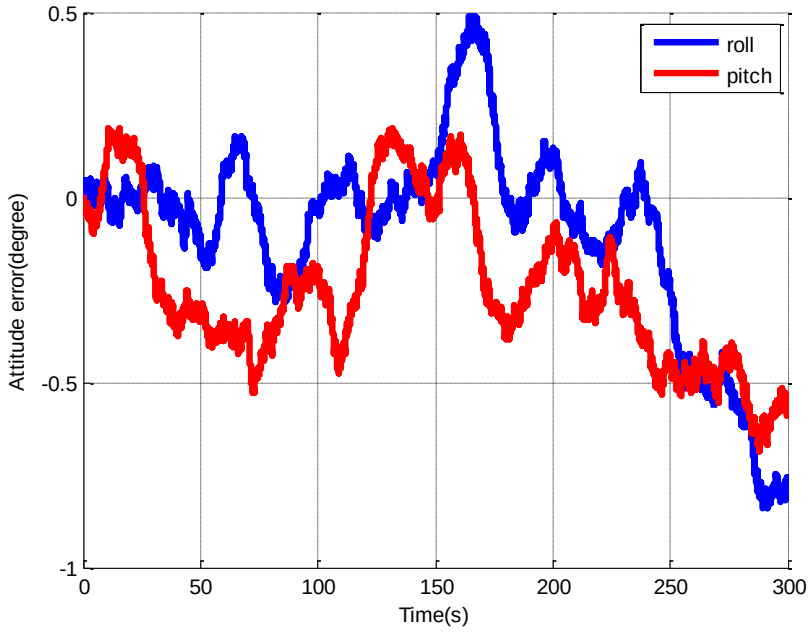

Figure 4.16 Attitude errors for rotary INS with MTi-G with Data Processing Strategy II

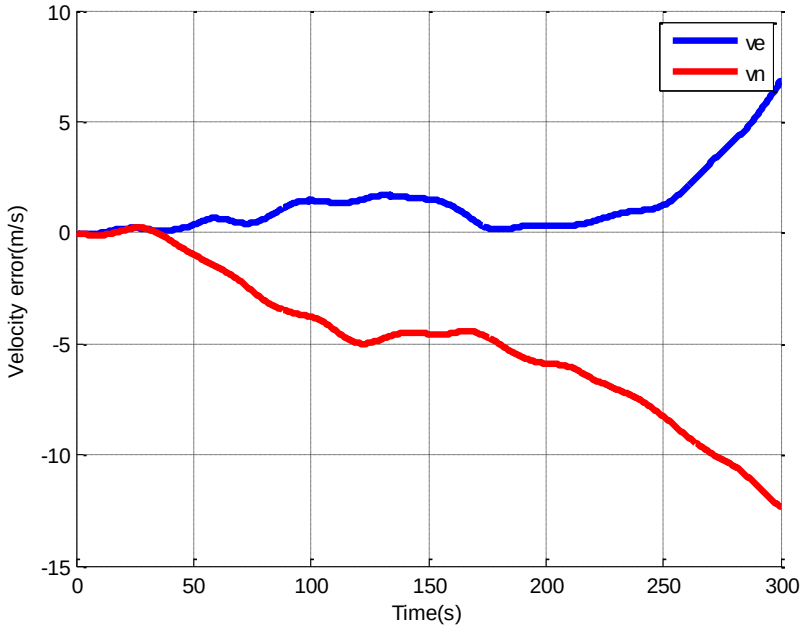

Figure 4.17 Velocity errors for rotary INS with MTi-G with Data Processing Strategy II

For different rotary tests using MTi-G, the RMS errors of position, velocity and attitude solutions are calculated and presented in Figures 4.18 and 4.19. By applying the estimates of the gyro installation errors and scale factors, not only are the horizontal position and velocity errors, and the pitch and roll errors, greatly decreased, but additionally the azimuth errors are reduced. The mean of the RMS of the horizontal position and velocity errors for all individual tests are further reduced to 1057.2 m and 10.4 m/s, respectively. As shown in Figure 4.18 and 4.19 that the horizontal position and velocity errors are not strongly related to the IMU rotation rate because of the significant gyro bias instability and noises of MTi-G.

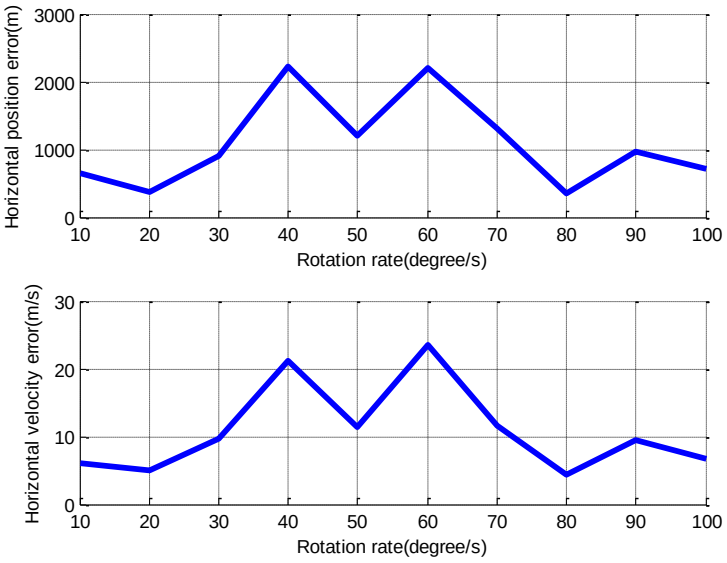

Figure 4.18 RMS of horizontal position and velocity errors for rotary INS with MTi-G with Data Processing Strategy II

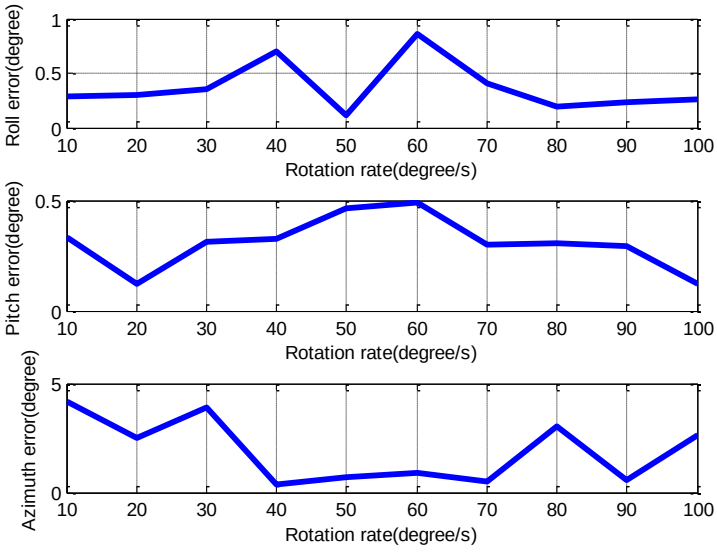

Figure 4.19 RMS of attitude errors for rotary INS with MTi-G with Data Processing Strategy II

4.1.2.5 Relations between IMU Rotation Rate and Error Mitigation Performance

To investigate the relationship between the IMU rotation rates and the error mitigation performance for the rotary INS with a low-cost MEMS IMU, another two rotary INS static tests, including 10 individual tests with IMU rotation rates ranging from 10 to 100 °/s respectively, are conducted using both MTi-G and NAV440. The test procedures are the same as those described previously, and only the Data Processing Strategy II is used to derive the navigation solutions. With the gyro installation errors and scale factor, as well as biases compensated, the obtained horizontal position and velocity errors, and the attitude errors for the two rotary tests using MTi-G are presented in Figures 4.20 and 4.21, respectively. Based on the results, we can see that, although theoretically the higher IMU rotation rates can more effectively modulate the sensor errors (Yang and Miao, 2004; Yuan, 2007; Ben et al., 2010), the gyro noise and bias instability also affect the error mitigation performance of the rotary INS. Given the significant gyro noise and bias instability of MTi-G, the low IMU rotation rate, such as 10°/s, offers similar results to the high rotation rate, such as 100 °/s. Considering the fact that the higher IMU rotation rate is more likely to cause mechanical issues and shorten the equipment lifetime, a low IMU rotation rate, such as 10 °/s, is recommended for the rotary INS with MTi-G.

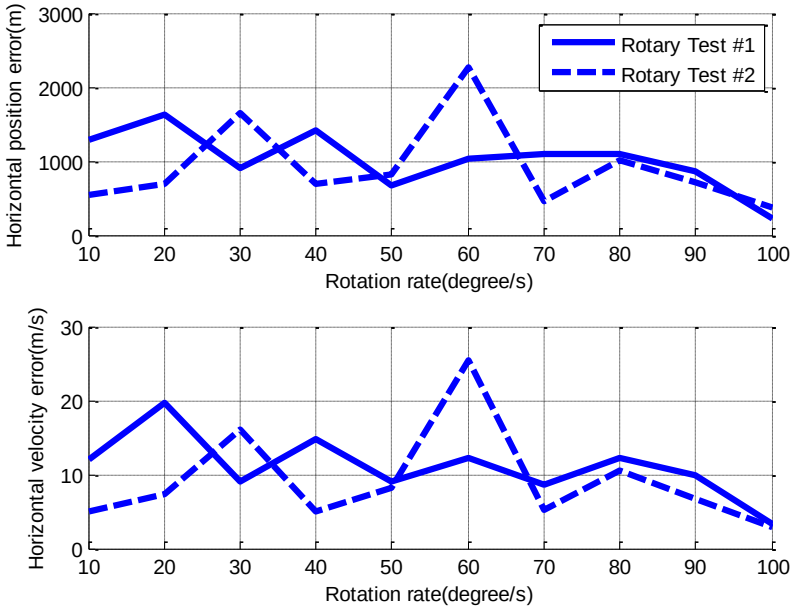

Figure 4.20 RMS of horizontal position and velocity errors for additional rotary INS tests with MTi-G

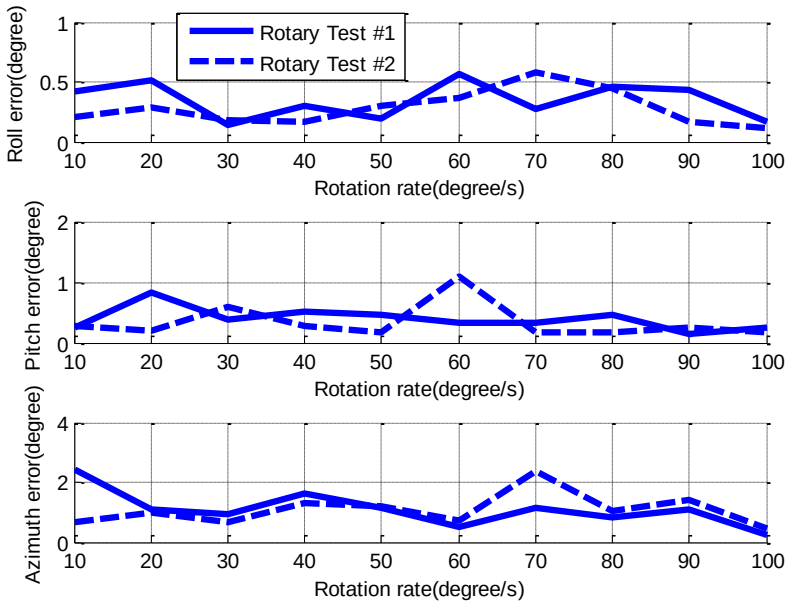

Figure 4.21 RMS of attitude errors for additional rotary INS tests with MTi-G

The horizontal position and velocity errors, as well as attitude errors, of the rotary tests using NAV440 are given in Figures 4.22 and 4.23, respectively. Obviously, the error mitigation is tightly associated with the IMU rotation rate, as NAV440 features much smaller gyro noise and bias instability compared to MTi-G. The higher IMU rotation rate essentially results in smaller navigation errors in the horizontal plane. The rotation rate of 20°/s is recommended for the rotary INS with NAV440, even though the higher rotation rate, which is not suitable for practical applications, may offer better error mitigation performance.

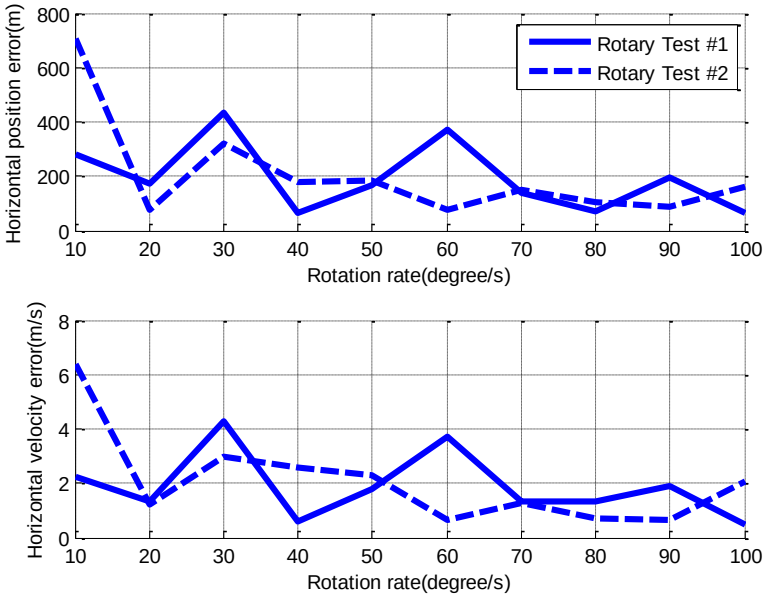

Figure 4.22 RMS of horizontal position and velocity errors for additional rotary INS tests with NAV440

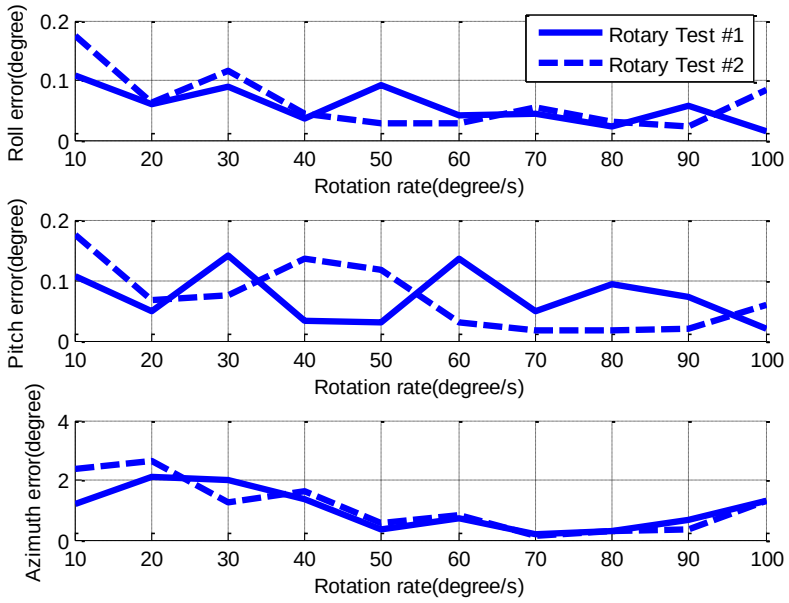

Figure 4.23 RMS of attitude errors for additional rotary INS tests with NAV440

Based on the above static tests for both the conventional and rotary INS, the following findings can be obtained: 1) the proposed calibration process can correctly estimate the gyro installation errors and the scale factor, and it largely removes the oscillating roll and pitch error, as well as the azimuth errors, caused by the rotation induced gyro biases; 2) the IMU rotation about the Z axis modulates the sensor errors and greatly reduces the navigation errors in the east-north plane for the rotary INS; 3) the azimuth errors are not related to IMU rotations but are highly dependent upon the gyro errors of the vertical axis, which cannot be modulated by IMU rotation about the Z axis; 4) the IMU rotation rate has limited effect on the error mitigation for the rotary INS with MTi-G, due to its significant gyro noise and bias instability; 5) for the rotary INS with NAV440, the IMU rotation rate affects the error mitigation, such that higher IMU rotation rate results in smaller navigation errors in east-north plane, due to the much smaller gyro noise and bias instability.

4.2 Kinematic Tests and Analysis

Kinematic field tests are also conducted based on a single-axis rotation platform to study the error mitigation of the rotary INS with a low-cost MEMS IMU in dynamic conditions. The single-axis rotation platform includes a rotation table and a console, as shown in Figure 4.24. The MEMS IMUs are firmly installed on the top of the platform using screws, as shown in Figure 4.25. Only IMU rotation about the Z axis can be implemented with this rotation table, and its technical parameters are given in Table 4.6. As analyzed in Chapter 2, the rotation rate error and the rotation angle error result in the navigation errors theoretically, such errors can be safely ignored because of the superior rotation rate and positioning accuracy of the rotation table.

Figure 4.24 Single-axis rotation platform

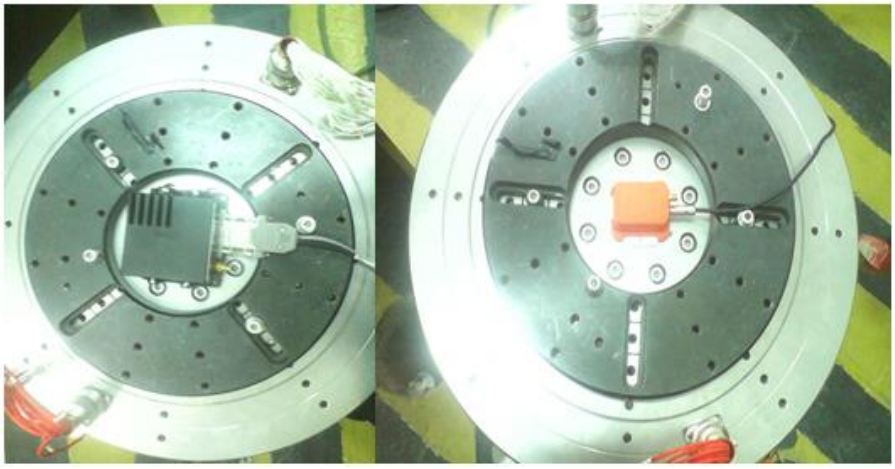

Figure 4.25 Installations of MEMS IMU on the single-axis rotation platform

Table 4.6 Technical parameters of single-axis rotation platform

Position Accuracy (°)	Rotation Rate Accuracy (°/s)	Maximum Rotation Rate (°/s)
8e-4	5e-5	±100

Kinematic field tests are conducted using a land vehicle. In addition to the single-axis rotation platform and two MEMS IMUs, the NovAtel SPAN system, which includes a high-end LCI IMU and a SE GNSS receiver, is employed to collect the data to generate the reference solutions. Other equipment includes the power supply and the antenna. The equipment set-up on the test vehicle is shown in Figure 4.26. The single-axis rotation table with the installed MEMS IMU and the power supply are placed at the trunk of the vehicle, and the console, as well as the NovAtel SPAN system, is placed on the back seat row. The body frame of the MEMS IMU is aligned to the body frame of the SPAN before the IMU rotations. The SPAN antenna is placed on the roof

of vehicle as shown in the figure. The SPAN data, including both GNSS data and inertial data, are collected with the data rates of 1 Hz and 100 Hz, respectively, and stored in the SD card of the GNSS receiver, while the MEMS IMU data and rotation angle data are collected by the rotation table console with the data rates of 100 Hz and 50 Hz, respectively.

Figure 4.26 Equipments set-up on the test vehicle

4.2.1 Field Test Descriptions

The designated trajectory for the kinematic field test includes straight lines, loops and turns, as shown in Figure 4.27. Its total length is about 2.3 km. When the vehicle travels along the

trajectory, it experiences accelerations and decelerations along west-to-east, north-to-south, and other different directions, as well as many velocity and azimuth variations. Consequently, the dynamic conditions of the kinematic test can represent the real scenario of the land vehicle.

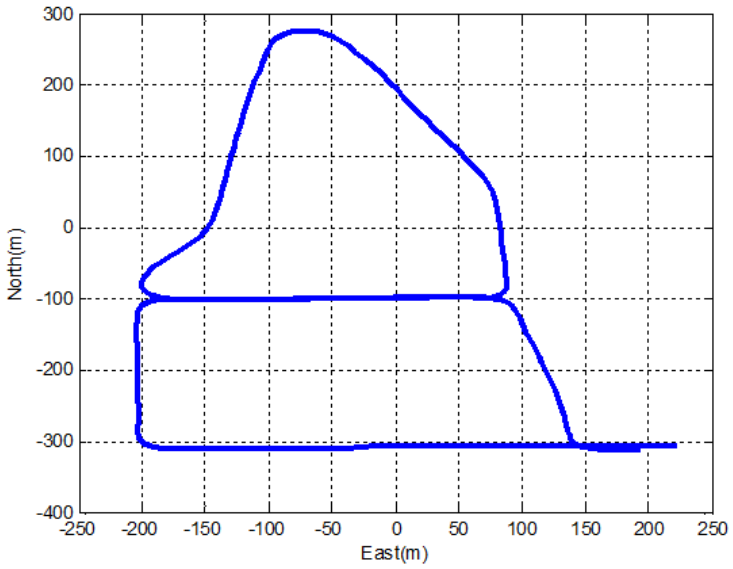

Figure 4.27 Trajectory of kinematic field tests

The kinematic field tests are conducted for the conventional and the rotary INS with both IMUs. For the conventional INS tests, a single test is conducted for each IMU, in which the vehicle remains static for five minutes, and then travels along the trajectory, and the IMU remains static relative to the vehicle during the entire test. In the rotary INS tests, the rotation rate of 10 °/s and 20 °/s are chosen for the rotary INS with MTi-G and NAV440, respectively. Six individual tests are conducted for each IMU and in each individual test, a calibration process is conducted while the vehicle remains static, and then the vehicle travels along the trajectory with the IMU rotating about the Z axis at the designated rate. The duration of the kinematic tests are about 210 seconds (not including the initial static period in the conventional INS test and the calibration time in the

rotary INS tests). As the heading information cannot be obtained from low-cost IMU due to its significant sensor errors, the initial attitudes of MEMS-based inertial systems in both conventional and rotary tests are obtained using SPAN data during the static period based on the 2-step coarse alignment, which includes the accelerometer leveling and the gyro compassing (Shin, 2001; Du, 2010).

The tests are conducted in an open sky environment and the reference solutions are generated by processing the SPAN data (including both GNSS and inertial data) using Waypoint Inertial Explorer from NovAtel, such that the reference solutions are accurate enough to evaluate the conventional and the rotary INS solutions. With the initial position and attitude from the SPAN system, the conventional INS solutions are derived with the estimates of the gyro biases obtained by averaging the gyro data collected during the static period (Skaloud 1999), while the rotary INS solutions are derived with the gyro biases, scale factors and installation errors from calibration process. Then the obtained conventional and rotary INS solutions are compared with the references to evaluate the navigation errors of both systems.

4.2.2 MEMS-based Rotary INS with NAV440

By using NAV440, the obtained roll and pitch errors for the conventional INS test and the 1st individual rotary test are presented the Figure 4.28. The major error sources for the roll and pitch errors are the gyro bias residuals (gyro biases are already removed). In the conventional INS, the maximum roll and pitch errors almost reach 1°, and they varied dramatically due to vehicle dynamics. Through the modulation of gyro bias residuals in the X and Y axes by IMU rotation about the Z axis, the roll and pitch errors are effectively reduced, compared to those errors in the

conventional INS. Additionally, they become oscillating signals with the period equals to IMU rotation period. Apparently, the gyro biases still can be effectively modulated under dynamics.

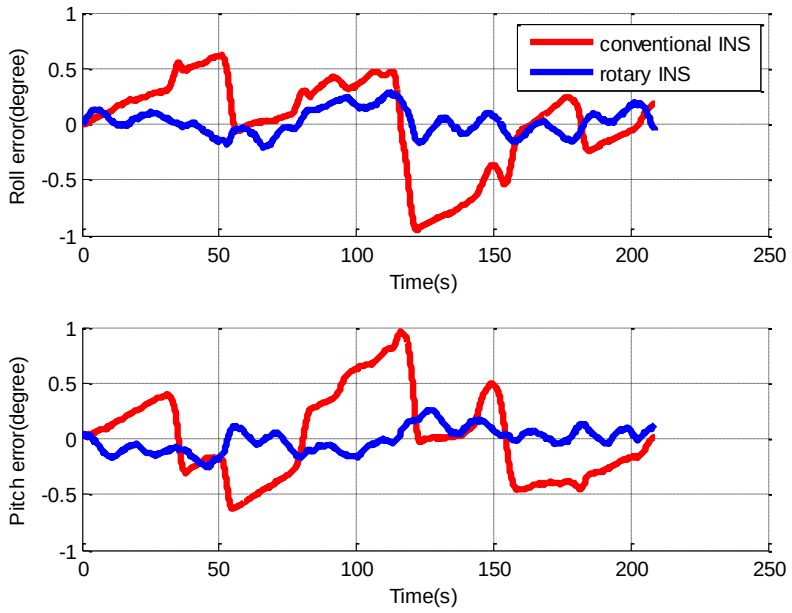

Figure 4.28 Roll and pitch errors for conventional INS and rotary INS with NAV440

The velocity errors in the east and north directions for the conventional INS test and the 1st rotary INS test are presented in Figure 4.29. The major error sources for the horizontal velocity errors are the accelerometer biases and the roll and pitch errors. As expected, the horizontal velocity errors accumulate quickly to over 10 m in the conventional INS after 200 seconds, while the modulation of accelerometer biases and the reduced roll and pitch errors effectively dampen their accumulation in the rotary INS. Similarly, the velocity errors in the rotary INS become oscillating signals with period equals to the IMU rotation period.

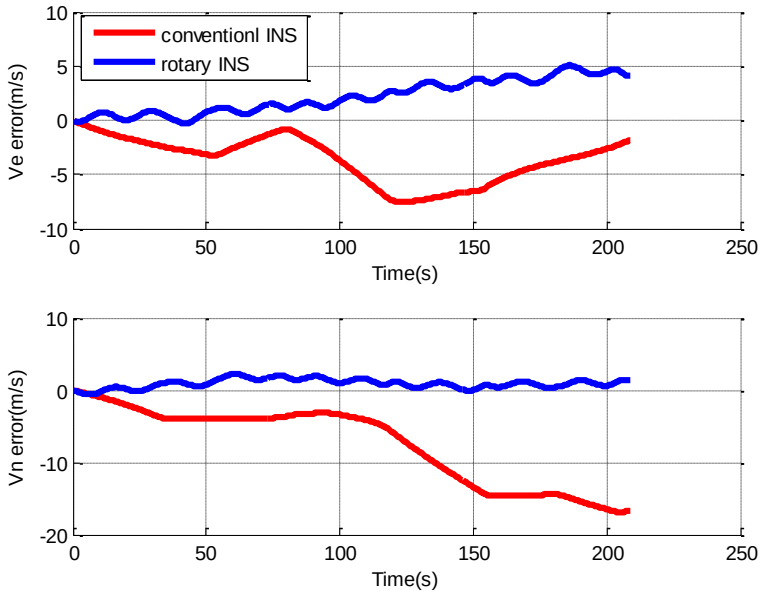

Figure 4.29 Velocity errors in east-north plane for conventional INS and rotary INS with NAV440

Figure 4.30 presents the trajectory of the conventional INS test, represented by red color, the trajectory of the 1st rotary INS test, represented by blue color, and the reference trajectory, represented by green color. Although both the conventional and rotary INS solutions drift away from the reference without external aiding, the conventional INS solutions are completely diverged after tens of seconds, whereas the rotary INS solution can still describe the shape of the traveled trajectory.

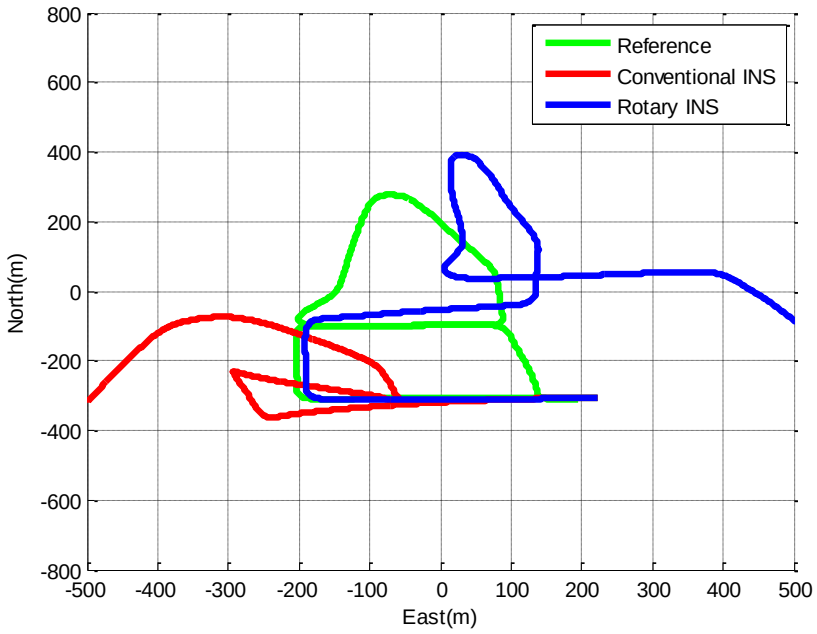

Figure 4.30 Trajectories for conventional INS and rotary INS with NAV440

The RMS errors of the conventional INS solutions and the rotary INS solutions in each individual test using NAV440 are summarized in Table 4.8. Through the IMU rotation, the horizontal position and velocity errors are reduced by about 3~5 times in the rotary INS as compared to the ones in the conventional INS. Although both the roll and pitch errors are significantly reduced in the rotary INS, no improvements are observed in the azimuth solution, as the gyro bias in the Z axis cannot be modulated. Based on the results, we can see that although sensor errors still can be effectively modulated by the IMU rotation, the error mitigation performance is slightly reduced with vehicle dynamics, compared to the static test results.

Table 4.7 RMS of navigation errors for conventional INS and rotary INS with NAV440

Rotation rate (°/s)	HP (m)	HV (m/s)	Roll (º)	Pitch (º)	Azimuth (°)
Conventional INS test	725.0	10.2	0.40	0.39	0.67
Rotary INS test #1	206.9	2.9	0.12	0.11	1.84
Rotary INS test #2	219.7	3.8	0.18	0.19	0.63
Rotary INS test #3	154.8	2.7	0.13	0.16	0.26
Rotary INS test #4	313.5	4.3	0.15	0.13	0.90
Rotary INS test #5	332.3	4.7	0.19	0.18	1.45
Rotary INS test #6	221.6	2.8	0.13	0.16	1.02
Mean of Rotary INS	241.5	3.5	0.15	0.16	1.02

4.2.3 MEMS-based Rotary INS with MTi-G

Similar results to the ones obtained using NAV440 are obtained for the conventional INS test and rotary tests with MTI-G. Through the IMU rotation about the Z axis, the accumulations of the roll and pitch errors, as well as the velocity errors in the east and north directions are effectively mitigated by the modulation of the gyro and accelerometer biases in the X and Y axes under dynamics.

The RMS errors of the conventional INS solutions and the rotary INS solutions in each individual test using MTi-G are calculated and summarized in Table 4.7. Greater navigation errors are obtained using MTi-G due to its greater sensor errors. Although sensor biases vary

with time, the IMU rotations effectively reduce the position and velocity errors in the east-north plane, as well as the roll and pitch errors, such that the horizontal position errors are reduced by about 2~3 times in the rotary INS in comparison to the ones in the conventional INS. Similarly, no obvious improvements are observed in azimuth solutions.

Table 4.8 RMS of navigation errors for conventional INS and rotary INS with MTi-G

Rotation rate (°/s)	HP (m)	HV (m/s)	Roll (º)	Pitch (º)	Azimuth (°)
Conventional INS test	1345.4	17.6	0.73	0.71	2.67
Rotary INS test #1	451.4	7.6	0.37	0.40	1.95
Rotary INS test #2	634.2	8.2	0.53	0.50	3.31
Rotary INS test #3	788.4	11.7	0.58	0.50	2.72
Rotary INS test #4	640.2	11.4	0.64	0.58	3.48
Rotary INS test #5	638.7	9.3	0.73	0.62	2.86
Rotary INS test #6	920.6	14.4	0.58	0.66	3.62
Mean of Rotary INS	678.9	10.4	0.57	0.54	2.94

Based on the kinematic field tests for both the conventional and rotary INS, we can conclude that, 1) the IMU rotation about the Z axis can still effectively modulate the sensor biases and greatly reduce the navigation errors in the east-north plane under kinematic environment; and, 2) compared to the static rotary tests, the error mitigation performance is slightly reduced under kinematic environments, and the reasons could be the vehicle vibrations and dynamics.

Additional equipments, such as jolt table, and more vehicle dynamics, are required for the future study of error mitigation of the rotary INS.

Chapter Five: Improving System Observability by Rotary Motions of IMU

In order to limit the error accumulation in the INS, the position and velocity from other sensors, such as GNSS or Doppler velocity sensors, are commonly applied to estimate the navigation errors, as well as inertial sensor errors, using an EKF. Although the INS position and velocity errors can be directly observed in the filter when external position and velocity measurements are available, the observability of other INS error terms (except the accelerometer bias in vertical direction) is still poor when system maneuvers are weak or not available (Goshen-Meskin and Bar-Itzhack, 1992; Hong et al., 2005). Poor system observability would result in inaccurate estimation of INS errors and eventually degrades the navigation performance. This chapter presents a method to improve the observability of INS errors in the absence of maneuvers by rotary IMU motions. The observability analysis methodology is first introduced, and is then followed by the observability analysis for both the conventional and rotary INS. The system observability improvements by IMU rotations, each rotating about the X, Y and Z axes, respectively, are identified. Based on a tri-axial rotation table, tests are conducted in laboratory with both NAV440 and MTi-G to verify the system observability improvements in the rotary INS.

5.1 Observability Analysis Methodology

The ability to estimate the state of a completely observable system depends only on the system driving noise and measurement noise; however, if the system is not observable, the accurate estimate of the state cannot be obtained, even if the noise level is negligible (Goshen-Meskin and Bar-Itzhack, 1992). The Kaman filter has been extensively employed in inertial systems to

estimate the INS errors with external measurements. The observability analysis assesses whether INS errors can be estimated from the filter.

For a linear continuous-time system described in Eq. (5.1), the observability analysis can be considered as finding a state vector $x(t)$ that satisfies the Eq. (5.2) for a time $t > t_0$ (Hong et al., 2005; Niu et al., 2012).

$$\begin{aligned} \dot{x}(t) &= F(t)x(t) \\ z(t) &= H(t)x(t) \end{aligned} \tag{5.1}$$

$$\begin{aligned} z(t) &= N_0(t)x(t) \\ \dot{z}(t) &= N_0(t)\dot{x}(t) + \dot{N}_0(t)x(t) \\ &= [N_0(t)F(t) + \dot{N}_0(t)]x(t) = N_1(t)x(t) \\ \ddot{z}(t) &= N_1(t)\dot{x}(t) + \dot{N}_1(t)x(t) \\ &= [N_1(t)F(t) + \dot{N}_1(t)]x(t) = N_2(t)x(t) \\ \dddot{z}(t) &= N_2(t)\dot{x}(t) + \dot{N}_2(t)x(t) \\ &= [N_2(t)F(t) + \dot{N}_2(t)]x(t) = N_3(t)x(t) \\ &\vdots \\ z^{n-1}(t) &= N_{n-2}(t)\dot{x}(t) + \dot{N}_{n-2}(t)x(t) \\ &= [N_{n-2}(t)F(t) + \dot{N}_{n-2}(t)]x(t) = N_{n-1}(t)x(t) \end{aligned} \tag{5.2}$$

where $F(t)$ is the dynamic matrix with size n×n, $H(t)$ is the design matrix with size p×n, $x(t)$ and $z(t)$ are the state vector and measurement vector, respectively, $N_0(t) = H(t), N_{n-1}(t) = N_{n-2}(t)F(t) + \dot{N}_{n-2}(t)$.

According to Goshen-Meskin and Bar-Itzhack (1992) and Hong et al (2005), the system is observable at t_0 if the rank of the matrix, $\begin{bmatrix} N_0(t) & N_1(t) & \cdots & N_{n-1}(t) \end{bmatrix}^T$, is n. In other words, the state vector can be determined based on Eq. (5.2).

For both the conventional and rotary INS, the state vector usually includes velocity errors, attitude errors, accelerometer and gyro biases, and the INS error model is employed as the dynamic model of the system. The position errors are excluded from the state vector, since they have very weak effect on attitude errors and sensor errors. The observability analysis for both the conventional and rotary inertial systems will be conducted in the local level frame.

5.2 Observability Analysis of Conventional INS

In the absence of system maneuvers, the error model of velocity and attitude for the conventional INS can be obtained by ignoring the horizontal accelerations and other insignificant terms as shown in Eq. (5.3) ~ (5.8). Although the sensor biases are actually slow-varying random variables, they are treated as random constants, whose time derivatives are zeroes, to simplify the analysis.

$$\delta \dot{V}_E = 2\omega_{ie} \sin\varphi \delta V_N - 2\omega_{ie} \cos\varphi \delta V_U + g\varepsilon_N + b_E \tag{5.3}$$

$$\delta \dot{V}_N = -2\omega_{ie} \sin\varphi \delta V_E - g\varepsilon_E + b_N \tag{5.4}$$

$$\delta \dot{V}_U = 2\omega_{ie} \cos\varphi \delta V_E + b_U \tag{5.5}$$

$$\dot{\varepsilon}_E = \frac{1}{M+h} \delta V_N + \omega_{ie} \sin\varphi \varepsilon_N - \omega_{ie} \cos\varphi \varepsilon_U + d_E \tag{5.6}$$

$$\dot{\varepsilon}_N = \frac{1}{N+h}\delta V_E - \omega_{ie}\sin\varphi\varepsilon_E + d_N \tag{5.7}$$

$$\dot{\varepsilon}_U = -\frac{\tan\varphi}{N+h}\delta V_E + \omega_{ie}\cos\varphi\varepsilon_E + d_U \tag{5.8}$$

where $\begin{bmatrix} b_E \\ b_N \\ b_U \end{bmatrix} = C_b^n \begin{bmatrix} b_X \\ b_Y \\ b_Z \end{bmatrix}$ and $\begin{bmatrix} d_E \\ d_N \\ d_U \end{bmatrix} = C_b^n \begin{bmatrix} d_X \\ d_Y \\ d_Z \end{bmatrix}$

The measurements used to estimate the INS errors are velocities, so $H(t)$ has the form of $\begin{bmatrix} I_{3\times3} & 0_{3\times3} & 0_{3\times3} & 0_{3\times3} \end{bmatrix}$. Based on the observability definition and the error model described above, the observable states and combinations of states are summarized in Table 5.1.

Table 5.1 Observable states and combinations of states in conventional INS

Observable states	$\delta V_E, \delta V_N, \delta V_U, b_U$
Observable combination of states	$g\varepsilon_N + b_E$, $-g\varepsilon_E + b_N$, $-\omega_{ie}\sin\varphi\varepsilon_E + d_N$, $\omega_{ie}\sin\varphi\varepsilon_N - \omega_{ie}\cos\varphi\varepsilon_U + d_E$, $\omega_{ie}\cos\varphi\varepsilon_E + d_U$

Apparently, three velocity errors can be obtained directly from the velocity measurements, so they are observable states. As shown in Eq. (5.5), the velocity error in the vertical direction is

associated with the velocity error in the east direction and the vertical accelerometer bias, so this bias can be uniquely determined and it is also observable state.

Given the velocity errors in the local level frame, the attitude error in the north direction is jointly observable with the accelerometer bias in the east direction, and the attitude error in the east direction is also jointly observable with the accelerometer bias in the north direction. Therefore, the estimation accuracy of the attitude error in the east or north direction is highly related to the accelerometer bias in the north or east direction, respectively. As shown in Table 5.1, other observable combinations of states consist of attitude errors and gyro biases. For most MEMS IMUs, as the gyro biases are usually much more significant than the earth rotation rate, the following can be concluded: 1) the state combination of $\omega_{ie}\cos\varphi\varepsilon_E + d_U$ cannot be determined, though it is observable theoretically; 2) the gyro biases in the east-north plane can be roughly determined, though they are not observable states. Evidently, the conventional INS is not a completely observable system in the absence of system maneuvers, and only the velocity errors and accelerometer bias in the vertical direction are observable.

5.3 Observability Analysis of Rotary INS

As the rotation does not introduce any linear movement of the IMU, the error model described by Eq. (5.3) ~ (5.8) can still be used to describe the navigation errors of the rotary INS in the absence of system maneuvers. Different from the conventional INS, the time derivatives of the sensor biases cannot be considered as zeroes due to the modulation of those errors by IMU rotations. The observable states and combinations of states are summarized in Table 5.2.

Table 5.2 Observable states and combinations of states in rotary INS

Observable states	$\delta V_E, \delta V_N, \delta V_U, b_U$
Observable combination of states	$g\varepsilon_N + b_E$, $-g\varepsilon_E + b_N$, $g(-\omega_{ie}\sin\varphi\varepsilon_E + d_N) + \dot{b}_E$, $-g(\omega_{ie}\sin\varphi\varepsilon_N - \omega_{ie}\cos\varphi\varepsilon_U + d_E) + \dot{b}_N$

Similar to the conventional INS, the velocity errors and accelerometer bias in the vertical direction are observable states in the rotary INS. With IMU rotations, other INS errors can be derived from the observable combinations of states. The improvements on system observability are analyzed as follows for each IMU rotation scheme, respectively.

5.3.1 System Observability with IMU Rotation about X Axis

When the IMU rotates about the X axis, the accelerometer bias in the vertical direction and its first time derivative can be described using Eq. (5.9) and (5.10), respectively. As both of them are observable, the accelerometer biases in the X, Y and Z axes can be determined with IMU rotation, which changes their geometry.

$$b_U = C_{31}b_X + C_{32}(b_Y\cos\omega t - b_Z\sin\omega t) + C_{33}(b_Y\sin\omega t + b_Z\cos\omega t) \tag{5.9}$$

$$\dot{b}_U = C_{32}\omega(-b_Y\sin\omega t - b_Z\cos\omega t) + C_{33}\omega(b_Y\cos\omega t - b_Z\sin\omega t) \tag{5.10}$$

where C_{ij} is the element in the i^{th} row and j^{th} column of the transformation matrix from the body frame to the navigation frame.

With estimates of the accelerometer biases in the X, Y and Z axes, the accelerometer biases in the east and north directions, as well as their first time derivatives, become observable, as shown in Eq. (5.11) ~ (5.14). According to Table 5.2, the attitude errors, ε_E and ε_N, also become observable states with the determination of the accelerometer biases.

$$b_E = C_{11}b_X + C_{12}(b_Y \cos\omega t - b_Z \sin\omega t) + C_{13}(b_Y \sin\omega t + b_Z \cos\omega t) \tag{5.11}$$

$$b_N = C_{21}b_X + C_{22}(b_Y \cos\omega t - b_Z \sin\omega t) + C_{23}(b_Y \sin\omega t + b_Z \cos\omega t) \tag{5.12}$$

$$\dot{b}_E = C_{12}\omega(-b_Y \sin\omega t - b_Z \cos\omega t) + C_{13}\omega(b_Y \cos\omega t - b_Z \sin\omega t) \tag{5.13}$$

$$\dot{b}_N = C_{22}\omega(-b_Y \sin\omega t - b_Z \cos\omega t) + C_{23}\omega(b_Y \cos\omega t - b_Z \sin\omega t) \tag{5.14}$$

As the attitude errors, as well as the first time derivatives of the accelerometer biases in the east and north directions, become observable states, the gyro biases in the east and north directions can be derived from their observable combination of states, $-g(\omega_{ie}\sin\varphi\varepsilon_N - \omega_{ie}\cos\varphi\varepsilon_U + d_E) + \dot{b}_N$ and $g(-\omega_{ie}\sin\varphi\varepsilon_E + d_N) + \dot{b}_E$, respectively. Subsequently the gyro biases in the X, Y and Z axes can be derived with IMU rotation as shown in Eq. (5.15) ~ (5.18). Finally, the vertical gyro bias can be obtained using Eq. (5.19).

$$d_E = C_{11}d_X + C_{12}(d_Y \cos\omega t - d_Z \sin\omega t) + C_{13}(d_Y \sin\omega t + d_Z \cos\omega t) \tag{5.15}$$

$$d_N = C_{21}d_X + C_{22}(d_Y \cos\omega t - d_Z \sin\omega t) + C_{23}(d_Y \sin\omega t + d_Z \cos\omega t) \tag{5.16}$$

$$\dot{d}_E = C_{12}\omega(-d_Y \sin\omega t - d_Z \cos\omega t) + C_{13}\omega(d_Y \cos\omega t - d_Z \sin\omega t) \tag{5.17}$$

$$\dot{d}_N = C_{22}\omega(-d_Y \sin\omega t - d_Z \cos\omega t) + C_{23}\omega(d_Y \cos\omega t - d_Z \sin\omega t) \tag{5.18}$$

$$d_U = C_{21}d_X + C_{22}(d_Y \cos\omega t - d_Z \sin\omega t) + C_{23}(d_Y \sin\omega t + d_Z \cos\omega t) \tag{5.19}$$

Obviously the attitude errors in the east and north directions, the accelerometer and gyro biases in the X, Y and Z axes become observable states through IMU rotation about the X axis. The azimuth error, however, is still unobservable, as the accurate estimation of it requires significant horizontal accelerations, as shown in Eq. (2.18). Even though the IMU rotation cannot improve the observability of azimuth errors, the estimation of vertical gyro bias can limit the azimuth error accumulation.

When the IMU rotates about the X axis, there is a potential issue affecting the system observability, such that the roll angle of zero reduces the observability of the accelerometer bias in the X axis. This is because the error coefficient, C_{31}, becomes zero when roll angle is zero, according to Eq. (2.1).

5.3.2 System Observability with IMU Rotation about Y Axis

Similar to the system with IMU rotation about the X axis, the accelerometer biases in the X, Y and Z axes can be determined from the vertical accelerometer bias and its first time derivative when IMU rotates about the Y axis, as shown in Eq. (5.20) and (5.21).

$$b_U = C_{31}(b_X \cos\omega t + b_Z \sin\omega t) + C_{32}b_Y + C_{33}(-b_X \sin\omega t + b_Z \cos\omega t) \quad (5.20)$$

$$\dot{b}_U = C_{31}\omega(-b_X \sin\omega t + b_Z \cos\omega t) + C_{33}\omega(-b_X \cos\omega t - b_Z \sin\omega t) \quad (5.21)$$

Then, the attitude errors, ε_E and ε_N, as well as the gyro biases, d_E and d_N, become observable states, with the determination of the accelerometer biases in the east and north directions using Eq. (5.22) and (5.23).

$$b_E = C_{11}(b_X \cos\omega t + b_Z \sin\omega t) + C_{12}b_Y + C_{13}(-b_X \sin\omega t + b_Z \cos\omega t) \quad (5.22)$$

$$b_N = C_{21}(b_X \cos\omega t + b_Z \sin\omega t) + C_{22}b_Y + C_{23}(-b_X \sin\omega t + b_Z \cos\omega t) \quad (5.23)$$

Similarly, the gyro biases in the X, Y and Z axes can be derived from the gyro biases in the east and north directions with IMU rotation, as shown in Eq. (5.24) ~ (5.27), and the vertical gyro bias can be derived using Eq. (5.28).

$$d_E = C_{11}(d_X \cos\omega t + d_Z \sin\omega t) + C_{12}d_Y + C_{13}(-d_X \sin\omega t + d_Z \cos\omega t) \quad (5.24)$$

$$d_N = C_{21}(d_X \cos\omega t + d_Z \sin\omega t) + C_{22}d_Y + C_{23}(-d_X \sin\omega t + d_Z \cos\omega t) \quad (5.25)$$

$$\dot{d}_E = C_{11}\omega(-d_X \sin\omega t + d_Z \cos\omega t) + C_{13}\omega(-d_X \cos\omega t - d_Z \sin\omega t) \quad (5.26)$$

$$\dot{d}_N = C_{21}\omega(-d_X \sin\omega t + d_Z \cos\omega t) + C_{23}\omega(-d_X \cos\omega t - d_Z \sin\omega t) \quad (5.27)$$

$$d_U = C_{31}(d_X \cos\omega t + d_Z \sin\omega t) + C_{32}d_Y + C_{33}(-d_X \sin\omega t + d_Z \cos\omega t) \quad (5.28)$$

As described above, the attitude errors in the east and north directions, and the accelerometer biases, as well as gyro biases in the X, Y and Z axes, become observable states through IMU rotations about the Y axis. Similarly, there is also a potential issue that affects the system observability, such that the pitch angle of zero reduces the observability of the accelerometer bias in the Y axis, as the error coefficient, C_{32}, becomes zero when pitch angle is zero according to Eq. (2.1).

5.3.3 System Observability with IMU Rotation about Z Axis

Similar to previous rotations about the X and Y axes, the accelerometer biases in the X, Y and Z axes can be derived from the vertical accelerometer bias and its first time derivative with IMU rotation about the Z axis, as described by Eq. (5.29) and (5.30).

$$b_U = C_{31}(b_X \cos\omega t - b_Y \sin\omega t) + C_{32}(b_X \sin\omega t + b_Y \cos\omega t) + C_{33} b_Z \tag{5.29}$$

$$\dot{b}_U = C_{31}\omega(-b_X \sin\omega t - b_Y \cos\omega t) + C_{32}\omega(b_X \cos\omega t - b_Y \sin\omega t) \tag{5.30}$$

The attitude errors and gyro biases in the east and north directions then become observable states with the determination of the accelerometer biases by Eq. (5.31) and (5.32). Finally, the gyro biases in the X, Y and Z axes, as well as the vertical gyro bias, can be determined.

$$b_E = C_{11}(b_X \cos\omega t - b_Y \sin\omega t) + C_{12}(b_X \sin\omega t + b_Y \cos\omega t) + C_{13} b_Z \tag{5.31}$$

$$b_N = C_{21}(b_X \cos\omega t - b_Y \sin\omega t) + C_{22}(b_X \sin\omega t + b_Y \cos\omega t) + C_{23} b_Z \tag{5.32}$$

Except for the azimuth error, other error states become observable when the IMU rotates about the Z axis. There is also a potential issue that affects the system observability. According to Eq. (2.1), C_{31} and C_{32} become zeroes when both the roll and pitch angles are zeroes. In that situation, the accelerometer biases in the X and Y axes become unobservable according to Eq. (5.29) and (5.30), which leads to a failure estimation of the accelerometer biases and attitude errors in the east and north directions, as well as the gyro biases. Eventually, the observable states reduce to velocity errors and vertical accelerometer bias.

Based on the above analysis, it appears that the three IMU rotations can improve the system observability without system maneuvers. The key for the improvements is twofold: 1) utilize the fact that the vertical accelerometer bias is observable with the velocity measurements; 2) IMU rotations change the geometry of the inertial sensor errors.

5.4 Turntable Tests and Analysis

Tests of the conventional and rotary INS are conducted using a tri-axial rotation table with both NAV440 and MTi-G to verify the improvements on system observability by IMU rotations. The rotary tests are conducted for IMU rotation about only the Y and Z axes, as the improvements by rotation about the X axis are similar to the ones by rotation about the Y axis. The MEMS IMU remains static on the rotation table for 5 minutes in the conventional INS test, while it rotates with the table at a designated rate for 5 minutes in rotary tests. As the rotation does not bring linear movement, the ZUPT is applied to estimate the attitude errors and inertial sensor errors in both the conventional and rotary INS tests using an EKF. The filter state vector includes 3 velocity errors, 3 attitude errors, 3 gyro biases and 3 accelerometer biases.

5.4.1 IMU Rotation about Y Axis

With the IMU axes defined as the X axis pointing right direction, the Y axis pointing forward, and the Z axis pointing upward, as shown in Figure 5.1, the rotation of the inner frame rotates the IMU about its Y axis when both the middle and outer frames remain still.

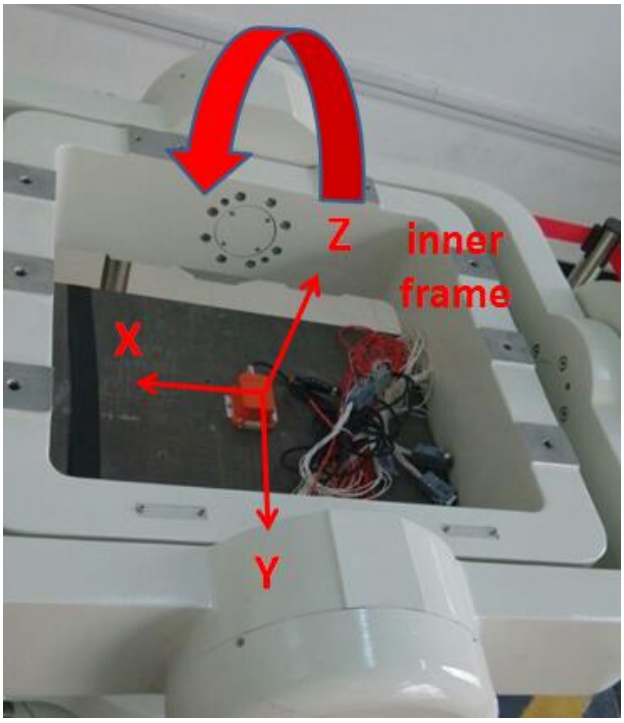

Figure 5.1 Rotation table set-up for IMU rotation about Y axis with middle frame at angle position of 0°

Two rotary INS tests are conducted with the middle frame remaining at angle positions of 0° and 30°, respectively, to study the effect of the pitch angle on the system observability, as shown in Figures 5.1 and 5.2. For each test, the IMU rotates about the Y axis with a constant rate of 10 °/s for 5 minutes. Apparently, the body frame of the IMU is aligned to the local level frame after the

initialization of the rotation table, with the middle frame remaining at the angle position of 0°, and the initial roll, pitch and azimuth are 0° 30° and 0°, when the middle frame remains at the angle position of 30°. The IMU data collections are same as the ones described in Chapter 4.

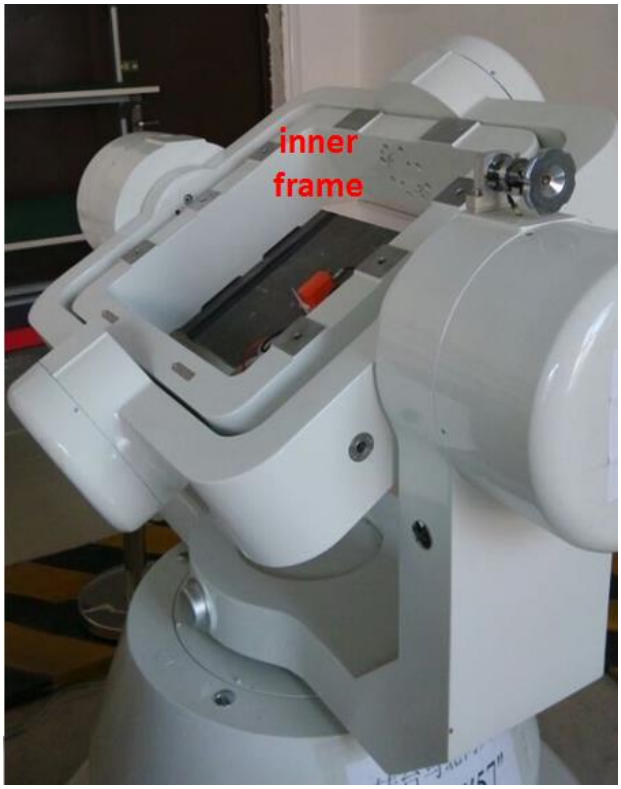

Figure 5.2 Rotation table set-up for IMU rotation about Y axis with middle frame at angle position of 30°

As the velocity errors can be directly observed with ZUPT, the analysis is focused on the attitude errors and inertial sensor biases. The obtained estimates of these errors using NAV440 and MTi-G are provided in the following paragraphs.

5.4.1.1 Rotary INS based on NAV440 with IMU Rotation about Y Axis

The obtained estimates of the accelerometer biases in the X and Y axes for the conventional INS test and the rotary INS tests with different pitch angles are given in Figure 5.3. The blue color represents the estimates in the conventional INS, the red color represents the estimates in the rotary INS with pitch of zero, and the green color represents the estimates in the rotary INS with pitch of 30°. As the accelerometer biases in both the X and Y axes are not observable states in the conventional INS, un-converged solutions are obtained. With the IMU rotation about the Y axis, the improved observability leads to quickly converged solutions for the bias of the X axis in the rotary INS with different pitch angles. Although the converged solution of the bias in the Y axis is obtained when pitch is 30 degrees, the reduced observability leads to the biased estimate when pitch is 0°.

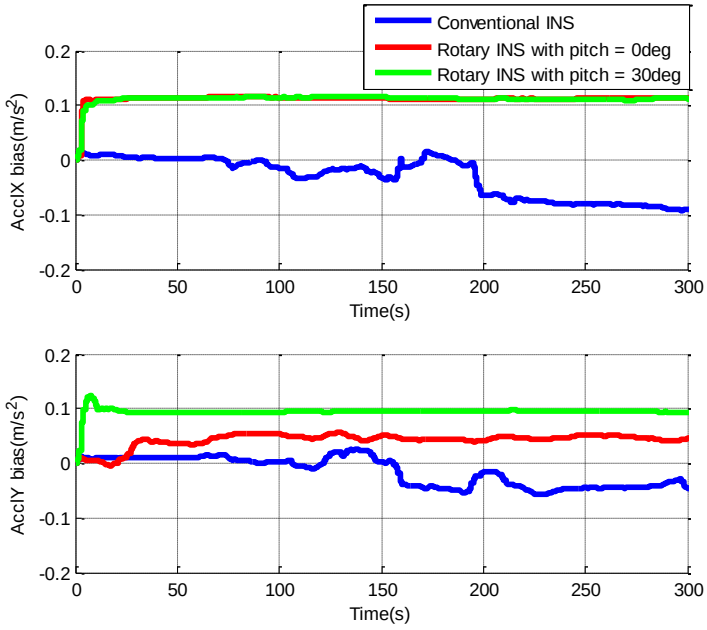

Figure 5.3 Estimates of accelerometer biases in X and Y axes for conventional INS and rotary INS with NAV440 when IMU rotates about Y axis

The means of the estimates of accelerometer biases in the X, Y and Z axes are summarized in Table 5.3 for the different inertial systems. Very similar estimates of the bias in the X axis are obtained in the rotary INS with different pitch angles, and the estimates of the bias in the Z axis are also consistent among the three inertial systems.

Table 5.3 Means of accelerometer bias estimates for conventional INS and rotary INS with NAV440 when IMU rotates about Y axis

	Accl X (m/s^2)	**Accl Y (m/s^2)**	**Accl Z (m/s^2)**
Conventional INS	-0.039	-0.021	0.058
Rotary INS with pitch of 0°	0.111	0.047	0.054
Rotary INS with pitch of 30°	0.113	0.095	0.052

The estimates of the roll and pitch errors for the three inertial systems with NAV440 are given in Figure 5.4. As the roll and pitch errors are coupled with the horizontal accelerometer biases, similar error characteristics are observed. The un-converged roll and pitch errors indicate that they are not observable in the conventional INS. With the improved observability by the IMU rotation, the quickly converged solutions of roll and pitch errors are obtained in the rotary INS with pitch angle of 30°. The reduced observability of the bias in the Y axis when pitch angle is zero also affects the pitch error estimation, as shown in the figure. The RMS of the roll and pitch errors are summarized in Table 5.4. In comparison to the errors in the conventional INS, the significantly reduced roll and pitch errors indicate that the horizontal accelerometer biases are more accurately estimated in the rotary INS.

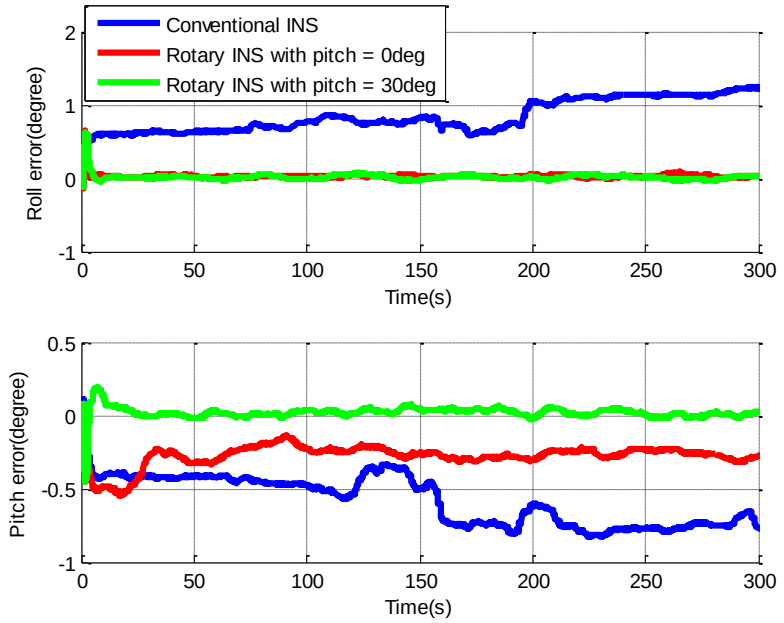

Figure 5.4 Estimates of roll and pitch errors for conventional INS and rotary INS with NAV440 when IMU rotates about Y axis

Figure 5.5 presents estimates of the azimuth errors and the gyro bias of the Z axis for the three inertial systems with NAV440. In the conventional INS, the azimuth error accumulates fast due to the fact that both the azimuth error and the gyro bias in the Z axis are unobservable in the absence of maneuvers. Because of the improved observability by IMU rotation, the gyro bias is quickly converged, and therefore, the azimuth error accumulation is effectively mitigated in the rotary inertial systems, though such error is still unobservable. The RMS of the azimuth errors are summarized in Table 5.4 for the different inertial systems. With IMU rotation, the azimuth error is reduced to less than 1° in the rotary INS.

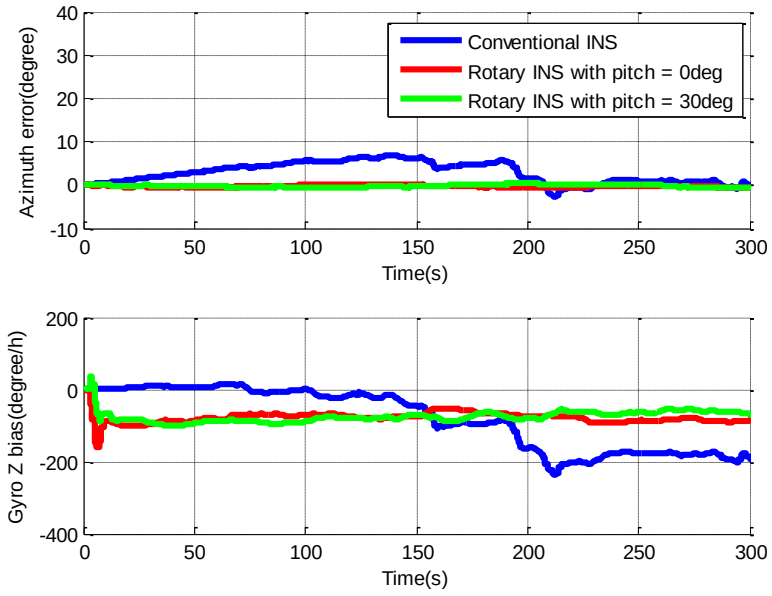

Figure 5.5 Estimates of azimuth errors and gyro bias in Z axis for conventional INS and rotary INS with NAV440 when IMU rotates about Y axis

Table 5.4 RMS of attitude errors for conventional INS and rotary INS with NAV440 when IMU rotates about Y axis

	Roll (°)	**Pitch (°)**	**Azimuth (°)**
Conventional INS	0.87	0.60	3.77
Rotary INS with pitch of 0°	0.03	0.28	0.35
Rotary INS with pitch of 30°	0.03	0.04	0.55

Figure 5.6 presents the estimates of gyro biases in the X and Y axes for different inertial systems. Consistent with previous analysis, quickly converged solutions are obtained for the biases in both the conventional INS and the rotary INS. The results do not show strong effects on the estimation of these biases by IMU rotation in the rotary INS.

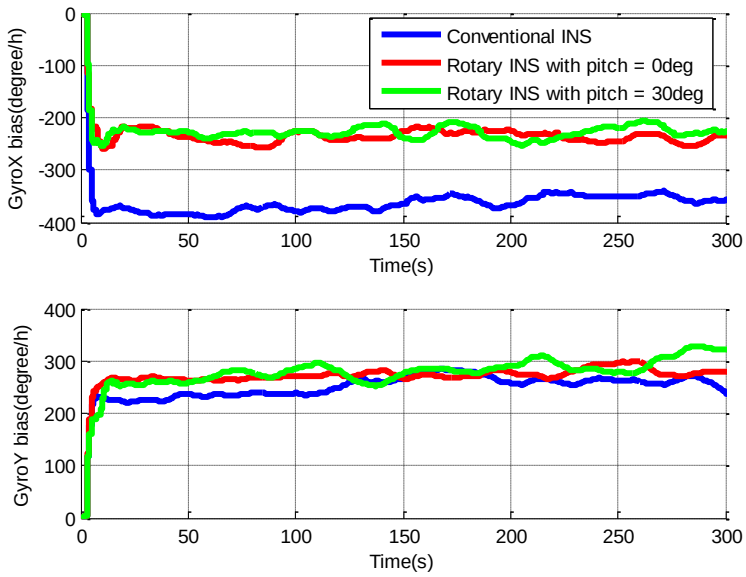

Figure 5.6 Estimates of gyro biases in X and Y axes for conventional INS and rotary INS with NAV440 when IMU rotates about Y axis

The means of the gyro bias estimates are summarized in Table 5.5 for different inertial systems with NAV440. Although there is no reference for these biases, the effective mitigations on the azimuth error accumulations indicate the correct estimation of the gyro bias of the Z axis in the rotary INS, whereas the accumulated azimuth error demonstrates the incorrect estimation of such error in the conventional INS. The stable pitch and roll errors also prove that the gyro biases of the X and Y axes are correctly estimated in the conventional and the rotary INS, as these attitude

errors are associated with the accelerometer and gyro biases of X and Y axes. The effect of incorrect gyro bias estimates on the attitude estimation will be discussed with the results for the IMU rotation about the Z axis. The differences between the horizontal gyro bias estimates in the conventional INS and the rotary INS mainly consist of the induced gyro biases by IMU rotation, the bias variations and the estimation errors.

Table 5.5 Means of gyro bias estimates for conventional INS and rotary INS with NAV440 when IMU rotates about Y axis

	Gyro X (°)	**Gyro Y (°)**	**Gyro Z (°)**
Conventional INS	-361.7	258.2	-98.5
Rotary INS with roll of 0°	-237.1	275.4	-75.0
Rotary INS with roll of 30°	-228.1	285.5	-74.0

5.4.1.2 Rotary INS based on MTi-G with IMU Rotation about Y Axis

The MTi-G sensor errors and attitude errors are also estimated in both the conventional and rotary INS tests. Figure 5.7 presents the estimates of the accelerometer biases in the X and Y axes for the different inertial systems. Although the converged solutions are obtained for both biases in the rotary INS with pitch angle of 30°, such errors cannot be estimated in the conventional INS. The reduced observability leads to fluctuated solutions for the accelerometer bias of the Y axis in the rotary INS when pitch angle is zero, as shown in Figure 5.8.

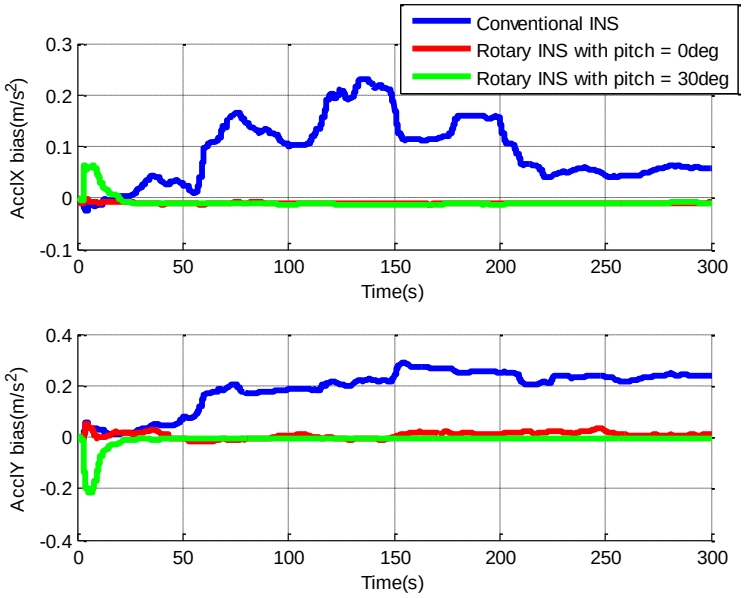

Figure 5.7 Estimates of accelerometer biases in X and Y axes for conventional INS and rotary INS with MTi-G when IMU rotates about Y axis

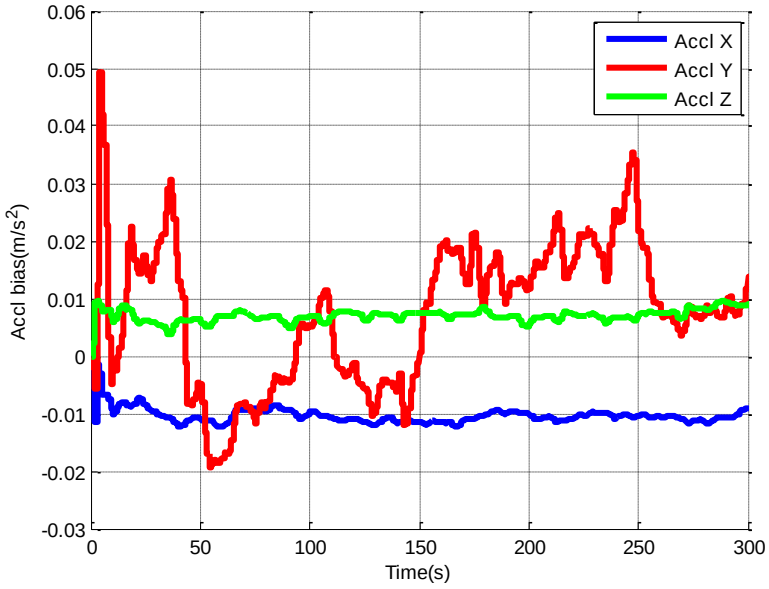

Figure 5.8 Estimates of accelerometer biases of rotary INS with MTi-G when pitch is zero and IMU rotates about Y axis

Figure 5.9 presents the estimates of the accelerometer bias in the Z axis for the three inertial systems with MTi-G. The quickly converged solutions indicate that such error is observable in the conventional INS and the rotary INS with different pitch angles. Table 5.6 summarizes the means of the accelerometer bias estimates.

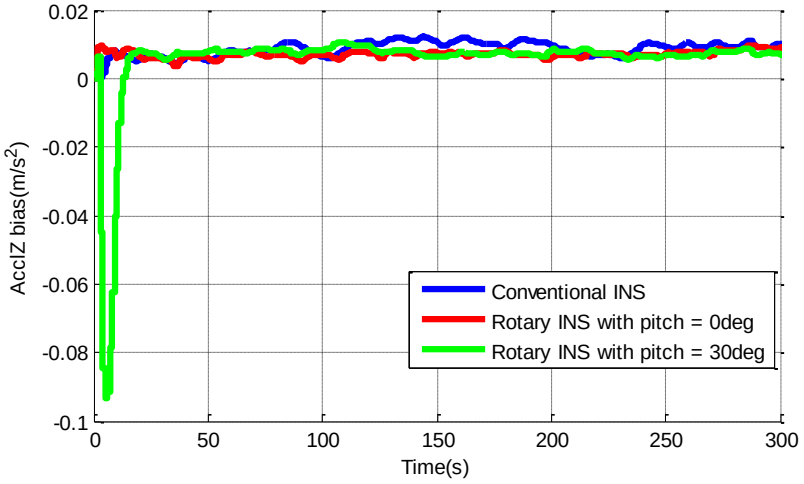

Figure 5.9 Estimates of accelerometer biases in Z axis for conventional INS and rotary INS with MTi-G when IMU rotates about Y axis

Table 5.6 Means of accelerometer bias estimates for conventional INS and rotary INS with MTi-G when IMU rotates about Y axis

	Accl X (m/s^2)	**Accl Y (m/s^2)**	**Accl Z (m/s^2)**
Conventional INS	0.112	0.223	0.009
Rotary INS with pitch of 0°	-0.010	0.007	0.007
Rotary INS with pitch of 30°	-0.011	-0.007	0.008

Figure 5.10 presents the estimates of the roll and pitch errors for different inertial systems. With the improved estimation of the accelerometer biases, the roll errors are quickly reduced to almost zero in the rotary systems. However, the reduced observability of the bias in the Y axis degrades the pitch accuracy when pitch is 0°, as shown in the figure. The RMS of the roll and pitch errors are summarized in Table 5.7. The greatly reduced roll and pitch errors verify the estimated accelerometer biases in the X and Y axes, though there is no reference.

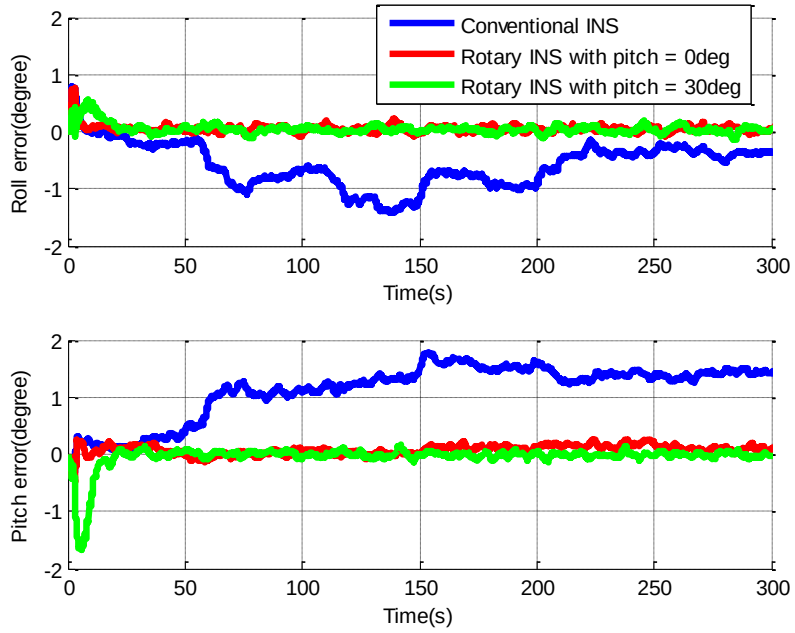

Figure 5.10 Estimates of roll and pitch errors for conventional INS and rotary INS with MTi-G when IMU rotates about Y axis

The estimates of the azimuth errors and the gyro bias of the Z axis are present in Figure 5.11 for the three inertial systems. Similarly, the improved observability by IMU rotation leads to the quickly converged estimates of the gyro bias, which effectively limits the azimuth error accumulation in the rotary INS. The RMS of the azimuth errors are summarized in Table 5.7,

and greater azimuth errors are obtained in the conventional INS, compared to the ones from NAV440, due to MTi-G's significant gyro errors.

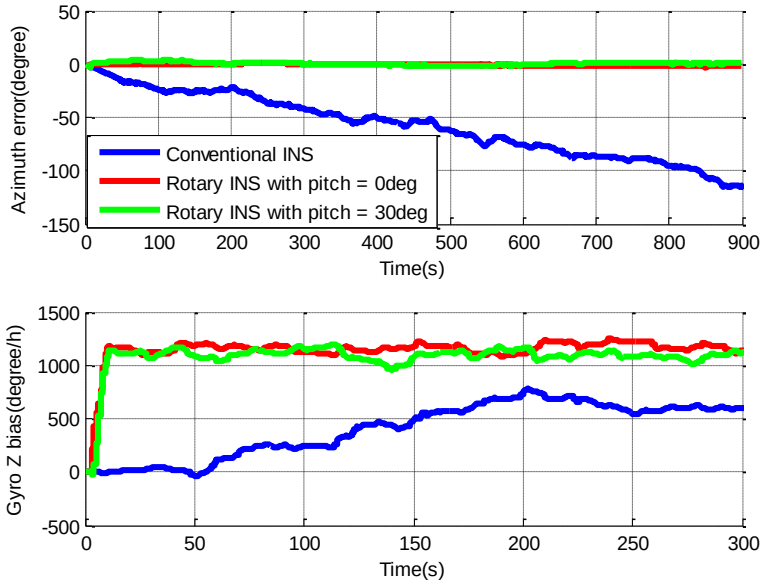

Figure 5.11 Estimates of azimuth errors and gyro bias in Z axis for conventional INS and rotary INS with MTi-G when IMU rotates about Y axis

Table 5.7 RMS of attitude errors for conventional INS and rotary INS with MTi-G when IMU rotates about Y axis

	Roll (°)	**Pitch (°)**	**Azimuth (°)**
Conventional INS	0.71	1.24	25.91
Rotary INS with pitch of 0°	0.07	0.11	0.78
Rotary INS with pitch of 30°	0.08	0.08	2.02

Figure 5.12 presents the obtained gyro biases of the X and Y axes for the different inertial systems and Table 5.8 summarizes their mean values. Similarly, converged estimates are obtained in the conventional and rotary systems and the IMU rotations do not have a strong effect on the estimations.

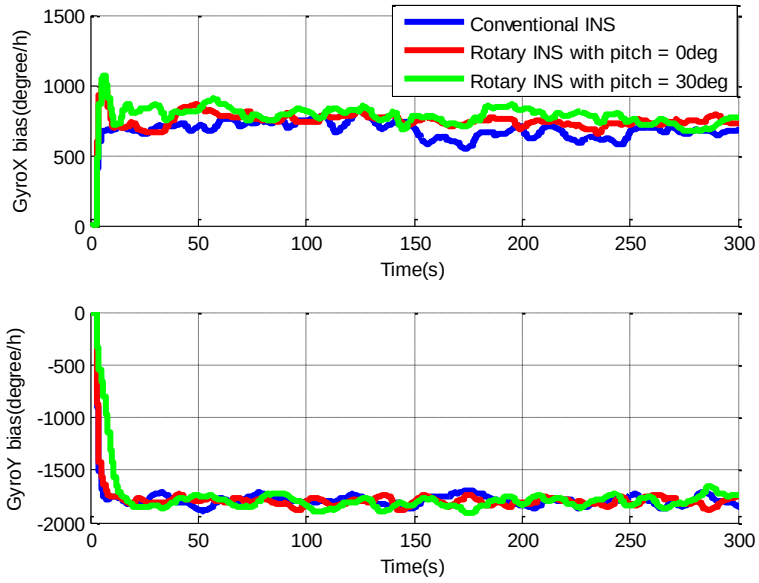

Figure 5.12 Estimates of gyro biases in X and Y axes for conventional INS and rotary INS with MTi-G when IMU rotates about Y axis

Table 5.8 Means of gyro bias estimates for conventional INS and rotary INS with MTi-G when IMU rotates about Y axis

	Gyro X (°/h)	**Gyro Y (°/h)**	**Gyro Z (°/h)**
Conventional INS	683.1	-1786.7	495.9
Rotary INS with pitch of 0°	748.2	-1802.1	1165.2
Rotary INS with pitch of 30°	777.1	-1804.9	1096.7

In summary, the rotary INS with IMU rotation about the Y axis significantly improves the observability of accelerometer biases in the X and Y axes, the roll and pitch errors, and the gyro bias in the Z axis. Even though the azimuth error is still unobservable, the estimation of the gyro bias in the Z axis can effectively limit its accumulation. The observability of the accelerometer bias in the Y axis and the pitch error is reduced when pitch is zero. Although only the results for IMU rotation about the Y axis are present, similar results can be obtained for IMU rotation about the X axis. The only difference is that the roll angle of zero will degrade the observability of accelerometer bias in the X axis and the roll error.

5.4.2 IMU Rotation about Z Axis

For the implementation of the IMU rotation about the Z axis, the middle frame of the rotation table is rotated to vertical position (90°), and the IMU axes are re-defined as the X axis pointing left direction, the Y axis pointing forward and the Z axis pointing upward, as shown in Figure 5.13. Then the rotation of the inner frame rotates the IMU about its Z axis.

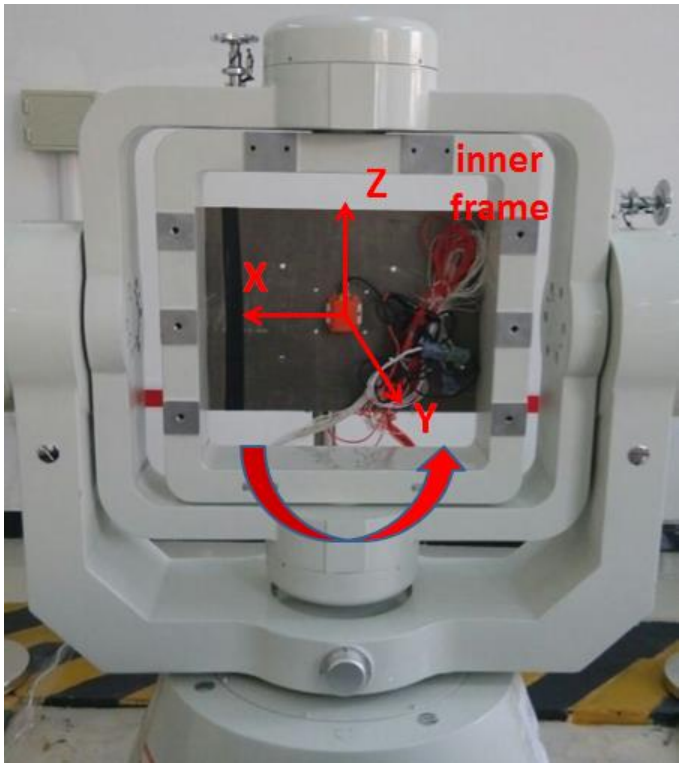

Figure 5.13 Rotation table set-up for IMU rotation about Z axis with middle frame at the angle position of 90°

To investigate the effect of the tilt angle on the system observability, two rotary INS tests are conducted with middle frame remaining at angle positions of 90° and 60°, respectively, as shown in Figures 5.13 and 5.14. For each test, the IMU rotates about the Z axis with the rotation rate of 10 °/s for 5 minutes. Similarly, the body frame is aligned to the local level frame after the initialization of the rotation table, with middle frame remaining at the angle position of 90°, and the initial roll, pitch and azimuth are 0° 30° and 0°, when the middle frame remains at the angle position of 60°.

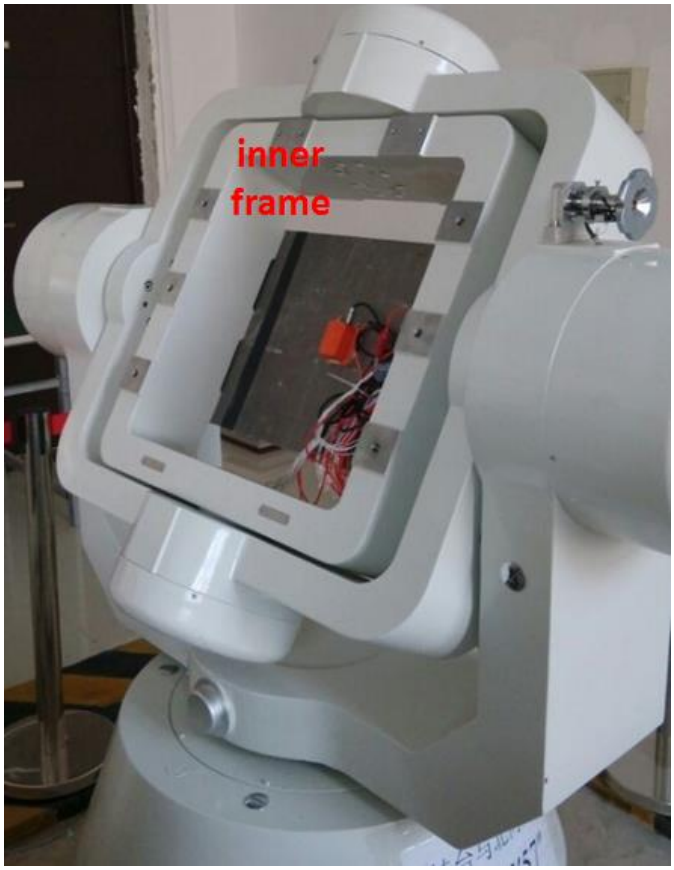

Figure 5.14 Rotation table set-up for IMU rotation about Z axis with middle frame at angle position of 60°

The estimates of the attitude errors, as well as inertial sensor biases, are analyzed to study the improvements on the system observability by IMU rotation about the Z axis.

5.4.2.1 Rotary INS based on NAV440 with IMU Rotation about Z Axis

The estimates of accelerometer biases in the X and Y axes for different inertial systems with NAV440 are given in Figure 5.15. Consistent with previous analysis, although the bias estimates in both axes are quickly converged in the rotary INS when pitch is 30°, they cannot converge when pitch is zero, due to the severely degraded observability. Table 5.9 summarizes the means

of the estimated accelerometer biases for different inertial systems. Apparently, the IMU rotation about the Z axis does not affect the observability of the bias in the Z axis.

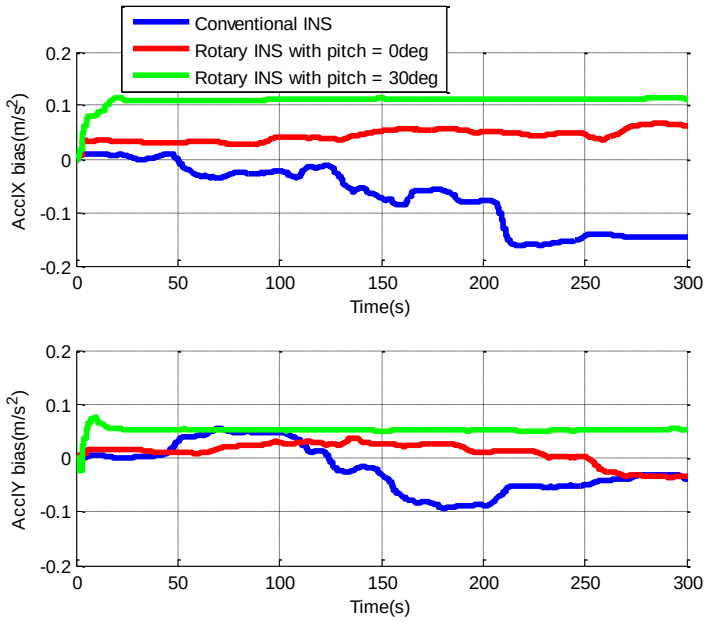

Figure 5.15 Estimates of accelerometer biases in X and Y axes for conventional INS and rotary INS with NAV440 when IMU rotates about Z axis

Table 5.9 Means of accelerometer bias estimates for conventional INS and rotary INS with NAV440 when IMU rotates about Z axis

	Accl X (m/s^2)	**Accl Y (m/s^2)**	**Accl Z (m/s^2)**
Conventional INS	-0.085	-0.027	-0.089
Rotary INS with roll of 0°	0.046	0.011	-0.091
Rotary INS with roll of 30°	0.112	0.052	-0.092

Figure 5.16 presents the estimates of the roll and pitch errors for the three inertial systems with NAV440. With converged estimates of the accelerometer biases in the X and Y axes, the roll and pitch errors are quickly reduced to around zero in the rotary INS with pitch of 30°. Obviously, oscillating errors are observed in the roll and pitch errors in the rotary INS when pitch is zero due to the degraded observability of horizontal accelerometer biases. According to the observable state combinations of the rotary INS, summarized in Table 5.2, the gyro biases in the east and north directions can be derived from the following two observable state combinations, $g(-\omega_{ie}\sin L\varepsilon_E + d_N) + \dot{b}_E$ and $-g(\omega_{ie}\sin L\varepsilon_N - \omega_{ie}\cos L\varepsilon_U + d_E) + \dot{b}_N$. However, the degraded observability of the accelerometer biases leads to incorrect estimates of gyro biases. Finally the modulation of the gyro bias residuals by IMU rotation results in the oscillating errors.

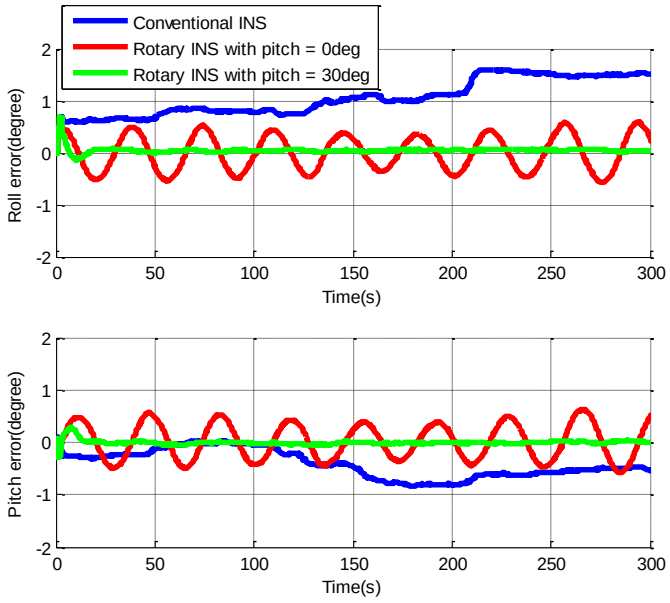

Figure 5.16 Estimates of roll and pitch errors for conventional INS and rotary INS with NAV440 when IMU rotates about Z axis

The RMS of the roll and pitch errors are summarized in Table 5.10. As expected, the severely degraded observability of the accelerometer and gyro biases in the X and Y axes results in significant roll and pitch errors in the rotary INS when pitch is zero.

Figure 5.17 presents the estimates of the azimuth errors and the gyro bias of the Z axis for the different inertial systems with NAV440. Although the azimuth error accumulation is effectively mitigated by the quickly converged estimates of gyro bias in the rotary INS when pitch is 30°, such error accumulates fast due to the incorrect estimate of the gyro bias when pitch is zero. The RMS of the azimuth errors are summarized in Table 5.10 for the different inertial systems.

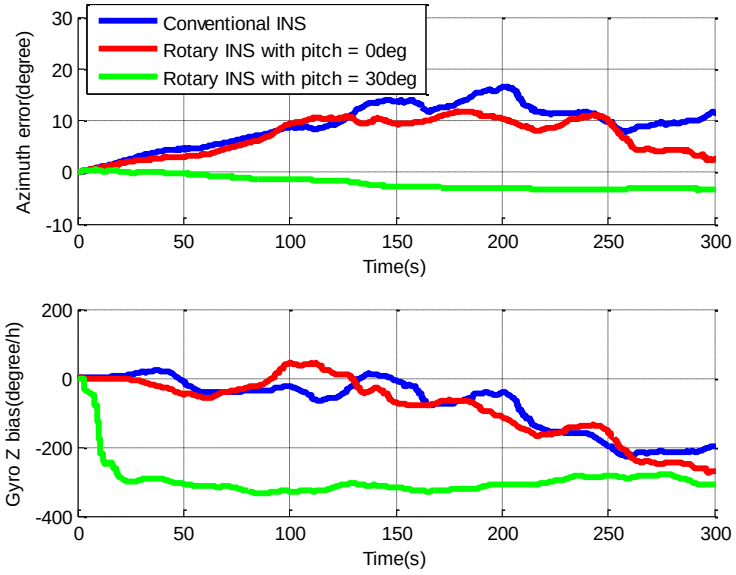

Figure 5.17 Estimates of azimuth errors and gyro bias in Z axis for conventional INS and rotary INS with NAV440 when IMU rotates about Z axis

Table 5.10 RMS of attitude errors for conventional INS and rotary INS with NAV440 when IMU rotates about Z axis

	Roll (°)	Pitch (°)	Azimuth (°)
Conventional INS	1.11	0.49	10.11
Rotary INS with roll of 0°	0.33	0.34	7.97
Rotary INS with roll of 30°	0.04	0.04	2.36

Figure 5.18 presents the estimates of the gyro biases in the X and Y axes for different inertial systems with NAV440. As mentioned previously, the degraded observability leads to the un-converged solutions for gyro biases of the X and Y axes in the rotary INS when pitch is zero, while converged solutions are obtained in the conventional INS and the rotary INS when pitch is 30°. Table 5.11 summarizes the means of gyro bias estimates for different inertial systems. The oscillating roll and pitch errors, and quickly accumulated azimuth errors, indicate the incorrect estimations of gyro biases of the X, Y and Z axes in the rotary INS with pitch of zero, while the small attitude errors demonstrate that such biases can be correctly determined when pitch is 30°.

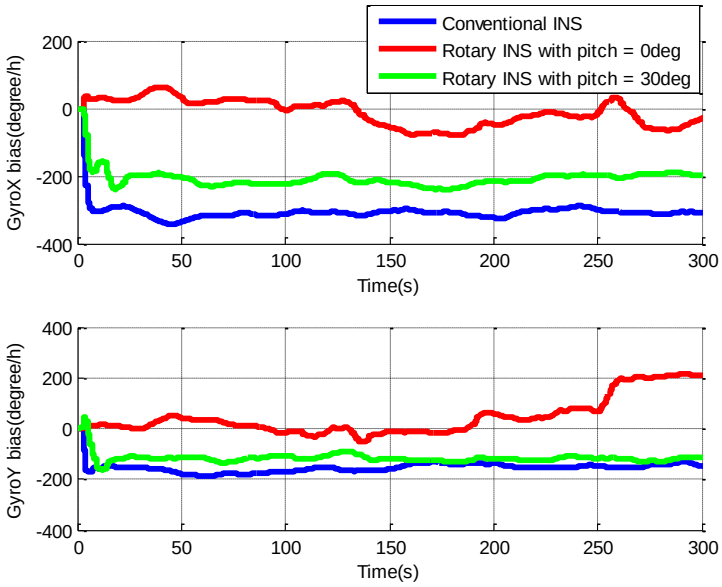

Figure 5.18 Estimates of gyro biases in X and Y axes for conventional INS and rotary INS with NAV440 when IMU rotates about Z axis

Table 5.11 Means of gyro bias estimates for conventional INS and rotary INS with NAV440 when IMU rotates about Z axis

	Gyro X (°)	Gyro Y (°)	Gyro Z (°)
Conventional INS	-308.4	-154.8	-92.3
Rotary INS with roll of 0°	-22.6	45.5	-95.2
Rotary INS with roll of 30°	-213.0	-118.5	-309.3

5.4.2.2 Rotary INS based on MTi-G with IMU Rotation about Z Axis

Similar results are obtained for the inertial systems with MTi-G. The estimates of the accelerometer biases in X and Y axes cannot be converged in the rotary INS when pitch is zero as shown in Figure 5.19, while converged estimates are obtained when pitch is 30°. The estimates of bias in the Z axis are still quickly converged in the conventional and rotary systems, as shown in Figure 5.20. Table 5.12 summarizes the means of the accelerometer bias estimates for the different inertial systems with MTi-G.

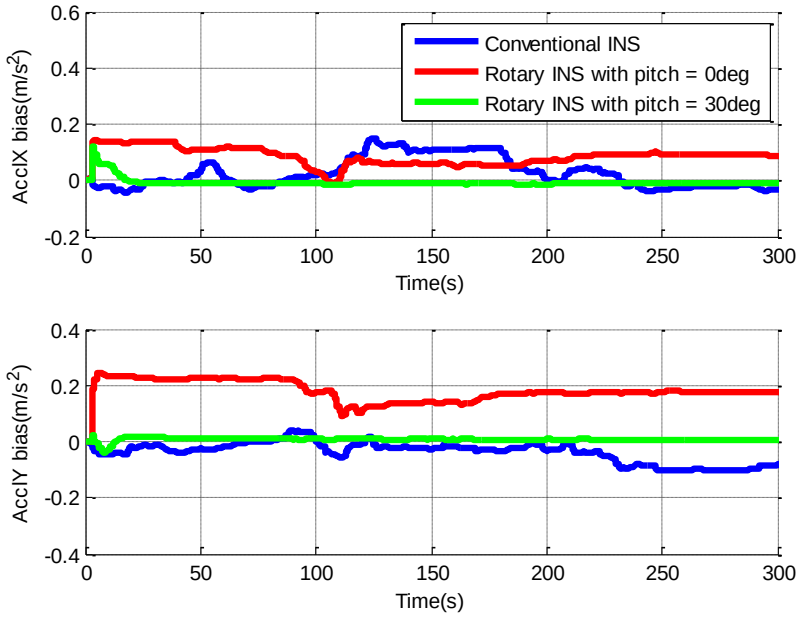

Figure 5.19 Estimates of accelerometer biases in X and Y axes for conventional INS and rotary INS with MTi-G when IMU rotates about Z axis

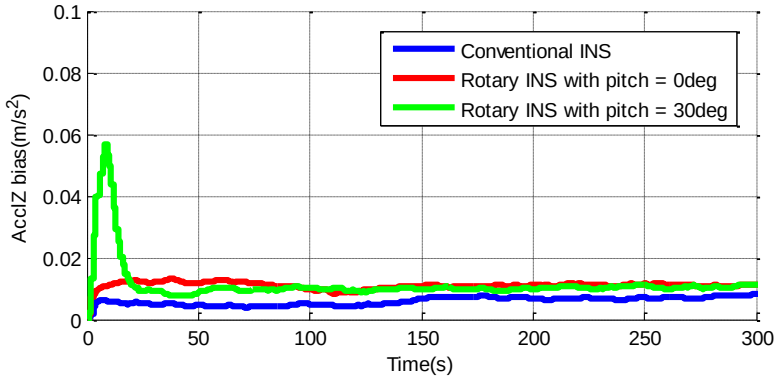

Figure 5.20 Estimates of accelerometer biases in Z axis for conventional INS and rotary INS with MTi-G when IMU rotates about Z axis

Table 5.12 Means of accelerometer bias estimates for conventional INS and rotary INS with MTi-G when IMU rotates about Z axis

	Accl X (m/s2)	**Accl Y (m/s2)**	**Accl Z (m/s2)**
Conventional INS	0.033	-0.039	0.006
Rotary INS with pitch of 0°	0.076	0.170	0.011
Rotary INS with pitch of 30°	-0.012	0.008	0.010

As mentioned previously that the roll and pitch errors are coupled with horizontal accelerometer biases, similar characteristics are observed in the roll and pitch errors as shown in Figures 5.21. The reduced system observability results in oscillating roll and pitch errors in rotary INS when pitch is zero. The RMS of the roll and pitch errors for different inertial system with MTi-G are summarized in Table 5.13.

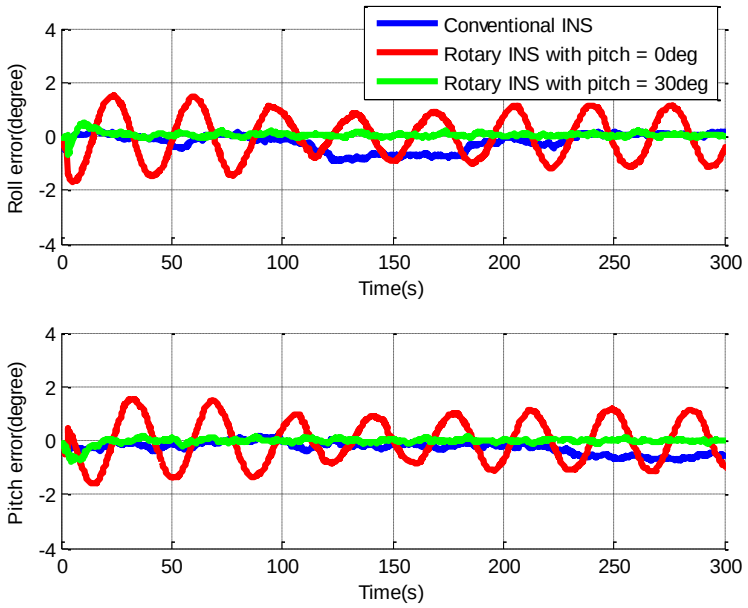

Figure 5.21 Estimates of roll and pitch errors for conventional INS and rotary INS with MTi-G when IMU rotates about Z axis

The estimates of the azimuth error and the gyro bias of the Z axis are presented in Figure 5.22 for the different inertial systems with MTi-G. Although the azimuth error accumulation is limited in the rotary INS with pitch of 30°, it grows rapidly when pitch is zero. A statistical summary of the azimuth errors is provided in Table 5.13 for the different inertial systems.

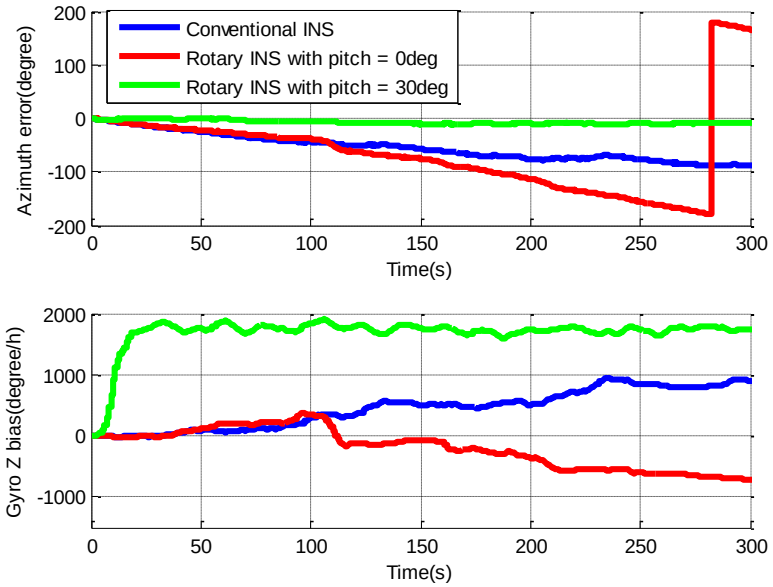

Figure 5.22 Estimates of azimuth errors and gyro bias in Z axis for conventional INS and rotary INS with MTi-G when IMU rotates about Z axis

Table 5.13 RMS of attitude errors for conventional INS and rotary INS with MTi-G when IMU rotates about Z axis

	Roll (°)	**Pitch (°)**	**Azimuth (°)**
Conventional INS	0.39	0.34	59.7
Rotary INS with pitch of 0°	0.82	0.85	101.13
Rotary INS with pitch of 30°	0.08	0.08	2.96

Figure 5.23 presents the estimated gyro biases of the X and Y axes for the different inertial systems with MTi-G. Similarly, the degraded observability leads to biased estimates in the rotary INS when pitch is zero. The means of the gyro bias estimates are summarized in Table 5.14 for different inertial systems. The small attitude errors verify that correct estimates are obtained for the gyro biases in the rotary INS with pitch of 30°, while the oscillating attitude errors and the quickly accumulated azimuth error indicate the incorrect estimation of these biases when pitch is zero.

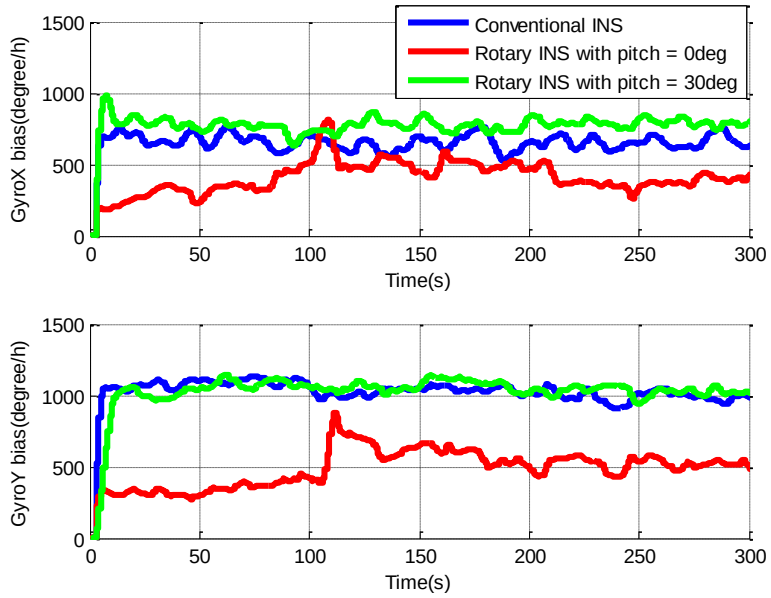

Figure 5.23 Estimates of gyro biases in X and Y axes for conventional INS and rotary INS with MTi-G when IMU rotates about Z axis

Table 5.14 Means of gyro bias estimates for conventional INS and rotary INS with MTi-G when IMU rotates about Z axis

	Gyro X (°/h)	Gyro Y (°/h)	Gyro Z (°/h)
Conventional INS	653.6	1028.1	538.3
Rotary INS with pitch of 0°	442.9	531.6	-243.4
Rotary INS with pitch of 30°	776.1	1056.4	1766.0

Different from the IMU rotation about the X or Y axes, the tilt angle plays a very important role for the rotary INS with IMU rotation about the Z axis. With the tilt angle, the IMU rotation significantly improves the observability of accelerometer biases in the X and Y axes, the roll and pitch errors, as well as the gyro bias in the Z axis, which leads to more accurate attitude solutions. However, the rotation about the Z axis severely degrades the system observability when no tilt angle is present, and the observable states are reduced to velocity errors and vertical accelerometer bias, which results in significant attitude errors.

Chapter Six: Development of Integrated GNSS and MEMS-based Rotary INS

Previous research has demonstrated that the IMU rotation about the Z axis can effectively reduce the navigation errors in the east-north plane. Based on that, this chapter presents an integrated system of GNSS and the rotary INS with a low-cost MEMS IMU for bridging GNSS outages. The proposed integrated system can significantly reduce the navigation errors during GNSS outages, and therefore offers longer autonomous navigation performance without external aiding in GNSS challenging environments. The integration scheme of the proposed system is present first, including the filter implementations. An observability analysis is then conducted for the proposed system, indicating that although the system observability is poor for a levelly placed rotary INS with IMU rotation about the Z axis, the vehicle maneuvers turn the system a completely observable system. By using a single-axis rotation table, kinematic field tests are conducted with both NAV440 and MTi-G to verify the improvements on the navigation performance of the proposed integrated systems during GNSS outages.

6.1 Integration of GNSS and MEMS-based Rotary INS

The GNSS and rotary INS are loosely integrated in this research due to its simplicity of implementation. The flowchart of the integrated system is given in Figure 6.1. The accelerometer and gyro readings collected in the sensor frame are first transformed to the body frame, then the mechanization algorithm is used to derive the INS solutions based on the transformed inertial data. An EKF is employed to fuse the position and velocity solutions from both GNSS and the rotary INS to derive the corrections for position, velocity and attitude solutions, as well as the

inertial sensor errors. Finally, the system outputs the corrected INS position, velocity and attitude solutions.

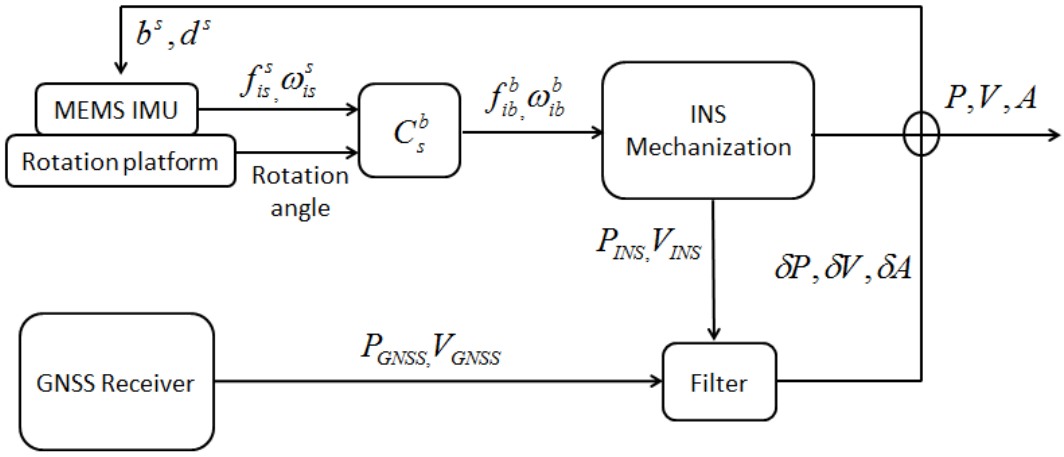

Figure 6.1 System flowchart of integrated GNSS and rotary INS

A 15-state vector, including 3 position errors in the local level frame, 3 velocity errors in the local level frame, 3 attitude errors in the local level frame, 3 accelerometer biases in the sensor frame, and 3 gyro biases in the sensor frame, is employed to represent the system errors as shown in Eq. (6.1).

$$x = \begin{bmatrix} \delta r^n & \delta v^n & \varepsilon^n & b^s & d^s \end{bmatrix}^T \tag{6.1}$$

where $\delta r^n = \begin{bmatrix} \delta\varphi & \delta\lambda & \delta h \end{bmatrix}^T$ represents the position errors in navigation frame

The error model given in Eq. (2.16) ~ (2.18) is employed to describe the position, velocity and attitude errors, and the 1st order Gauss-Markov (GM) random process is used to model the random variation for both the accelerometer and gyro biases. The GM model parameters are

obtained from the autocorrelation analysis of the collected MEMS IMU data under static condition (Nassar, 2003)**.**

In a loose integration scheme, the GNSS position and velocity are used as measurements to estimate the INS errors, so the measurement model of the integration filter can be described by Eq. (6.2). More details regarding the implementation of the integration filter can be referred to Shin (2001) and Du (2010).

$$H = \begin{bmatrix} I_{3\times3} & 0_{3\times3} & 0_{3\times3} & 0_{3\times3} & 0_{3\times3} \\ 0_{3\times3} & I_{3\times3} & 0_{3\times3} & 0_{3\times3} & 0_{3\times3} \end{bmatrix} \tag{6.2}$$

6.2 Observability Analysis of Integrated System

As the integrated GNSS and inertial systems are usually involved in the kinematic applications, the system observability is analyzed in conditions where strong maneuvers are frequently experienced. The observability analysis of the integrated system with the conventional INS is present first, then followed by the analysis for the integrated system with the rotary INS.

With the horizontal accelerations, the velocity error model can be rewritten as Eq. (6.3) ~ (6.5). The azimuth error is present in the velocity error equation of the east and north directions, and the roll and pitch errors are present in the velocity error equation of the vertical direction. So with the horizontal accelerations and their variations, the roll, pitch and azimuth errors can be determined and become observable states.

$$\delta\dot{V}_E = 2\omega_{ie}\sin\varphi\delta V_N - 2\omega_{ie}\cos\varphi\delta V_U - f_N\varepsilon_U + g\varepsilon_N + b_E \tag{6.3}$$

$$\delta\dot{V}_N = -2\omega_{ie}\sin\varphi\delta V_E + f_E\varepsilon_U - g\varepsilon_E + b_N \tag{6.4}$$

$$\delta\dot{V}_U = 2\omega_{ie}\cos\varphi\delta V_E + f_N\varepsilon_E - f_E\varepsilon_N + b_U \tag{6.5}$$

According to Table 5.1, the accelerometer biases in the east and north directions become observable with the determination of the roll and pitch errors, and the gyro biases, especially the bias in the Z axis, also become observable after the determination of the attitude errors. Apparently, the presence of the horizontal accelerations makes the system completely observable.

Eq. (6.3) ~ (6.5) can still be used to describe the velocity errors in the rotary INS, as the rotation does not introduce any linear movement in the IMU. According to Table 5.2, the accelerometer biases in the east and north directions, as well as three gyro biases, become observable with the determination of the attitude errors, and then the system becomes a completely observable system.

In summary, for the integrated systems of GNSS with both the conventional INS and rotary INS, the horizontal accelerations and their variations make them completely observable systems. However, in the absence of the horizontal accelerations, the observability of most error states are still poor, as described in Chapter 5. Based on the kinematic field tests, a covariance analysis is conducted to further study the observability of INS errors for the integrated systems.

6.3 Field Tests and Analysis

The kinematic field tests are conducted based on a land vehicle and the single-axis rotation table is used as the rotation platform. The descriptions of the rotation table, the test equipment set-up, as well as the data collections, are the same as those used for the kinematic tests described in Chapter 4.

6.3.1 Field Test and Data Descriptions

A loop trajectory is designated for the field tests, which includes the rectangular turn, the circle and the straight line, as shown in Figure 6.2. Two types of field tests, namely tests of integrated system with the conventional INS, and tests of integrated system with the rotary INS, are conducted and their details are provided below.

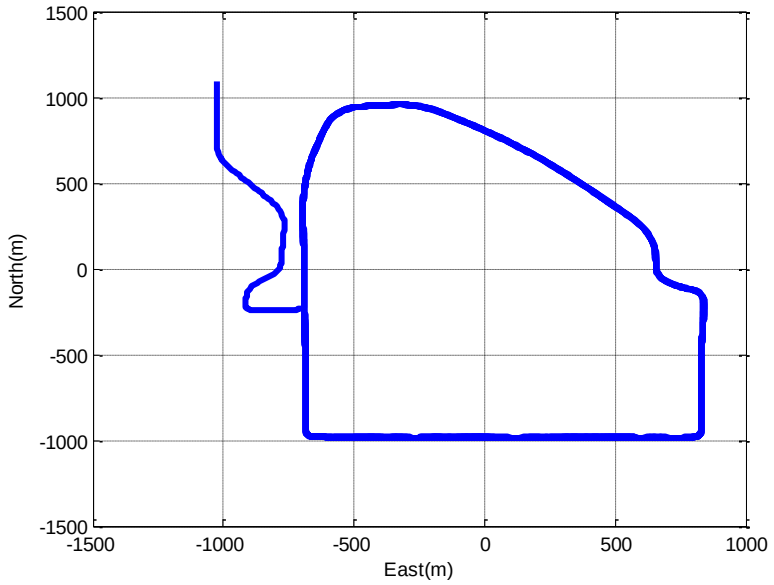

Figure 6.2 Trajectory of kinematic field tests

1) Tests of Integrated Systems with the Conventional INS

The tests start with an initialization process during which the vehicle remains static for 5 minutes to solve the initial attitude solutions using the SPAN system. Subsequently, the vehicle remains still for 30 seconds before it travels along the designated trajectory. During the whole test, the MEMS IMU remains static relative to the vehicle (the rotating table is non-rotating). Not including the initialization time, the test lasts for approximately 33 minutes (30 seconds for static period and 32.5 minutes for kinematic period). The collected GNSS data of SPAN is processed by the Waypoint GrafNav from NovAtel to derive the position and velocity information, which is loosely integrated with the collected MEMS IMU data to derive the solutions for the integrated system, with initial attitude obtained from the SPAN. The reference solutions are generated by processing the SPAN data (including both the GNSS data and LCI data) using Waypoint Inertial Explorer. The MTi-G and NAV440 are employed in the tests separately.

2) Tests of Integrated Systems with the Rotary INS

After the same initialization process, the vehicle remains still for about 30 seconds and then is driven along the trajectory. The MEMS IMU remains still during the initialization process and it starts rotating about the Z axis with designated rotation rates immediately after the initialization. The test also lasts for 33 minutes, excluding the time for the initialization process. The position and velocity obtained by processing the collected GNSS data of SPAN using Waypoint GrafNav are loosely integrated with rotary MEMS IMU data to derive the navigation solutions for the integrated system, with initial attitude obtained from the SPAN. The reference solutions are obtained in the same way as in 1). MTi-G and NAV440 are employed in the tests separately.

According to the analysis in Chapter 4, the designated rotation rate for MTi-G is 10 °/s, while the rate for NAV440 is 20 °/s.

6.3.2 Covariance Analysis of the Integrated Systems

The covariance matrices from the integration filter are analyzed to study the observability of INS errors for both the integrated systems with the conventional and rotary INS. As INS position and velocity errors are directly observed with the GNSS measurements, the covariance analysis will be focused on the attitude errors, as well as sensor biases. The results obtained with MTi-G are given below.

The obtained STDs of the pitch and roll errors for both of the integrated systems are provided in Figure 6.3. The STDs are dramatically reduced in both integrated systems when the vehicle starts moving, which indicates the improved observability of the pitch and roll errors with horizontal accelerations.

As the roll and pitch errors are coupled with the horizontal accelerometer biases, similar STDs are obtained for the accelerometers biases in the X and Y axes, compared to the ones for the roll and pitch errors, as shown in Figure 6.4.

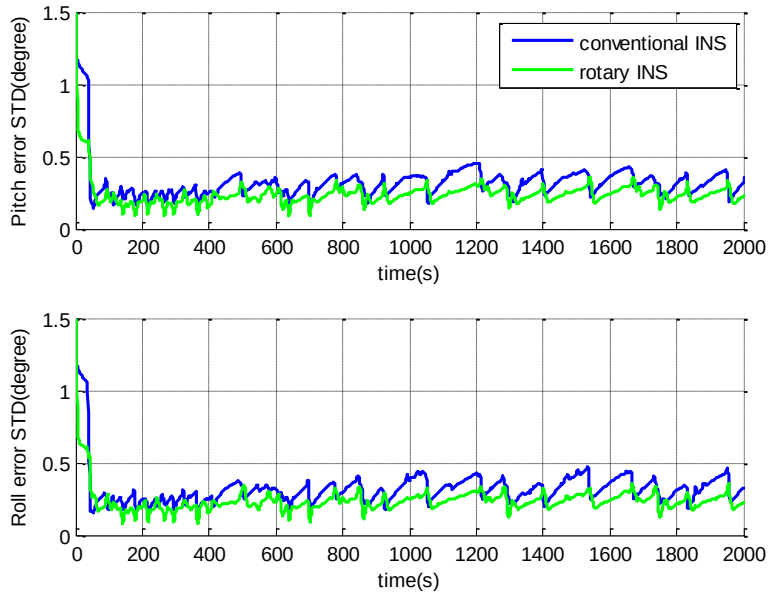

Figure 6.3 STDs of pitch and roll errors for integrated systems with MTi-G

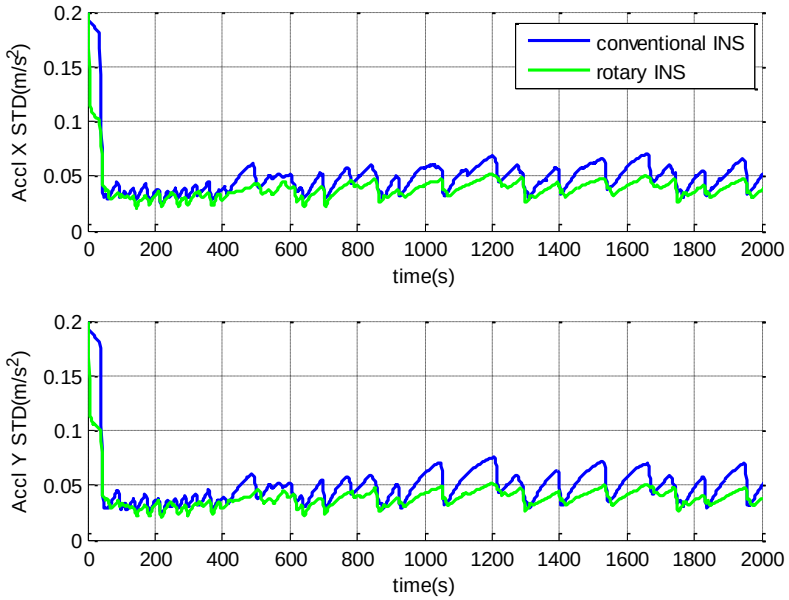

Figure 6.4 STDs of accelerometer biases in X and Y axes for integrated systems with MTi-G

The STDs of the azimuth error and the gyro bias in the Z axis are given in Figure 6.5. Before the vehicle movement, the STDs of the azimuth error accumulate in both systems, as such error and the gyro bias are unobservable without maneuvers. With the horizontal accelerations by the vehicle movement, the observability of the two errors is improved, and their STDs are largely reduced immediately.

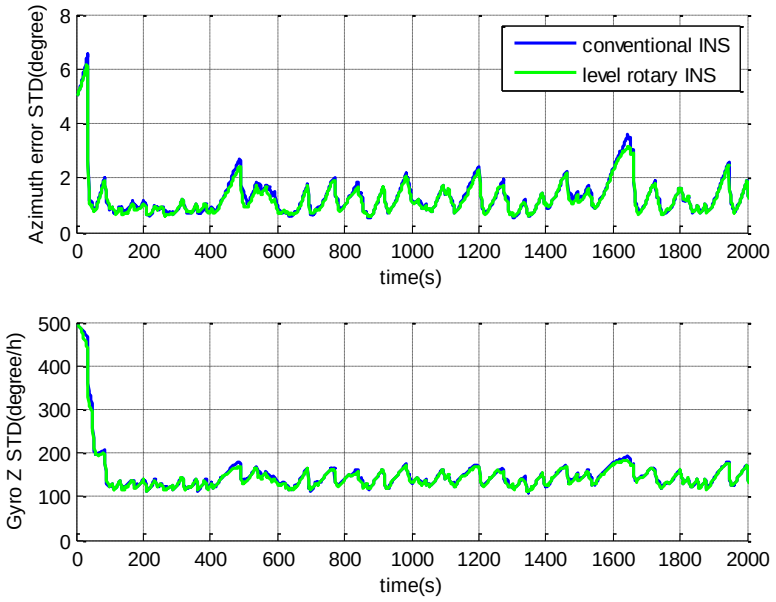

Figure 6.5 STDs of azimuth error and gyro bias in Z axis for integrated systems with MTi-G

The STDs of the gyro biases in the X and Y axes are specified in Figure 6.10. The STDs are quickly dropped during the static period for the integrated system with the conventional INS, while they are reduced after the vehicle movement for the integrated system with the rotary INS. This is consistent to the analysis in Chapter 5, which states that the horizontal gyro biases are unobservable for the levelly-installed rotary INS without maneuvers. It should be noted that the

system with the conventional INS outputs the smaller and more stable STDs. This is because the estimation error of the horizontal accelerometer biases will affect the estimation of the horizontal gyro biases in the rotary INS.

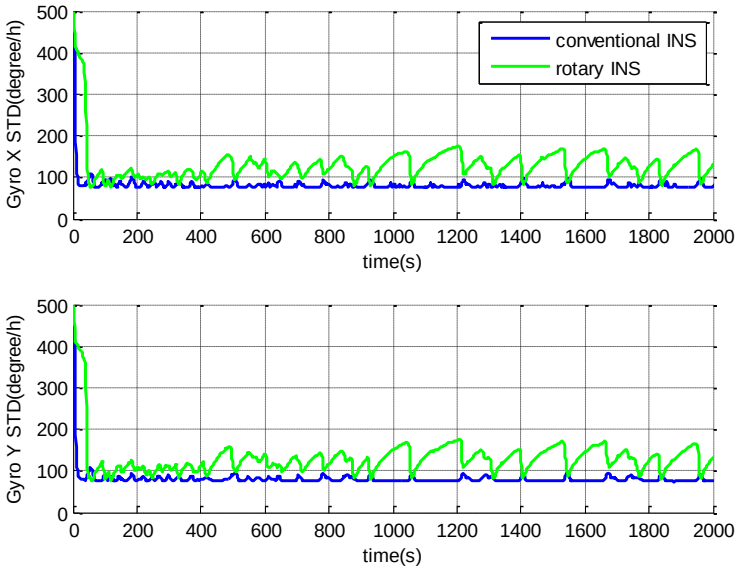

Figure 6.6 STDs of gyro biases in X and Y axes for integrated systems with MTi-G

Although only the error STDs from the integrated systems with MTi-G are present, similar results can be obtained by using NAV440. In summary, the system maneuvers significantly improve the system observability of both integrated systems. Although the attitude errors, the horizontal accelerometer biases, and the gyro biases are unobservable in the rotary INS with IMU rotation about the Z axis when both roll and pitch are zeroes, the maneuvers make all these errors become observable states.

6.3.3 Navigation Error Analysis of Integrated Systems without GNSS Outages

Without simulating any GNSS outages, the navigation errors of both the integrated systems with the conventional and rotary INS are evaluated by comparing them to the corresponding reference solutions.

6.3.3.1 Navigation Error Analysis of Integrated Systems with NAV440

The attitude errors of both the integrated systems with NAV440 are given in Figure 6.7. With continuous GNSS measurements, the roll and pitch errors are well bounded in small values for both integrated systems. The oscillating errors are not observed in the roll and pitch for the integrated systems with the rotary INS, which indicates that the gyro biases in the X and Y axes are correctly estimated. The RMS values of the attitude errors are calculated for both the integrated systems and summarized in Table 6.1, which demonstrates that very similar attitude accuracies are obtained for both systems.

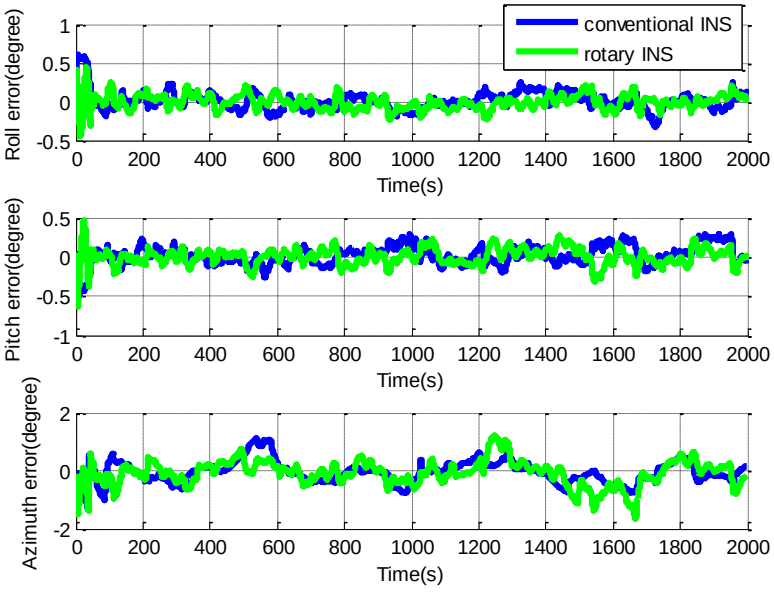

Figure 6.7 Attitude errors of integrated systems with NAV440

Table 6.1 RMS of attitude errors for integrated systems with NAV440

RMS	Roll (°)	Pitch (°)	Azimuth (°)
Integrated System with Conventional INS	0.12	0.12	0.39
Integrated System with rotary INS	0.11	0.12	0.44

Table 6.2 summarizes the RMS values of the position and velocity errors. As the GNSS position and velocity integrated with MEMS IMU data are derived from the SPAN data that is used to generate the reference solutions, the solutions of both integrated systems are highly consistent with the reference solutions.

Table 6.2 RMS of position and velocity errors for integrated systems with NAV440

RMS	Latitude (cm)	Longitude (cm)	Height (cm)	Ve (cm/s)	Vn (cm/s)	Vu (cm/s)
Integrated System with Conventional INS	1.9	1.8	1.5	1.9	1.9	1.3
Integrated System with rotary INS	1.9	1.7	1.5	1.8	1.9	1.3

6.3.3.2 Navigation Error Analysis of Integrated Systems with MTi-G

Figure 6.8 presents the attitude errors of both the integrated system with MTi-G. The roll and pitch errors are well bounded in 0.5° in most of the time for both systems, and the oscillating errors are not observed. During the initial static period, the azimuth errors accumulate in both the integrated systems, and they are quickly reduced to around zero after the vehicle starts moving, as shown in the figure. Table 6.3 summarizes the RMS values of the attitude errors. Obviously, both systems offer similar results.

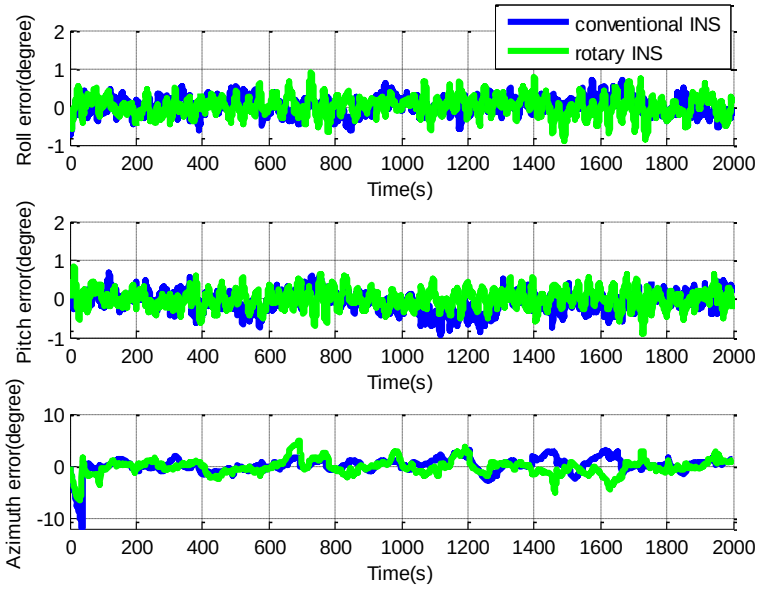

Figure 6.8 Attitude errors of integrated systems with MTi-G

Table 6.3 RMS of attitude errors for integrated systems with MTi-G

RMS	Roll (°)	Pitch (°)	Azimuth (°)
Integrated System with Conventional INS	0.22	0.26	1.43
Integrated System with rotary INS	0.26	0.24	1.39

Given the attitude errors are well maintained at small values, the position and velocity solutions are highly consistent with reference solutions for both the integrated systems, as shown in Table 6.4, which summarizes the RMS errors for position and velocity solutions.

Table 6.4 RMS of position and velocity errors for integrated systems with MTi-G

RMS	Latitude (cm)	Longitude (cm)	Height (cm)	Ve (cm/s)	Vn (cm/s)	Vu (cm/s)
Integrated System with Conventional INS	2.8	2.5	1.7	3.2	3.3	1.2
Integrated System with rotary INS	2.8	2.6	1.7	3.2	3.3	1.2

6.3.4 Navigation Error Analysis of Integrated Systems during GNSS Outages

The GNSS outages are simulated to study the navigation performance of the integrated systems in situations where GNSS measurements are not available, such as travelling in tunnels. 3 outages with the length of 5 minutes are simulated in the GNSS data collected in each field test, and the 3 corresponding sections of the trajectory for the different tests are the same. This can evaluate the navigation performance of the integrated systems during GNSS outages under similar dynamic conditions.

6.3.4.1 Navigation Error Analysis of Integrated Systems with NAV440 during GNSS Outages

As external GNSS measurements are not available, the integrated systems work in the stand-alone mode of inertial navigation. The roll and pitch errors for both the integrated systems with NAV440 during the 1st outage are present in Figure 6.9. As the gyro bias residuals in the X and Y axes are modulated by IMU rotation, the roll and pitch errors of the integrated system with the rotary INS becomes oscillating signals and they are reduced to less than 0.2 degree, while such errors in the integrated system with the conventional INS drift to about 0.4 degree. The oscillating period is the same as the IMU rotation period, and the varied oscillating amplitudes indicate the variation on gyro bias residuals. The velocity errors in the east-north plane for both the integrated systems with NAV440 during the 1st outage are given in Figures 6.10. The oscillating errors are barely observed in the velocity errors, as the accelerometer biases are estimated in the integration filter and are removed from the inertial data. With the modulation of the accelerometer bias residuals and the reduced roll and pitch errors, the velocity errors are also effectively reduced in the integrated system with the rotary INS.

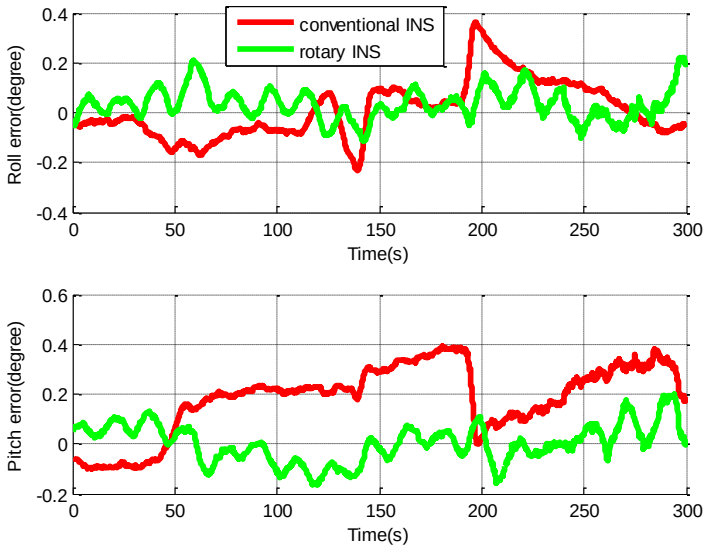

Figure 6.9 Roll and pitch errors of the integrated systems with NAV440 during the 1st GNSS outage

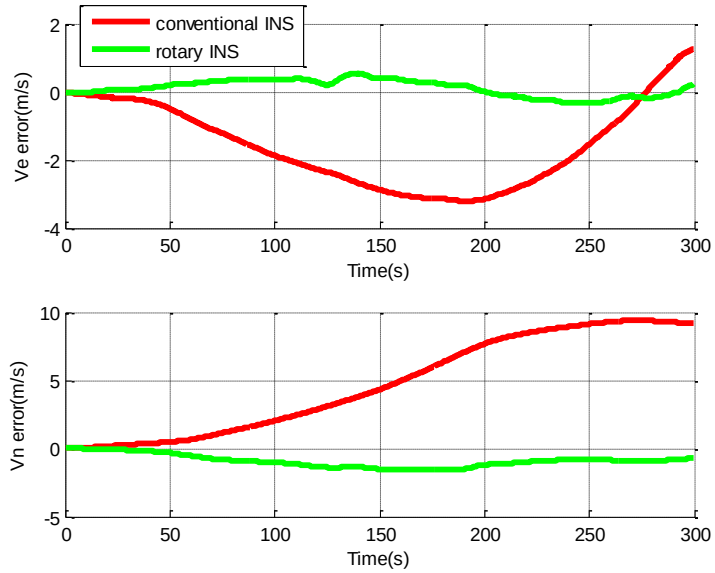

Figure 6.10 Horizontal velocity errors of the integrated systems with NAV440 during the 1st GNSS outage

The obtained roll and pitch errors, as well as the velocity errors in the east and north directions during the 2nd and 3rd outages are presented in Figure 6.11~6.14, respectively. The RMS errors of the PVA solutions during all outages are calculated for both systems and given in Table 6.5. Although no obvious improvements are observed in the azimuth solutions, the horizontal position errors are reduced from more than one thousand meters, to about four hundred meters. Figure 6.15 presents the RMS of horizontal position and velocity errors versus the outage time for the integrated systems with NAV440. Apparently, the IMU rotation effectively dampens the accumulation of the position and velocity errors.

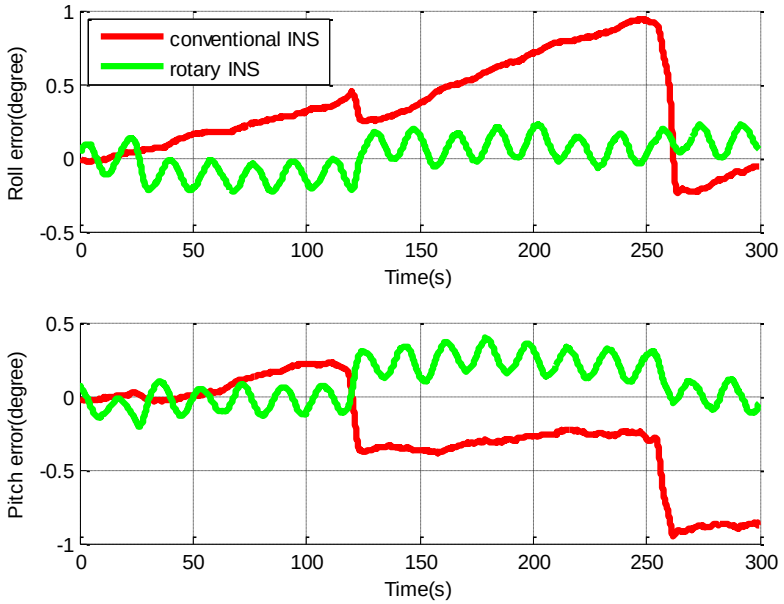

Figure 6.11 Roll and pitch errors of the integrated systems with NAV440 during the 2nd GNSS outage

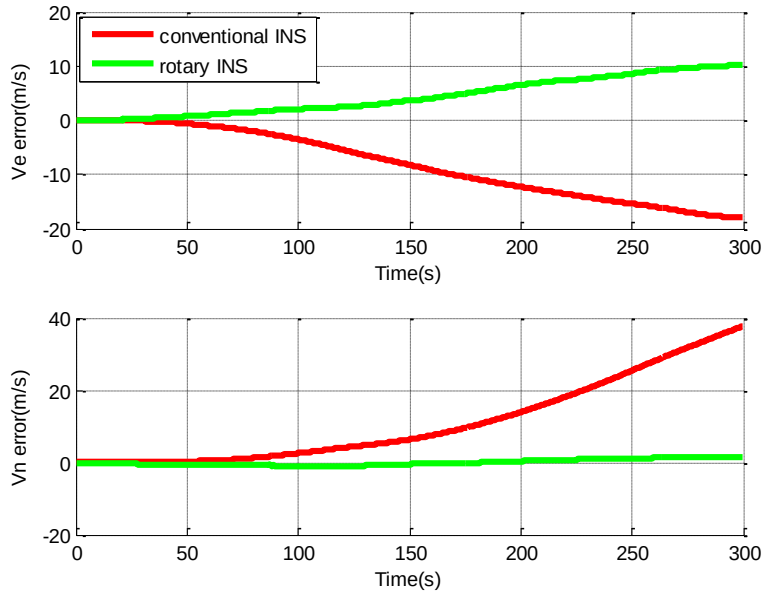

Figure 6.12 Horizontal velocity errors of the integrated systems with NAV440 during the 2nd GNSS outage

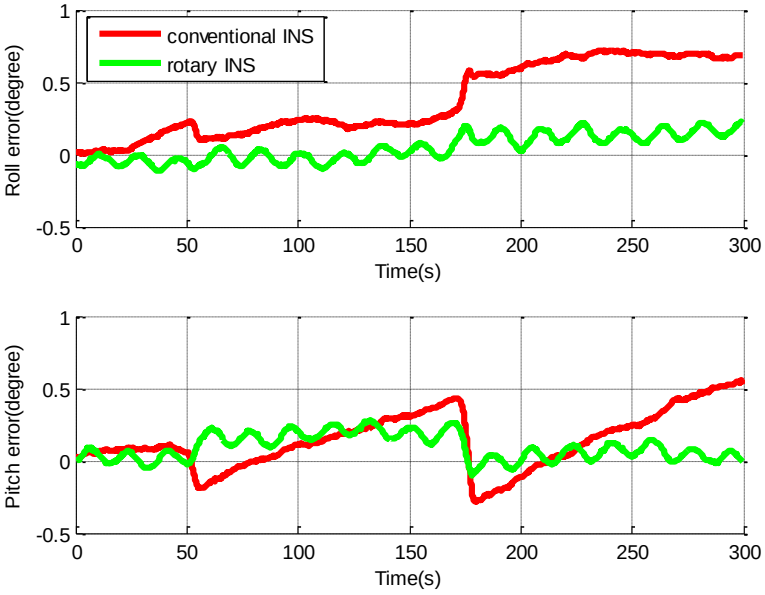

Figure 6.13 Roll and pitch errors of the integrated systems with NAV440 during the 3rd GNSS outage

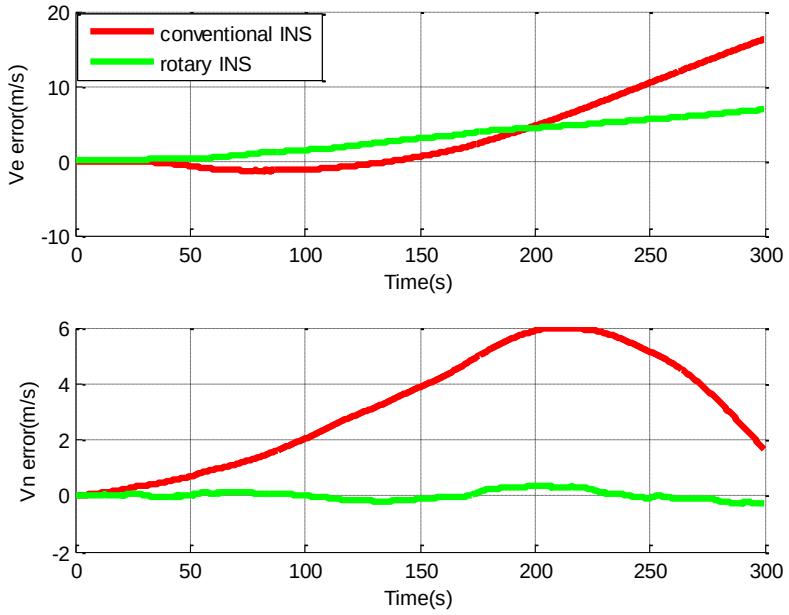

Figure 6.14 Horizontal velocity errors of the integrated systems with NAV440 during the 3rd GNSS outage

Table 6.5 RMS of PVA errors of integrated systems with NAV440 for all GNSS outages

RMS	HP (m)	HV (m/s)	Roll (º)	Pitch (º)	Azimuth (º)
Integrated System with Conventional INS	1095.0	14.4	0.64	0.50	0.42
Integrated System with Rotary INS	440.2	4.8	0.13	0.18	0.76

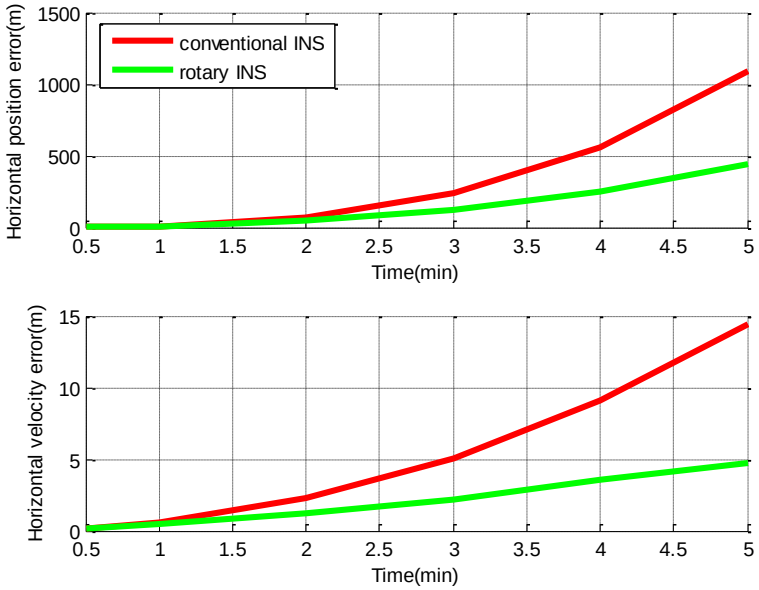

Figure 6.15 RMS of horizontal position and velocity errors of integrated systems with NAV440 vs. time

6.3.4.2 Navigation Error Analysis of Integrated Systems with MTi-G during GNSS Outages

Similar results are obtained for the systems with MTi-G, such that the navigation errors in the horizontal are also greatly reduced in the integrated system with rotary INS during GNSS outages, compared to the errors with conventional INS. The RMS values of the PVA errors during all outages are calculated and summarized in Table 6.6 for both systems with MTi-G. Although much greater navigation errors are obtained due to MTi-G's significant gyro errors, compared to those errors from NAV440, the navigation errors are still effectively mitigated by IMU rotation. The horizontal position and velocity errors are reduced about 2 times in the integrated system with the rotary INS, compared to those errors with the conventional INS. Figure 6.13 presents the RMS of horizontal position and velocity errors versus the outage time.

Table 6.6 RMS of PVA errors of integrated systems with MTi-G for all GNSS outages

RMS	HP (m)	HV (m/s)	Roll (°)	Pitch (°)	Azimuth (°)
Integrated System with Conventional INS	3458.3	31.9	0.83	0.75	2.39
Integrated System with Rotary INS	1645.3	17.3	0.59	0.57	1.67

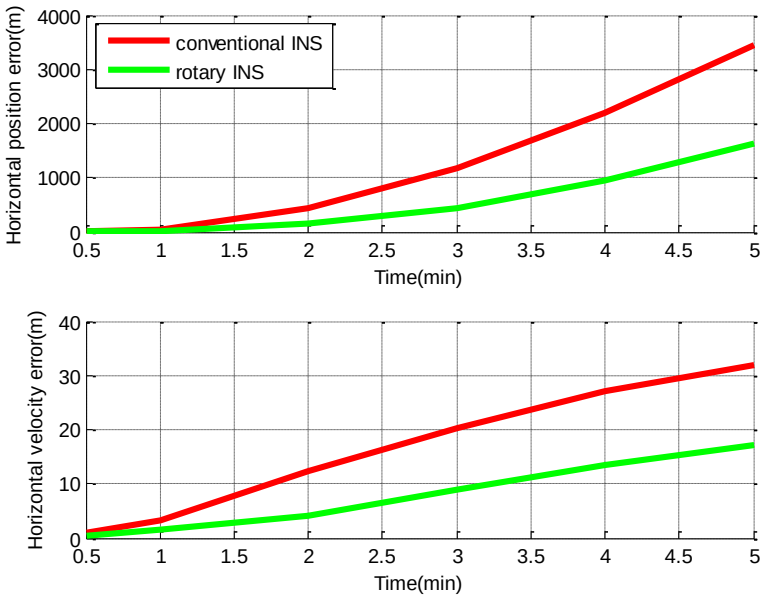

Figure 6.16 RMS of horizontal position and velocity errors of integrated systems with MTi-G vs. time

Based on the kinematic field tests and analysis, there are the following findings: 1) although the INS errors, such as the azimuth error, the accelerometer biases in the horizontal plane, and the gyro biases, are unobservable for a rotary INS when both the roll and pitch are zeroes, the maneuvers significantly improve their observability; 2) both the integrated systems with the conventional and rotary INS offer similar PVA solutions with continuous GNSS measurements; 3) through sensor error modulation by IMU rotation about the Z axis, the navigation errors in the east-north plane are significantly reduced during GNSS outages for the integrated system with the rotary INS, and therefore such a system can more effectively bridge GNSS outages, in comparison to the system with a conventional INS.

Chapter Seven: Conclusions and Recommendations

MEMS IMU has been applied in a wide range of applications in recent years for its low-cost, small size and low power assumption. MEMS IMU however, features significant sensor errors such that the navigation errors for a MEMS-based inertial system will accumulate very quickly. External aiding from other enabling sensors, such as GNSS, has become the main approach to help limit the growth of the navigation errors over time. In this research, the concept of rotary INS is investigated for mitigating inertial navigation errors through rotating IMU sensors. Comparing to the conventional external sensor aiding approach, the rotary INS based method requires no external sensors, which can be an effective approach for inertial navigation error mitigation particularly when no external aiding information is available in applications (e.g. navigation during GNSS outages in challenging environments). The concept of rotary INS based on high-end IMUs has been investigated with respect to certain applications, but no work has been conducted for low-cost MEMS IMUs. In addition to the error mitigations, rotary INS also has the potential to improve a navigation system's observability, which is critical to ensure high navigation precision, as well as reliability. The major contributions of this research include:

i. The investigation of rotary INS with MEMS IMU from mathematical equations of error mitigations, IMU rotation schemes and the rotation-induced sensor errors, as well as their calibrations, simulation analysis, turntable tests and kinematic field tests to study the error mitigation performance;

ii. The investigation of the observability of both the conventional and rotary inertial navigation systems, and the improvement on system observability by IMU rotations, and turntable tests, as well as results analyses;

iii. The development of the integrated system of GNSS and the rotary INS with a low-cost MEMS IMU for bridging GNSS outages, including the system observability analysis, and kinematic field tests, as well as results analyses.

The following sections outline the major conclusions drawn from this research and the recommendations for future improvements.

7.1 Conclusions

The following conclusions can be drawn from the aspect of the error mitigation by IMU rotations.

i. The IMU rotation modulates the constant biases of inertial sensors that are perpendicular to the rotation axis, and the attitude and velocity errors caused by such biases are self-eliminated after a complete rotation cycle. The constant biases of inertial sensors in the rotation axis cannot be modulated, and the attitude and velocity errors caused by such errors propagate in the same way as in the conventional INS.

ii. The IMU rotation induces an extra gyro error in the rotation axis due to the gyro scale factor, and this error results accumulated attitude errors in the direction of the corresponding rotation axis. The IMU rotation also induces extra errors in the gyros that are perpendicular to the rotation axis due to the gyro installation errors, resulting in the oscillating attitude and velocity errors.

iii. The rotation about the X or Y axis effectively mitigates the navigation errors in the vertical directions, while the rotation about the Z axis largely reduces the navigation errors in the east and north directions. In this research, the rotation about the Z axis is employed for land vehicle navigation.

iv. When the IMU rotates about the Z axis, IMU rotation induces gyro biases due to the gyro scale factor of Z axis, K_{gz}, and the installation errors, K_{gxz} and K_{gyz}. The proposed calibration method can effectively remove these errors and further reduce the navigation errors with a rotating MEMS IMU.

v. With the calibration process in a rotary INS with a rotating MTi-G about the Z axis, the position and velocity errors in the east-north plane can be reduced by about 2~3 times compared to the ones in the conventional INS. Although theoretically the higher IMU rotation rates can more effectively modulate the sensor errors, the IMU rotation rate has limited effect on the error mitigations due to the significant gyro noise and bias instability of MTi-G.

vi. For a rotary INS with a rotating NAV440 about the Z axis, the position and velocity errors in the east-north plane are reduced by about 3~5 times, in comparison to the ones in the conventional INS. As NAV440 features much smaller gyro noise and bias instability, the IMU rotation rate has stronger effect on the error mitigations, such that higher IMU rotation rate result smaller navigation errors.

The following conclusions can be drawn from the aspect of improvements on system observability by IMU rotations.

i. The conventional INS is not a completely observable system in the absence of system maneuvers, the observable states are the velocity errors in the east, north and vertical directions, and the accelerometer bias in the vertical direction.

ii. The IMU rotation about the X axis significantly improves the observability of the accelerometer biases in the X and Y axes, the roll and pitch errors, and the gyro bias in the Z axis. While only the azimuth error is still unobservable, the estimation of the gyro bias of the Z axis, however, can limit its accumulation. When roll is zero, the observability of the accelerometer bias in the X axis and the roll error is reduced.

iii. The improvements on the system observability by the IMU rotation about the Y axis are similar to those for the rotation about the X axis. The only difference is that the pitch angle of zero will degrade the observability of the accelerometer bias in the Y axis and the pitch error.

iv. The IMU rotation about the Z axis also significantly improves the observability of the accelerometer biases in the X and Y axes, the roll and pitch errors, as well as the gyro bias in the Z axis. However, if both the roll and pitch are zeroes, IMU rotation about the Z axis severely degrades the observability of the horizontal accelerometer biases as well as the gyro biases, which results in significant attitude errors. Therefore, a tilt angle is required for the rotary INS with a rotating IMU about the Z axis to improve the system observability.

The following conclusions can be drawn from the aspect of bridging GNSS outages based on a rotary INS with a low-cost MEMS IMU.

i. Although the attitude errors, the horizontal accelerometer biases, as well as the gyro biases, are unobservable in the rotary INS with a rotating MEMS IMU about the Z axis when both the roll and pitch are zeros. The vehicle maneuvers make the integrated system of GNSS and rotary INS a completely observable system.

ii. With continuous GNSS measurements, both the integrated systems with the conventional and rotary INS offer similar navigation solutions.

iii. The integrated system with the rotary INS outperforms the system with the conventional INS during GNSS outages, as the modulation of the sensor errors by IMU rotation greatly reduces the navigation errors in the horizontal plane.

7.2 Recommendations

The following recommendations can be made for future investigation:

i. The turntables are used in this research to rotate the MEMS IMU to isolate the effect of the vibrations and unstable rotations on error mitigations. However, the turntables are expensive and cumbersome, which is not practical for commercial application. A low-cost and portable rotation device must be considered in the future investigations.

ii. The error mitigation performance of a rotary INS is largely constrained by the noise and the gyro bias instability of a MEMS IMU. Currently, there are different grades of MEMS IMU available on the commercial market, with gyro bias instability ranges from several degrees per hour to hundreds degrees per hour; therefore, more MEMS IMUs should be tested and analyzed to fully investigate the error mitigation performance of the rotary INS with MEMS IMUs

iii. As shown in the kinematic field tests, the vibrations and the vehicle dynamics affect the error mitigations of a rotary INS. Additional equipment, such as the jolt table, and more dynamics, are required for the future study of the error mitigation of a rotary INS with MEMS IMUs.

iv. Only the continuous rotation of the IMU is considered in this research. More rotation schemes, such as the rotation-dwell scheme, should be tested for the rotary INS with MEMS IMUs.

v. The findings of IMU rotations substantially improving the system observability in the absence of maneuvers is critical to applications where strong maneuvers are difficult, such as the marine navigation or the underwater navigation. The field tests should be conducted in such environments to investigate the enhancements on the navigation performance by IMU rotations.

References

Antonio, A. (2010). GNSS/INS Integration Methods. Ph.D. Thesis, The University of Calgary, Canada, 2010.

Artese, G. and Trecroci, A. (2008). CALIBRATION OF A LOW COST MEMS INS SENSOR FOR AN INTEGRATED NAVIGATION SYSTEM. In Proceedings of the International Archives of the Photogrammetry, Remote Sensing and Spatial Information Sciences, Beijing, China, 2008.

Ben, Y. Y., Chai, Y. L., Gao, W. and Sun, F. (2010). Analysis of Error for a Rotating Strap-down Inertial Navigation System with Fiber Gyro. J. Marine. Sci. Appl. 9: 419-424. DOI: 10.1007/s11804-010-1028-z.

Carvalho, H., Del Moral, P., Monin, A. and Salut, G. (1997). Optimal nonlinear filtering in GPS/INS integration. Aerospace and Electronics Systems IEEE Transactions, Vol. 33, No. 3, pages 835-850, July 1997.

Du, S. (2010). Integration of Precise Point Positioning and Low Cost MEMS IMU, M.Sc. Thesis, The University of Calgary, Canada, 2010.

Du, S. and Gao, Y. (2012a). Inertial aided cycle slip detection and identification for integrated PPP GPS and INS. Sensor, 2012; 12 (14344-14362), doi: 10.3390/s121114344.

Du, S. and Gao Y. (2012b). Integration of Precise Point Positioning and the Latest MEMS IMU for Precise Applications. In Proceedings of the ION GNSS 2012, Nashville, Teneeesee, U.S., September 18 – 21, 2012.

Du, S., Huang, B. and Gao, Y. (2012). An Integrated MEMS IMU/Camera System for Pedestrian Indoor Navigation Using Smartphones. In China Satellite Navigation Conference (CSNC) 2012 Proceedings, Guangzhou, China, May 2012.

Du, S., Huang, B. and Gao, Y. (2013). Integration of Floor Plan, Vision and Inertial Sensors for Pedestrian Navigation in Indoor Environments. In Proceedings of ION PLAN 2013, Honolulu, Hawaii, U.S., April 19-23, 2013

Du, S., Sun, W. and Gao, Y (2014). An Investigation on MEMS IMU Error Mitigation Using Rotation Modulation Technique. In Proceedings of ION GNSS 2014, Tempa, FL, U.S., September 8~12, 2014

Du, S., Sun, W. and Gao, Y. (2015). Integration of GNSS and MEMS-based Rotary INS with MEMS IMU. In China Satellite Navigation Conference (CSNC) 2015, Xian, China, May, 2015.

Fang, J. and Gong X. (2010). Predictive iterated Kalman filter for INS/GPS integration and its application to SARmotion compensation. IEEE trans. Instrum. Meas. 2010, 6, 909-915.

Geller, E. S. (1968). Inertial system platform rotation. IEEE Transactions on Aerospace and Electronic Systems, 1968, pages, 627-634

Giovanni, S. C. and Levinson, E. (1981). Performance of a Ring Laser Strapdown Marine Gyrocompass. In the Proceedings of the ION 7th Annual Meeting, Annapolis, Maryland, U.S., 1981

Godha, S. (2006) Performance Evaluation of Low Cost MEMS-based IMU Integrated with GPS for Land Vehicle Navigation Application, M.Sc. Thesis, Department of Geomatics Engineering, The University of Calgary, Canada.

Godha, S. and Cannon, M. E. (2007). GPS/MEMS INS integrated system for navigation in urban areas. GPS Solutions 11(3):193-203

Goshen-Meskin, D. and Bar-Itzhack, I. Y. (1992). Observability analysis of piece-wise constant systems. I. Theory. IEEE Trans. Aerosp. Electron Syst. Vol. 28, No.4, pp1056-1067

Guo, J. and Zhong, M. Y. (2013). Calibration and Compensation of the Scale Factor Errors in DTG POS. IEEE trans. Instrum. Meas., 2013, vol. 62 (2784-2794), doi: 10.1109/TIM.2013.2261631.

Hartman, R., Hawkinson, W., Sweeney, K. and Gurgaon, H. (2008) Tactical underwater navigation system (TUNS). Proceedings of Position, Location and Navigation Symposium, New York, Institute of Electrical and Electronics Engineers, pp.898-911.

He, K. P. (2008). Parametric Identification and Error Compensation of MEMS Inertial Sensors and IMU. Ph.D. Thesis, Harbin Engineering University, Harbin, China, 2008.

Heckman, D. W. and Baretela, L. M. (2000). Improved Affordability of High Precision Submarine Inertial Navigation by Insertion of Rapidly Developing Fiber Optic Gyro Technology. In Proceedings of IEEE PLANS. San Diego, CA, USA., 2000.

Hibbard, R., Wylie, B. and Levinson E. (1996). Sperry Marine MK-49, The World's Best Ring Laser Gyro Ship's Inertial Navigation System. JSDE Proceedings, Orlando, 1996

Hide, C., Botterill, T. and Andreotti M. (2010). Low cost vision-aided IMU for pedestrian navigation. Ubiquitous Positioning Indoor Navigation and Location Based Service (UPINLBS), pages 1-7.

Hong, S., Lee, M. H., Chun, H. H., Kwon, S. and Speyer, J. L. (2005). Observability of error states in GPS/INS integration. IEEE Trans. Veh. Tech. Vol. 54, No.2,pp731-743

Huang, B., Du, S. and Gao, Y. (2011). An Integrated MEMS IMU/Camera System for Pedestrian Navigation in GPS-denied Environment. In Proceedings of ION GNSS 2011, Portland, Oregon, U.S., September 9-12, 2011

Ishibashi, S., S. Tsukioka, H. Yoshida, T. Hyakudome and T. Sawa (2006a). The Method to Improve the Performance of an Inertial Navigation System using a Turntable. The Proceedings of the Sixteenth (2006) International Offshore and Polar Engineering Conference, pp. 229-232, 2006

Ishibashi, S., S. Tsukioka, H. Yoshida, T. Hyakudome and T. Sawa (2006b). The Research of an Inertial Navigation System Installed in an Autonomous Underwater Vehicle. in Proceeding of Techno-Ocean 2006/19th JASNAOE Ocean Engineering Symposium, Kobe, 2006, No.95

Jekeli, C. (2001). Inertial Navigation System with Geodetic Applications. Walter de Gryter GmBH and Co.

Karumuri, S. R., Srinivas, Y., Sekhar, J. V. and Sravani, K. G. (2011). Review on Break Through MEMS Technology. Archives of Physics Research, 2011. 2(4): pp.158-165

Lahham, J. and Brazell, J. (1992). Acoustic Noise Reduction in the MARLIN Dithered Laser Gyro Marine Navigator. PLANS 1992

Levinson, E. and Giovanni, S. C. (1980). Laser gyro potential for long endurance marine navigation. In Proceedings of IEEE Position, Location and Navigation Symposium. New York, 1980

Levinson, E. and Majure, R. (1987). Accuracy enhancement techniques applied to the Marine Ring Laser Inertial Navigator (MARLIN). Journal of The Institute of Navigation, 1987 vol. 34 (71-80).

Levinson, E. ter Horst, J. and Willcocks, M. (1994). The next generation marine inertial navigation is here now. In Proceedings of IEEE Position Location and Navigation Symposium, 1994.

Li, T. (2009). Use of Wheel Speed Sensors to Enhance a Reduced IMU Ultra-Tight GNSS Receiver. M.Sc. Thesis, Department of Geomatics Engineering, The University of Calgary, Canada

Li, Y., Efatmaneshnik, M. and Dempster, A. G. (2012). Attitude determination by integration of MEMS inertial sensors and GPS for autonomous agriculture applications. GPS Solut. (2012) 16:41-52 DOI 10.1007/s10291-011-0207-y

Liu, C. (2006). Foundations of MEMS. Published by Pearson Education Inc., Upper Saddle River, New Jersey 07458

Lu, Z. D., and X. B. Wang (2010). Error analysis and calibration of systematic dual-axis rotation-modulating SINS. Journal of Chinese Inertial Technology, 2010, 18 (2): 135-141.

Morrow, R. B. and Heckman, D. W. (1998). High precision IFOG insertion into the strategic submarine navigation system. In Proceedings of IEEE Position Location and Navigation Symposium, 1998, pages 332-338

Nassar, S. (2003). Improving the Inertial Navigation System (INS) Error Model for INS and INS/DGPS Applications. Ph.D. Thesis, The University of Calgary, Canada, 2003.

Nassar, S., Schwarz, K.P. and El-Sheimy, N. (2003). INS and INS/GPS Accuracy Improvement Using Autoregressive Modeling of INS Sensor Errors. In Proceedings of the ION NTM, San Diego, California, U.S., 26-28 January 2003.

Nassar, S. and El-Sheimy, N. (2005). A Combined Algorithm of Improving INS Error Modeling and Sensor Measurements for Accurate INS/GPS Navigation. GPS Solutions, DOI:10.1007/s10291-005-0149-3

Niu, X., T. Hassan, C, Ellum, and N. El-Sheimy (2006). Directly Georeferencing Terrestrial Imagery using MEMS-based INS/GNSS Integrated Systems. XXIII FIG Congress. Munich, Germany, October 8-13.

Niu, X., Nassar, S., and El-Sheimy N. (2007). An Accurate Land-Vehicle MEMS IMU/GPS Navigation System Using 3D Auxiliary Velocity Updates. Journal of the Institute of Navigation Vol.54, No.3, pp.177-188

Niu, X., Li, Y., Zhang, Q., Cheng, Y. and Shi, C. (2012). Observability Analysis of Non-Holonomic Constraints for Land-Vehicle Navigation Systems. Journal of Global Positioning Systems (2012) Vol. 11, No.1: 80-88 DOI: 10.5081/jgps.11.1.80

Niu, X., Li, Y., Zhang, H. P., Wang, Q. J. and Ban, Y. L. (2013). Fast Thermal Calibration of Low-Grade Inertial Sensors and Inertial Measurement Units. Sensors, 2013, 13, 12192-12217; doi:10.3390/s130912192.

Noureldin, A., El-Shafie, A. and El-Sheimy, N. (2007). Adaptive neurofuzzy module for inertial navigation system/global positioning system integration utilising position and velocity updates with realtime cross-validation. Radar, Sonar & Navigation, IET, 2007, vol. 1 (388-396).

Ren, Y. F. and Ke, X. Z. (2010). Particle Filter Data Fusion Enhancements for MEMS-IMU/GPS. Intelligent Information Management, 2010, 2, pages 417-421.

Rhee, I., Abdel-Hafez, M. and Speyer, J. L. (2004). Observability of an Integrated GPS/INS during Maneuvers, IEEE Trans. on Aerosp. and Electr. Syst., Vol. 40, No.2.

Schwarz, K. P. and M. Wei (2000). INS/GPS Integration for Geodetic Applications. ENGO-623 Lecture Notes, Department of Geomatics Engineering, The University of Calgary, Canada.

Shin, E. (2001). Accuracy Improvement of Low Cost INS/GPS for Land Application. M.Sc. Thesis, Department of Geomatics Engineering, The University of Calgary, Canada.

Shin, E. (2005). Estimation Techniques for Low-Cost Inertial Navigation. Ph.D. Thesis, University of Calgary, Canada, 2005.

Shin, E., Niu, X. and El-Sheimy N. (2005). Performance Comparison of the Extended and the Unscented Kalman Filter for Integrated GPS and MEMS-based Inertial Systems. In Proceedings of ION NTM, San Diego, California, U.S., 24-26 January, 2005.

Skalund, J. (1999). Optimizing Georeferencing of Airborne Survey Systems by INS/DGPS. Ph.D. Thesis, The University of Calgary, Canada, 1999.

Sun, F., Sun, W., Gao, W. and Ben, Y. Y. (2009) Research on the Technology of Rotational Motion for FOG Strapdown Inertial Navigation System. Proceedings of the 2009 IEEE International Conference on Mechatronics and Automation, August 9-12, Changchun, China.

Sun, W. (2011). Research on the Modulated Strapdown Inertial Navigation System. Ph.D. Thesis, Harbin Engineering University, Harbin, China.

Sun, W., Wang, D. X., Xu, L. W. and Xu, L. L. (2013). MEMS-based rotary strapdown inertial navigation system. Measurement, 2013, 46, 2585–2596.

Terry, T. and Emanuel, L. (2000). The AN/WSN-7B marine gyrocompass/navigator. In Proceedings of the National Technical Meeting of the Institute of Navigation, 2000, pages 348-357.

Titterton, D. and Weston, J. (2004). Strapdown Inertial Navigation Technology, 2nd Edition. Progress in Astronautics and Aeronautics Series, Published by AIAA, 2004

Tucker, T. and E. Levinson (2000), "The AN/WSN-7B Marine Gyro-compass/Navigator.", ION NTM Anaheim, CA, U.S.A.

Wang, J. H. (2006), "Intelligent MEMS INS/GPS Integration For Land Vehicle Navigation", Ph.D. Thesis, Department of Geomatics Engineering, The University of Calgary, Canada.

Wang, J. H. and Gao, Y. (2005). Multi-sensor data fusion for land vehicle attitude estimation using fuzzy expert system, Data Science Journal, Vol. 4, pages 127-139

Weston, J. L. and Titterton, D. H. (2000). Modern inertial navigation technology and its application. Electronics & Communication Engineering Journal, April 2000.

Yang, Y. and Miao, L. J. (2004). Fiber-optic Strapdown Inertial System with Sensing Cluster Continuous Rotation. IEEE Transactions on Aerospace and Electronic Systems, 2004, Vol. 40, No.4, pages 1173-1178

Yuan, B. L. (2007). Research on Rotating Inertial Navigation System with Four-Frequency Differential Laser Gyro. Ph.D. Thesis, National University of Defense Technology, Changsha, 2007

Yuan, B. L. and Rao, G. Y. (2006). On the theory of optical gyro rotating inertial navigation system. Journal of National University of Defense Technology, 2006, 28 (6): 76-80.

Yukel, Y. (2011). Design and Analysis of Inertial Navigation Systems with Skew Redundant Inertial Sensors. Ph.D. Thesis, University of Calgary, Calgary, Canada.

Zha, F., Hu, B. Q., Qin, F. J. and Luo, Y. B. (2012). A rotating inertial navigation system with the rotating axis error compensation consisting of fiber optic gyros. OPTOELECTRONICS LETTERS, Vol.8, No.2, March 2012

Zhang, L. D., Lian, J. X., Wu, M. P. and Zheng, Z. Q. (2009). Research on auto compensation technique of strap-down inertial navigation system. International Asia Conference on Information in Control, Automation and Robotics, pages 350-353